Modification of inorganic surfaces with 1-alkenes and 1-alkynes

Jurjen ter Maat

Modification of inorganic surfaces with 1-alkenes and 1-alkynes

Jurjen ter Maat

Thesis committee

Thesis supervisor

Prof dr. Han Zuilhof
Professor of Organic Chemistry
Wageningen University

Other members

Prof. dr. ir. Jurriaan Huskens	Twente University, Enschede
Prof. dr. Hauke Smidt	Wageningen University
Dr. Alexander Kros	Leiden University
Dr. ir. Marko Blom	Micronit Microfluidics BV, Enschede

This research was conducted under the auspices of graduate school VLAG.

Modification of inorganic surfaces with 1-alkenes and 1-alkynes

Jurjen ter Maat

Thesis

submitted in fulfillment of the requirements for the degree of doctor
at Wageningen University
by the authority of the Rector Magnificus
Prof. dr. M.J. Kropff,
in the presence of the
Thesis Committee appointed by the Academic Board
to be defended in public
on Wednesday April 4 2012
at 4 p.m. in the Aula.

Jurjen ter Maat
Modification of inorganic surfaces with 1-alkenes and 1-alkynes,
168 pages
PhD thesis, Wageningen University, Wageningen, NL (2012)
ISBN 978-94-6173-201-9

"Oh sorry honey, I guess I must have been really involved in my scientific work there for a minute."

Dr. Paul Armstrong in '*The lost skeleton of Cadavra*' (2001).

Table of Contents

Chapter 1

Introduction

1.1 Monolayers on inorganic surfaces

With the ever-decreasing size of devices, surfaces determine the relevant material characteristics to an increasing extent. The surface properties of a solid material can be modified by adsorbing a monomolecular layer of an organic compound, as has already been a topic of intense investigations for over 75 years.[1,2] Properties such as surface wettability can be greatly affected by the presence of a monolayer, while the structural properties of the surface are fully retained. What is more, monolayers can even introduce physical properties such as conductivity and magnetism to a surface.[3] In addition, they may allow further coupling of functional molecules to the surface by introducing reactive functional groups. In this way, monolayers enable us to combine the well-defined physical properties of inorganic materials with the specificity encountered in (bio)chemical interactions. This makes them particularly useful for sensing and detection purposes.

Molecules can associate to inorganic surfaces via physical and/or chemical interactions. In the classical monolayer example of the Langmuir-Blodgett (LB) film,[4] the interactions with the substrate are merely physical. The LB technique exploits the self-organization of surfactant molecules at the air-water interface by transferring these pre-formed monolayers to a solid substrate.[5] The technique offers great control over the intermolecular interactions,[6] but the physisorbed monolayer lacks stability in aqueous environments, which has limited its application.[7]

1.1.1 Self-assembled monolayers.[8]

In comparison to Langmuir-Blodgett films, self-assembled monolayers (SAMs) display increased stability.[9] In these SAMs, molecules self-organize on a surface by chemisorption, resulting in well-ordered monolayers. One of the earliest examples was the formation of alkylsilane monolayers on silicon oxide surfaces.[10,11] These are formed upon the condensation reaction of trichloro- or trialkoxyalkylsilanes with surface hydroxyl groups, resulting in the formation of three covalent bonds with the surface. Such monolayers can also form on other hydroxylated surfaces, although the monolayer stability on these surfaces may be somewhat different compared to silicon oxide.

Organosilane adsorption can take place from mM solutions or even from the gas phase. It is compatible with several functional groups, such as -SH and -NH_2. However, one of the disadvantages of using trichloro- or trialkoxysilanes is their tendency to form multilayers, which is often undesirable as this limits reproducibility.[8] Multilayer formation is due to silane condensation in solution, followed by adsorption of the resulting oligomers to the surface. To prevent this, it is necessary to strictly control the water content of the solution.[12] Nevertheless, organosilane monolayers have found many applications and can nowadays be found in several commercial products.

The other well-known self-assembled monolayer system is that of alkylthiols on gold.[8,13] Here, the thiol is adsorbed to form a surface thiolate. The corresponding sulfur-gold interaction has a semi-covalent character, which allows the adsorbed molecules to migrate over the surface. For unbranched alkylthiols, this results in the formation of a closely packed monolayer, in which the molecules are tilted ca. 30° from the surface normal to maximize the Van der Waals interactions. Thiolate monolayers can also be obtained from disulfides, which are cleaved upon adsorption. The thiolate surface chemistry is rather selective and therefore compatible with many functional groups and complex molecules. Moreover, monolayer formation is simple and reproducible, requiring just (sub)mM solutions. Yet the semi-covalent character of the surface bond, combined with the tendency of thiols to oxidize, limits the stability of gold monolayers, which has thwarted its application on an industrial scale.

1.1.2 1-Alkenes and/or 1-alkynes on inorganic surfaces

In addition to these classical systems, many other monolayer systems exist, e.g. those based on the adsorption of hydroxamic acids[14] or phosphonic acids[15,16] on metal oxide surfaces. Of special interest is the surface chemistry based on terminally unsaturated hydrocarbons. Whereas these compounds have initially been shown to form monolayers onto silicon,[17] they have since then been demonstrated to react to other inorganic surfaces as well. This thesis may serve as an illustration of this versatility, as it consists of studies that are based on the reaction of terminally unsaturated hydrocarbons with silicon, silica and alumina, respectively.

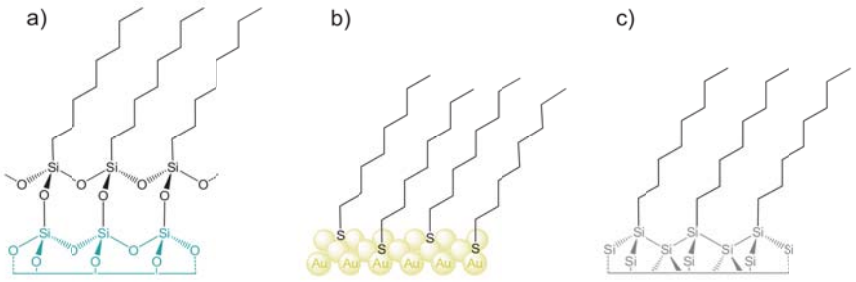

Figure 1.1. Monolayers of alkylsilanes on silica (a), alkylthiols on gold (b), and 1-alkenes on silicon (c).

In order to get an overview of the reactivity of 1-alkenes and 1-alkynes on inorganic surfaces, a short review is given in this chapter. It starts with the surface modification of silicon (as this is well understood), then continues with silicon-related materials (such as silicon nitride and germanium), and finally treats the surface modification of metal oxides. The review is limited to wet-chemical methods only, because this offers wider flexibility and is often more easily applicable than gas-phase methods. Furthermore, it only considers flat substrates, thereby excluding the surface chemistry on nanoparticles, nanowires and porous substrates. Porous anodic alumina is the only notable exception, since this material can be regarded as a flat surface with a well-defined array of pores running perpendicularly to the surface.

1.2 Monolayers of 1-alkenes and 1-alkynes on silicon[18-20]

Silicon is a semiconducting material with a band gap of 1.1 eV that is widely used in the semiconductor industry. It is grown as a single crystal, which is then cut along specific directions to obtain surfaces with a well-defined orientation, such as <100> or <111>. Under ambient conditions, these surfaces are covered with a thin layer of native oxide, which affects the electrical properties of the material. Therefore, this oxide layer is usually removed by etching in (buffered) hydrogen fluoride solution, yielding an atomically flat hydrogen-terminated silicon surface (H-Si). The semiconducting properties of the material can be further tuned by doping with e.g.

boron or phosphorus. In this way, electron-enriched (n-type) or hole-enriched (p-type) silicon is obtained. By combining n-type and p-type material, functional devices such as diodes and transistors can be fabricated.

Because of the dominant position of silicon in the semiconductor industry, interest rose in the surface modification of this material. It was envisaged that the resulting hybrid materials combine the semiconducting properties of silicon with the specific binding properties of the organic monolayer. This may, for example, result in devices that can monitor the adsorption of specific compounds by means of the electric field effect.

In a landmark publication, Linford and Chidsey described the formation of organic monolayers on hydrogen-terminated silicon from terminally unsaturated compounds.[17] The covalent Si-C bond that is formed upon the reaction is non-polar, and therefore very stable. Moreover, the monolayer can effectively passivate the surface, preventing the formation of silicon oxide at the interface. However, modification with long-chain hydrocarbons has been shown to leave part of the Si-H sites unreacted. These sites are then prone to oxidation, which may undermine the electrical properties of the well-defined interface. Effective and highly stable surface passivation with long-chain hydrocarbons has therefore been developed, to yield a close-to-maximum surface coverage. The maximum surface coverage is dependent on steric factors and was shown to be ~55 % for 1-alkenes[21] and 69 % for 1-alkynes.[22]

In contrast to self-assembled monolayer systems, the formation of alkene monolayers on silicon requires concentrated solutions and significant activation: In the initial publication elevated temperatures and radical initiators were used to initiate the reaction.[17] Since then, several thermal,[23] catalytic,[24] photo-,[25,26] electro-,[27] mechano-[28] and sonochemical[29] methods have been introduced, which are compatible with ever milder reaction conditions. Currently, methods are available under conditions that approach self-assembly at room temperature.[29,30]

Regardless of the method employed, there is consensus on the mechanism behind monolayer formation. The hydrosilylation reaction is thought to proceed over the surface via a radical-chain mechanism. This was supported by scanning tunneling microscopy studies, that clearly showed island formation.[31] The reaction initiation is dependent on the modification method. For example, thermal or UV methods may

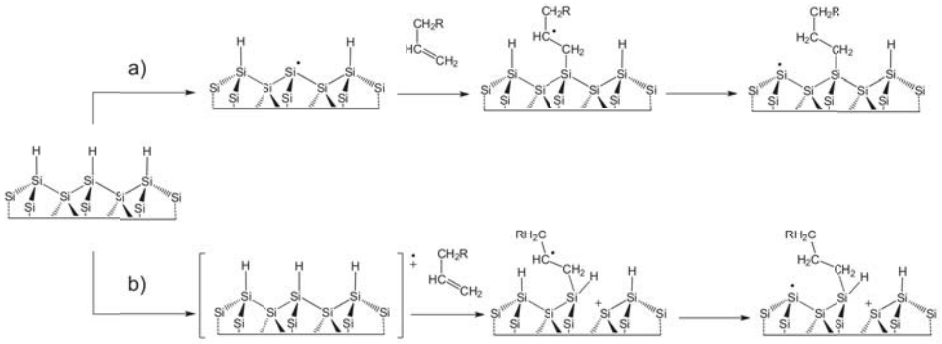

Figure 1.2. Initial stages of monolayer formation on H-Si(111): a) Homolytic cleavage of Si-H by UV illumination or a radical initiator, b) Exciton-based initiation by thermal or visible light activation.

favor homolytic cleavage of the Si-H bond, whereas for mild photochemical modification an excitation mechanism was proposed (
Figure **1.2**).[32,33]

In contrast to thiolate monolayers on gold, only a limited number of functional groups are compatible with monolayer formation on H-Si. This has hampered the applicability of this monolayer system. It has been shown that many functional groups, including $-NH_2$ and $-SH$, can react with the silicon surface. Therefore, initial functionalization approaches mainly relied on functional group protection. Yet in recent years, there have been several reports on successful functionalization with $-COOH$,[34] $-COF$[35] and $-CH=CH_2$ functional groups[36] that may open the way to further applications.

Lateral control over surface functionality can be obtained by patterning. A wide range of patterning methods has been developed for self-assembled monolayer systems.[11,13] However, most of these methods are not compatible with H-Si, because of its tendency to oxidize in the unmodified regions.

Therefore, most reports deal with the patterning of preformed monolayers on oxide-free Si.[35-39] Nevertheless, several studies on the constructive patterning of H-Si have been reported. These include methods based on scanning probe microscopy,[40,41]

photolithography[42] and soft lithography.[43,44] The soft lithographic methods rely on using a stamp in combination with a catalyst to locally initiate monolayer formation. In this thesis, a new soft lithographic method is introduced that does not rely on a catalyst, but instead uses light to enhance the surface modification reaction (Chapter 2).

1.3 Monolayers on Si-based materials

When it was established that 1-alkenes and 1-alkynes could successfully form monolayers on silicon surfaces, the surface modification of other silicon-containing materials with these compounds was also investigated.

1.3.1 Silicon nitride

Silicon nitride is a wide-band gap material (band gap ~5 eV) that can be easily deposited and is therefore often used as an insulator in the semiconductor industry. Moreover, because of its mechanical hardness and chemical inertness, it has found applications in bearings, microsieves and cantilevers. The reactivity of 1-alkenes with the silicon nitride surface was first demonstrated by Pignataro et al., who reacted 1-octadecene with the silicon nitride at 200 ºC.[45] These results could be improved by using Si-enriched silicon nitride (Si_nX_4, $n \geq 3$) in combination with HF etching. Reaction with 1-alkenes or 1-alkynes at elevated temperatures (165 ºC) resulted in the formation of fairly dense yet disordered monolayers.[46] These monolayers were shown to display good stability in a wide pH range ($1 < pH < 11$).[47] It was shown that the modification reaction mainly yielded Si-C bonds on the surface, although some N-C bond formation was also indicated. Functional monolayers could be obtained by coupling protected acids and amines, followed by a deprotection step. Subsequently, the functional surfaces could be biofunctionalized by coupling proteins and oligopeptides.[47]

The coupling of 1-alkenes can also be performed photochemically. Coiffinier et al. performed the sample pretreatment and modification under UHV conditions.[48] They used UV light (254 nm) to couple a functional alkene bearing a protected semicarbazide group to the Si_nX_4 surface at elevated temperatures. Rosso et al. used

wet-chemical methods to perform the photochemical modification.[49] The grafting reaction was found to require a wavelength shorter than 270 nm, and was not strictly limited to monolayer formation, presumably due radical formation on the monolayer surface. Under these photochemical conditions, the majority of grafted sites were bound via N-C bonds, in contrast to thermal modification where mostly Si-C bonds were formed. Functionalized surfaces can be obtained by coupling protected acids[49] or in a single step by reacting 1,2-epoxy-9-decene.[50] The latter surfaces were used as a starting point to graft zwitterionic polymer brushes to the surface, which resulted in excellent protein-repelling properties.

1.3.2 Silicon carbide

Silicon carbide is a very hard semiconducting material that has a band gap of 2.3 - 3.2 eV. Combined with its high thermal conductivity and high maximum current density, this makes SiC a preferred material for high-power applications. Moreover, its chemical inertia would make it a suitable material for (bio)chemical sensing under highly demanding conditions. This requires removal of the native oxide layer, which can be performed by HF etching. Yet instead of the expected H-termination, etching yields an OH-terminated surface.[51] 1-Alkenes have been shown to react to these etched SiC surfaces both thermally and photochemically, resulting in fairly dense yet disordered monolayers.[49,51] It was proposed that this chemisorption follows Markovnikov addition, in which the 1-alkene is bound to the surface O atoms at C_2. The resulting monolayers show extremely high stability, with little or no degradation in a very wide pH range ($-1 < pH < 11$). This allowed the formation of carboxylic acid-functionalized surfaces from the corresponding methyl ester-terminated monolayers by acidic hydrolysis. Alternatively, the direct UV-induced formation of COOH-terminated monolayers on C-enriched, H-terminated SiC surfaces has also been demonstrated.[52] These surfaces could be further functionalized by amide bond formation.[49,52] In addition, protein-repelling surfaces have been fabricated by coupling oligo(ethylene glycol) terminated alkenes to the SiC surface.[53]

1.3.3 Silicon oxide

Silicon oxide (SiO_2) is an abundant material that has found many applications. Silica glasses are used for optical substrates because of their excellent transparency, but silicon oxide is also present as a native oxide on silicon wafers.

In contrast to SiN and SiC, silicon oxide was not expected to show any reactivity towards 1-alkenes. Yet in control experiments, Mischki et al. showed that the SiO_2 surface is not completely unreactive under both thermal (T = 150 °C) and photochemical (λ = 300 nm) conditions.[54] Characterization of the obtained partial monolayers showed that, similar to SiC, the attachment likely involves Markovnikov addition of the surface silanol groups to the 1-alkene. Improved reactivity was observed when the SiO_2 was illuminated at λ = 254 nm, yielding fairly dense monolayers, but prolonged illumination led to multilayer formation. The results of this study are described in more detail in chapter 3. Since the reaction is photochemical in nature, it allows constructive patterning by photolithography. This was used to locally functionalize enclosed surfaces, which is described in chapter 4. Moreover, biofunctionalization of enclosed silica surfaces was also demonstrated by coupling an activated ester to the surface, followed by the attachment of a DNA oligomer.

1.4 Other group 14 materials

1.4.1 Germanium[18]

With the successful modification of silicon, interest rose in the modification of other materials consisting of group 4A elements, such as germanium and carbon-based materials. Germanium (Ge) is often considered as a promising alternative to silicon because of its higher electron mobility and lower processing temperature.[55] Nevertheless, the instability of its oxide has thwarted the application of Ge in the semiconductor industry so far, and studies on its surface modification are limited. Germanium shows similar reactivity to silicon: Treatment with HF renders a hydrogen-terminated surface, which can react with terminal alkenes and alkynes by hydrogermylation, the Ge analogue of hydrosilylation.[56] This reaction can be performed catalytically, but better results are obtained by thermal or photochemical

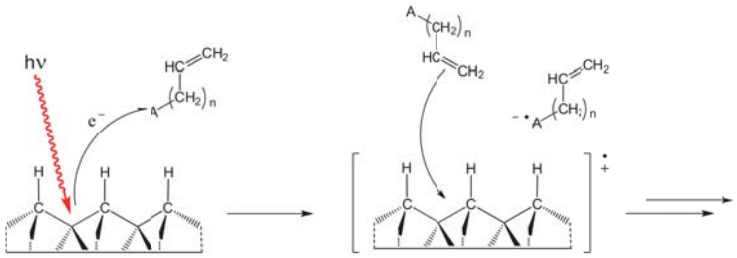

Figure 1.3. Mechanism of 1-alkene monolayer formation on diamond: initiation by photoelectron emission. Upon illumination, a substrate electron is ejected from the surface and accepted by a molecule that has a high electron affinity, such as trifluoroacetic acid-protected 10-aminodec-1-ene. The resulting holes on the surface are subsequently attacked by the alkene.

(UV) modification. Long-chain alkenes and alkynes (> C_{12}) can form densely packed monolayers on Ge, as was demonstrated by the complete blocking of HfO_2 atomic layer deposition.[57]

1.4.2 Carbon materials: Diamond

Carbon has many allotropes that can react with terminal alkenes or alkynes. However, the only material that will be treated here is diamond. Diamond is a material that is often applied for its hardness and stability. Even though it is strictly not a semiconductor (with a bandgap of 5.47 eV), it is treated similarly, including dopants. Its high stability, combined with its tunable electrical properties, would make diamond thin films an excellent choice for a biosensor substrate under demanding conditions. The reactivity of unsaturated hydrocarbons with diamond has been extensively investigated.[58-60] It was found that the reactivity of diamond with unfunctionalized alkenes upon UV-irradiation is limited. However, the presence of molecules with a high electron affinity near the diamond surface can increase the reactivity. This was explained by UV-induced photoemission of diamond valence band electrons into the liquid phase.[61,62] The resulting positively charged surface can react with 1-alkenes to form a very stable covalent C-C bond. Surface functionalization can be achieved by grafting protected amines[63] or carboxylic acids.[64] This has enabled the coupling of DNA,[65] enzymes[66] and antibodies[67] to the diamond surface. Moreover,

subsequent binding of antigens to an antibody-modified diamond surface could be detected with electrochemical impedance spectroscopy.[68] Finally, the photochemical nature of the reaction allows surface patterning by means of photolithography.[64,69]

1.5 Other oxide materials

In addition to SiO_2, 1-alkenes and/or 1-alkynes have also been shown to react to other oxide surfaces, including titanium oxide and aluminum oxide.

1.5.1 Titanium oxide

Titanium oxide is a semiconductor material with a band gap of ~3 eV. Whereas it is mainly used as a pigment, it is also present as the native oxide on titanium devices, such as medical implants. In the presence of oxygen or water, titanium oxide is known to photochemically oxidize organic molecules. However, under more controlled conditions, the titanium oxide surface has been shown to react with 1-alkenes, resulting in the formation of an organic adlayer.[70] During this coupling reaction, which is photochemically initiated, surface hydroxyl groups presumably react with the 1-alkene at the terminal carbon, forming a surface ether bond. Initial studies on the adsorption of 1-dodecene showed that the obtained adlayer is disordered, yet has a very high surface coverage, indicating that it is not strictly a monolayer. Nevertheless, these formed layers were shown to display good stability in a wide pH range (1 - 10), even at elevated temperature. Moreover, the photochemical nature of the reaction allows constructive patterning by photolithography.[70]

Functionalization of the titanium oxide requires protected functional groups. However, methyl-protected esters were shown to react with the titanium oxide surface as well, forming surface carboxylates. Trifluoroacetic acid-protected 10-amino-1-decene was shown to react selectively at the alkene moiety, but could only partially be deprotected (< 70 % yield) afterwards.[71] Higher deprotection yields (~ 90 %) were obtained using a trimethylgermanium-protected alkyne as the functional group.[72] These functionalization approaches allowed the subsequent coupling of DNA and peptides to the titanium oxide surface.[71,72]

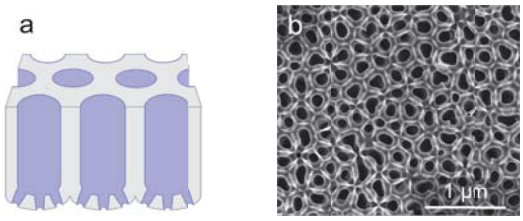

Figure 1.4. a) Schematic drawing of asymmetric porous anodic alumina. b) Scanning electron micrograph of (symmetric) porous anodic alumina, showing the quasi-hexagonal porous structure.

1.5.2 Porous anodic alumina

Porous anodic alumina (PAA) is an interesting nanostructured material. It is formed upon anodic oxidation of aluminum as an oxide layer that has a well-defined porous structure, in which parallel pores of uniform diameter run perpendicularly to the surface. By optimizing the anodization parameters, such as anodization voltage and electrolyte composition, the pore diameter can be tuned in the range of 10 to 450 nm. Freestanding oxide films can be formed by selectively etching the underlying aluminum, or by gradually reducing the anodization voltage, which results in lift-off.[73] Films obtained by the former method will require an additional etching step to dissolve the base of the pore, resulting in symmetric membranes. Films obtained by the latter method are asymmetric, as reduction of the anodization voltage will decrease the pore diameter at the base of the pore, and field-enhanced dissolution of the barrier layer dominates over oxide formation.[74]

Because of its well-ordered structure, ease of fabrication and good mechanical properties, PAA has found applications in many fields. It has been used as a structural template in the fabrication of carbon nanotubes[75-77] and metal nanowires,[78,79] and as a mold for self-assembly[80] and nanoimprinting.[81] It has also been applied as a membrane for protein filtration[82,83] and as a substrate for cell cultivation.[84] Moreover, PAA has found use as a substrate material in several biosensor systems,[85-87] which may, for example, be based on optical waveguide sensing.[88,89]

PAA can also be modified with 1-alkenes and 1-alkynes. In contrast to silicon oxide and titanium oxide, the modification of porous aluminum oxide with these compounds

does not require illumination with UV light. Instead, the reaction already proceeds at room temperature, even though higher surface coverages are obtained at elevated temperature (80 °C). The 1-alkyne reacts by oxidative chemisorption, i.e. it is oxidized to form the adsorbing species. This 1-alkyne oxidation product is presumably its α-hydroxy carboxylate, which is coordinated to the surface via its OH-groups. Chapter 5 of this thesis describes the formation of these monolayers, as well as their stability and functionalization. Chapter 6 focuses on the biofunctionalization of such modified PAA surfaces from the viewpoint of specific microbial adsorption. Here, the specific binding of the lectin peanut agglutinin to lactosyl-terminated PAA is shown, and the adsorption of the pathogens *Neisseria gonorrhoeae* and *Candida albicans* to these surfaces is studied.

1.5.3 Zirconium oxide and other metal oxides

Based on their reactivity with silicon oxide, titanium oxide and aluminum oxide, it is likely that terminally unsaturated hydrocarbons may show reactivity towards other oxides as well. Preliminary results on the photochemical grafting of trifluoroacetic acid-protected 10-amino-1-decene onto zirconium oxide were reported.[90] However, these results indicate that 1) the surface coverage may be limited, and 2) that the molecule does not stay intact upon chemisorption. Preliminary results from our lab also show different reactivity between oxides. Therefore, the reactivity with terminally unsaturated hydrocarbons cannot be regarded as a general trait of oxide materials. Further investigations should point out which oxides do form monolayers of 1-alkenes and/or 1-alkynes.

1.6 Outline

The previous sections have shown that terminally unsaturated hydrocarbons can react with several inorganic materials. From this overview, it follows that these compounds can react by different mechanisms, depending on the substrate material and reaction conditions. The reactions on silicon and diamond are well-understood, and studies can now focus on applications. Conversely, the understanding of e.g. the

UV-mediated reactions on silicon-based materials is limited, and these reactions thus require further fundamental investigation.

This thesis comprises several studies that are all based on the coupling of 1-alkenes and/or 1-alkynes on inorganic substrates. The first study, Chapter 2, deals with the surface modification of silicon. Here, a new patterning method is introduced that enables the local hydrosilylation of 1-alkynes on silicon surfaces. It uses microcontact printing, where a stamp is used to create chemical patterns on a surface, in combination with illumination to enhance the coupling reaction. Chapter 3 and 4 are based on the reaction of 1-alkenes on the silicon oxide surface. In Chapter 3, the conditions for this photochemical reaction are explored, and it is shown that photolithography can be used for surface patterning. This knowledge is exploited in Chapter 4 to locally modify the inner surface of a capillary with single-stranded DNA. In chapters 5 and 6, the focus is on the surface modification of porous anodic alumina. In Chapter 5 it is shown that 1-alkynes can form monolayers onto the PAA surface and the coupling reaction is investigated. In Chapter 6, the PAA surface is modified with a lactosyl moiety and the subsequent binding of the lectin peanut agglutinin and of the pathogenic microorganisms *Neisseria gonorrhoeae* and *Candida albicans* is investigated. Finally, Chapter 7 discusses opportunities for further research.

1.7 References

(1) Blodgett, K. B. *J. Am. Chem. Soc.* **1934**, *56*, 495-495.

(2) Bigelow, W. C.; Pickett, D. L.; Zisman, W. A. *J. Coll. Sci. Imp. U. Tok.* **1946**, *1*, 513-538.

(3) Roberts, G. G. *Adv. Phys.* **1985**, *34*, 475-512.

(4) Blodgett, K. B. *J. Am. Chem. Soc.* **1935**, *57*, 1007-1022.

(5) Ulman, A. *An introduction to Ultrathin Organic Films: From Langmuir-Blodgett to Self-Assembly*; Academic Press: Boston, 1991.

(6) Talham, D. R. *Chem. Rev.* **2004**, *104*, 5479-5501.

(7) Zasadzinski, J. A.; Viswanathan, R.; Madsen, L.; Garnaes, J.; Schwartz, D. K. *Science* **1994**, *263*, 1726-1733.

(8) Ulman, A. *Chem. Rev.* **1996**, *96*, 1533-1554.

(9) Gun, J.; Iscovici, R.; Sagiv, J. *J. Colloid Interf. Sci.* **1984**, *101*, 201-213.

(10) Sagiv, J. *J. Am. Chem. Soc.* **1980**, *102*, 92-98.

(11) Onclin, S.; Ravoo, B. J.; Reinhoudt, D. N. *Angew. Chem. Int. Ed.* **2005**, *44*, 6282-6304.

(12) Silberzan, P.; Leger, L.; Ausserre, D.; Benattar, J. J. *Langmuir* **1991**, *7*, 1647-1651.

(13) Love, J. C.; Estroff, L. A.; Kriebel, J. K.; Nuzzo, R. G.; Whitesides, G. M. *Chem. Rev.* **2005**, *105*, 1103-1169.

(14) Folkers, J. P.; Gorman, C. B.; Laibinis, P. E.; Buchholz, S.; Whitesides, G. M.; Nuzzo, R. G. *Langmuir* **1995**, *11*, 813-824.

(15) Lukes, I.; Borbaruah, M.; Quin, L. D. *J. Am. Chem. Soc.* **1994**, *116*, 1737-1741.

(16) Gao, W.; Dickinson, L.; Grozinger, C.; Morin, F. G.; Reven, L. *Langmuir* **1996**, *12*, 6429-6435.

(17) Linford, M. R.; Fenter, P.; Eisenberger, P. M.; Chidsey, C. E. D. *J. Am. Chem. Soc.* **1995**, *117*, 3145-3155.

(18) Buriak, J. M. *Chem. Rev.* **2002**, *102*, 1271-1308.

(19) Aswal, D. K.; Lenfant, S.; Guerin, D.; Yakhmi, J. V.; Vuillaume, D. *Anal. Chim. Acta* **2006**, *568*, 84-108.

(20) Ciampi, S.; Harper, J. B.; Gooding, J. J. *Chem. Soc. Rev.* **2010**, *39*, 2158-2183.

(21) Sieval, A. B.; van den Hout, B.; Zuilhof, H.; Sudholter, E. J. R. *Langmuir* **2001**, *17*, 2172-2181.

(22) Scheres, L.; Giesbers, M.; Zuilhof, H. *Langmuir* **2010**, *26*, 4790-4795.

(23) Sung, M. M.; Kluth, G. J.; Yauw, O. W.; Maboudian, R. *Langmuir* **1997**, *13*, 6164-6168.

(24) Zazzera, L. A.; Evans, J. F.; Deruelle, M.; Tirrell, M.; Kessel, C. R.; Mckeown, P. *J. Electrochem. Soc.* **1997**, *144*, 2184-2189.

(25) Cicero, R. L.; Linford, M. R.; Chidsey, C. E. D. *Langmuir* **2000**, *16*, 5688-5695.

(26) Sun, Q. Y.; de Smet, L.; van Lagen, B.; Wright, A.; Zuilhof, H.; Sudholter, E. J. R. *Angew. Chem. Int. Ed.* **2004**, *43*, 1352-1355.

(27) G. Robins, E.; P. Stewart, M.; M. Buriak, J. *Chem. Commun.* **1999**, 2479-2480.

(28) Niederhauser, T. L.; Jiang, G. L.; Lua, Y. Y.; Dorff, M. J.; Woolley, A. T.; Asplund, M. C.; Berges, D. A.; Linford, M. R. *Langmuir* **2001**, *17*, 5889-5900.

(29) Zhong, Y. L.; Bernasek, S. L. *J. Am. Chem. Soc.* **2011**, *133*, 8118-8121.

(30) Scheres, L.; Giesbers, M.; Zuilhof, H. *Langmuir* **2010**, *26*, 10924-10929.

(31) Cicero, R. L.; Chidsey, C. E. D.; Lopinski, G. P.; Wayner, D. D. M.; Wolkow, R. A. *Langmuir* **2002**, *18*, 305-307.

(32) Sun, Q. Y.; de Smet, L. C. P. M.; van Lagen, B.; Giesbers, M.; Thune, P. C.; van Engelenburg, J.; de Wolf, F. A.; Zuilhof, H.; Sudhölter, E. J. R. *J. Am. Chem. Soc.* **2005**, *127*, 2514-2523.

(33) Rijksen, B.; van Lagen, B.; Zuilhof, H. *J. Am. Chem. Soc.* **2011**, *133*, 4998-5008.

(34) Faucheux, A.; Gouget-Laemmel, A. C.; de Villeneuve, C. H.; Boukherroub, R.; Ozanam, F.; Allongue, P.; Chazalviel, J. N. *Langmuir* **2006**, *22*, 153-162.

(35) Scheres, L.; ter Maat, J.; Giesbers, M.; Zuilhof, H. *Small* **2010**, *6*, 642-650.

(36) Campos, M. A. C.; Paulusse, J. M. J.; Zuilhof, H. *Chem. Commun.* **2010**, *46*, 5512-5514.

(37) Rosso, M.; Giesbers, M.; Schroen, K.; Zuilhof, H. *Langmuir* **2010**, *26*, 866-872.

(38) Shestopalov, A. A.; Clark, R. L.; Toone, E. J. *Langmuir* **2010**, *26*, 1449-1451.

(39) Yang, M. L.; Wouters, D.; Giesbers, M.; Schubert, U. S.; Zuilhof, H. *Acs Nano* **2009**, *3*, 2887-2900.

(40) Hurley, P. T.; Ribbe, A. E.; Buriak, J. M. *J. Am. Chem. Soc.* **2003**, *125*, 11334-11339.

(41) Wacaser, B. A.; Maughan, M. J.; Mowat, I. A.; Niederhauser, T. L.; Linford, M. R.; Davis, R. C. *Appl. Phys. Lett.* **2003**, *82*, 808-810.

(42) Effenberger, F.; Gotz, G.; Bidlingmaier, B.; Wezstein, M. *Angew. Chem. Int. Ed.* **1998**, *37*, 2462-2464.

(43) Arafat, S. N.; Dutta, S.; Perring, M.; Mitchell, M.; Kenis, P. J. A.; Bowden, N. B. *Chem. Commun.* **2005**, 3198-3200.

(44) Mizuno, H.; Buriak, J. M. *J. Am. Chem. Soc.* **2008**, *130*, 17656-+.

(45) Pignataro, B.; Grasso, G.; Renna, L.; Marletta, G. *Surf. Interface Anal.* **2002**, *33*, 54-58.

(46) Arafat, A.; Schroën, K.; de Smet, L. C. P. M.; Sudhölter, E. J. R.; Zuilhof, H. *J. Am. Chem. Soc.* **2004**, *126*, 8600-8601.

(47) Arafat, A.; Giesbers, M.; Rosso, M.; Sudhölter, E. J. R.; Schroën, K.; White, R. G.; Yang, L.; Linford, M. R.; Zuilhof, H. *Langmuir* **2007**, *23*, 6233-6244.

(48) Coffinier, Y.; Boukherroub, R.; Wallart, X.; Nys, J.-P.; Durand, J.-O.; Stiévenard, D.; Grandidier, B. *Surf. Sci.* **2007**, *601*, 5492-5498.

(49) Rosso, M.; Giesbers, M.; Arafat, A.; Schroën, K.; Zuilhof, H. *Langmuir* **2009**, *25*, 2172-2180.

(50) Nguyen, A. T.; Baggerman, J.; Paulusse, J. M. J.; van Rijn, C. J. M.; Zuilhof, H. *Langmuir* **2011**, *27*, 2587-2594.

(51) Rosso, M.; Arafat, A.; Schroën, K.; Giesbers, M.; Roper, C. S.; Maboudian, R.; Zuilhof, H. *Langmuir* **2008**, *24*, 4007-4012.

(52) Touahir, L.; Niedziółka-Jönsson, J.; Galopin, E.; Boukherroub, R.; Gouget-Laemmel, A. C.; Solomon, I.; Petukhov, M.; Chazalviel, J.-N. l.; Ozanam, F. o.; Szunerits, S. *Langmuir* **2010**, *26*, 6058-6065.

(53) Qin, G.; Zhang, R.; Makarenko, B.; Kumar, A.; Rabalais, W.; Lopez Romero, J. M.; Rico, R.; Cai, C. *Chem. Commun.* **2010**, *46*, 3289-3291.

(54) Mischki, T. K.; Donkers, R. L.; Eves, B. J.; Lopinski, G. P.; Wayner, D. D. M. *Langmuir* **2006**, *22*, 8359-8365.

(55) Loscutoff, P. W.; Bent, S. F. *Annu. Rev. Phys. Chem.* **2006**, *57*, 467-495.

(56) Choi, K.; Buriak, J. M. *Langmuir* **2000**, *16*, 7737-7741.

(57) Chen, R.; Bent, S. F. *Chem. Mater.* **2006**, *18*, 3733-3741.

(58) Szunerits, S.; Boukherroub, R. *J. Solid State Electr.* **2008**, *12*, 1205-1218.

(59) Wang, X. Y.; Landis, E. C.; Franking, R.; Hamers, R. J. *Acc. Chem. Res.* **2010**, *43*, 1205-1215.

(60) Zhong, Y. L.; Loh, K. P. *Chem-Asian J.* **2010**, *5*, 1532-1540.

(61) Nebel, C. E.; Shin, D.; Takeuchi, D.; Yamamoto, T.; Watanabe, H.; Nakamura, T. *Diamond Relat. Mater.* **2006**, *15*, 1107-1112.

(62) Nichols, B. M.; Butler, J. E.; Russell, J. N.; Hamers, R. J. *J. Phys. Chem. B* **2005**, *109*, 20938-20947.

(63) Strother, T.; Knickerbocker, T.; Russell, J. N.; Butler, J. E.; Smith, L. M.; Hamers, R. J. *Langmuir* **2002**, *18*, 968-971.

(64) Zhong, Y. L.; Chong, K. F.; May, P. W.; Chen, Z. K.; Loh, K. P. *Langmuir* **2007**, *23*, 5824-5830.

(65) Yang, W. S.; Auciello, O.; Butler, J. E.; Cai, W.; Carlisle, J. A.; Gerbi, J.; Gruen, D. M.; Knickerbocker, T.; Lasseter, T. L.; Russell, J. N.; Smith, L. M.; Hamers, R. J. *Nat. Mater.* **2002**, *1*, 253-257.

(66) Rubio-Retama, J.; Hernando, J.; Lopez-Ruiz, B.; Hartl, A.; Steinmuller, D.; Stutzmann, M.; Lopez-Cabarcos, E.; Garrido, J. A. *Langmuir* **2006**, *22*, 5837-5842.

(67) Stavis, C.; Clare, T. L.; Butler, J. E.; Radadia, A. D.; Carr, R.; Zeng, H. J.; King, W. P.; Carlisle, J. A.; Aksimentiev, A.; Bashir, R.; Hamers, R. J. *P. Natl. Acad. Sci. USA* **2011**, *108*, 983-988.

(68) Yang, W. S.; Butler, J. E.; Russell, J. N.; Hamers, R. J. *Analyst* **2007**, *132*, 296-306.

(69) Wang, X.; Colavita, P. E.; Metz, K. M.; Butler, J. E.; Hamers, R. J. *Langmuir* **2007**, *23*, 11623-11630.

(70) Franking, R. A.; Landis, E. C.; Hamers, R. J. *Langmuir* **2009**, *25*, 10676-10684.

(71) Li, B.; Franking, R.; Landis, E. C.; Kim, H.; Hamers, R. J. *ACS Appl. Mater. Interfaces* **2009**, *1*, 1013-1022.

(72) Li, Y.; Zhao, M. R.; Wang, J.; Liu, K.; Cai, C. Z. *Langmuir* **2011**, *27*, 4848-4856.

(73) Furneaux, R. C.; Rigby, W. R.; Davidson, A. P. *Nature* **1989**, *337*, 147-149.

(74) O'Sullivan, J. P.; Wood, G. C. *Proc. R. Soc. Lon, Ser. A* **1970**, *317*, 511-&.

(75) Ciambelli, P.; Sannino, D.; Sarno, M.; Fonseca, A.; Nagy, J. B. *J. Nanosci. Nanotechno.* **2004**, *4*, 779-787.

(76) Lee, D. H.; Condrate, R. A. *Mater. Lett.* **1995**, *23*, 241-246.

(77) Yu, G. J.; Wang, S.; Gong, J. L.; Zhu, D. Z.; He, S. X.; Li, Y. L.; Zhu, Z. Y. *Chin. Sci. Bull.* **2005**, *50*, 1097-1100.

(78) Borissov, D.; Isik-Uppenkamp, S.; Rohwerder, M. *J. Phys. Chem. C* **2009**, *113*, 3133-3138.

(79) Matefi-Tempfli, S.; Matefi-Tempfli, M.; Vlad, A.; Antohe, V.; Piraux, L. *J. Mater. Sci.-Mater. El.* **2009**, *20*, 249-254.

(80) Sakurai, M.; Shimojima, A.; Yantauchi, Y.; Kuroda, K. *Langmuir* **2008**, *24*, 13121-13126.

(81) Yanagishita, T.; Nishio, K.; Masuda, H. *Appl. Phys. Express* **2009**, *2*.

(82) Thormann, A.; Teuscher, N.; Pfannmoller, M.; Rothe, U.; Heilmann, A. *Small* **2007**, *3*, 1032-1040.

(83) Yeu, S.; Lunn, J. D.; Rangel, H. M.; Shantz, D. F. *J. Membr. Sci.* **2009**, *327*, 108-117.

(84) Ingham, C. J.; van den Ende, M.; Pijnenburg, D.; Wever, P. C.; Schneeberger, P. M. *Appl. Environ. Microbiol.* **2005**, *71*, 8978-8981.

(85) Koutsioubas, A. G.; Spiliopoulos, N.; Anastassopoulos, D.; Vradis, A. A.; Priftis, G. D. *J. Appl. Phys.* **2008**, *103*.

(86) Kondo, T.; Nishio, K.; Masuda, H. *Appl. Phys. Express* **2009**, *2*.

(87) Lu, Z. C.; Ruan, W. D.; Yang, J. X.; Xu, W. Q.; Zhao, C.; Zhao, B. *J. Raman Spectrosc.* **2009**, *40*, 112-116.

(88) Lau, K. H. A.; Tan, L. S.; Tamada, K.; Sander, M. S.; Knoll, W. *J. Phys. Chem. B* **2004**, *108*, 10812-10818.

(89) Yamaguchi, A.; Hotta, K.; Teramae, N. *Anal. Chem.* **2009**, *81*, 105-111.

(90) Hamers, R. J.; Chambers, S. A.; Evans, P. E.; Franking, R.; Gerbec, Z.; Gopalan, P.; Kim, H.; Landis, E. C.; Li, B.; McCoy, M. W.; Ohsawa, T.; Ruther, R. In *Physica Status Solidi C: Current Topics in Solid State Physics, Vol 7, No 2* 2010, p 200-205.

Chapter 2

Light-Enhanced Microcontact Printing of 1-Alkynes onto Hydrogen-Terminated Silicon

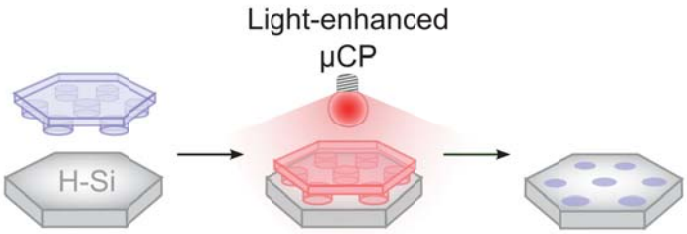

This chapter was published as:

ter Maat, J.; Yang, M. L.; Scheres, L.; Kuypers, S.; Zuilhof, H. "Light-Enhanced Microcontact Printing of 1-Alkynes onto Hydrogen-Terminated Silicon", *Chem. Commun.* **2010**, *46*, 8005-8007.

2.1 Abstract

A method for the direct patterning of 1-alkynes onto hydrogen-terminated silicon is presented. It combines microcontact printing with illumination by visible light through the stamp, and results in the formation of an alkenyl monolayer. The formation of heterogeneous monolayers is demonstrated by subsequent backfilling.

2.2 Introduction

Since the mid-90's many studies have appeared on monolayer formation onto hydrogen-terminated silicon (H-Si) from terminally unsaturated hydrocarbons (1-alkenes/1-alkynes).[1] The resulting monolayers are intrinsically very stable, as the alkenes and alkynes bind covalently to the silicon surface via robust Si-C linkages.[1-2] In addition, the absence of an interfacial oxide layer provides a true hybrid organic monolayer/semiconductor interface with excellent electrical characteristics.[3-5] Such hybrid materials introduce the flexibility of organics into the well-developed infrastructure of the semiconductor industry, and display great potential for electronics, sensors and other devices.[6-9]

Around the same time, the technique of microcontact printing (μCP) was developed by Whitesides et al.[10-11] In μCP patterned polymer stamps are inked, e.g. with molecules or proteins, after which the ink is transferred to a surface by stamping, thereby allowing the easy reproduction of (sub)μm patterns. Compared to other patterning methods, e.g. photolithography or scanning probe methods, μCP is cheap, efficient and easy-to-use.[12-13] Recent reviews give a good overview of the current status of and developments in μCP.[13-16]

Whereas μCP has been performed on many surfaces, most notably on gold and silicon oxide, the number of μCP studies on oxide-free silicon is very limited. Given the potential of Si-C bound monolayers on silicon, there is a need for techniques that allow the cheap and efficient patterning hereof. μCP seems an obvious candidate. However, its application has been hampered up to now, as the modification of H-Si is frequently performed under conditions at which commonly used PDMS stamps are not stable (high T, UV light), while the typically required reaction time of hours may limit the pattern resolution.[17-18] To circumvent harsh modification conditions and to reduce modification times, μCP has been performed onto a Cl-terminated Si surface, using alcohols as ink.[19] Yet this yields a Si-O-C surface bond, which is more prone to hydrolysis than the (rather apolar) Si-C bond. Another approach therefore describes catalytic μCP on H-Si.[20] In this elegant study the surface of a PDMS-based stamp was loaded with a patterned catalyst array and then inked with 1-alkenes/1-alkynes to pattern alkyl/alkenyl monolayers directly onto H-Si via in-situ catalyzed

hydrosilylation. That approach allowed the reproducible formation of rather small features, i.e. < 100 nm, but the preparation of the stamp may not be trivial, whereas the resulting monolayers were not as densely packed as obtainable via other attachment reactions.[21] Micromolding in capillaries, a soft lithographic technique closely related to μCP, has been performed on H-Si as well.[22] This resulted in the formation of an alkyl monolayer on the non-contacted areas. However, the method requires a radical initiator and the filling of the channels limits the possible pattern structures. Finally, several recent studies use μCP onto preformed high-quality monolayers on oxide-free silicon rather than directly onto H-Si. Examples include the coupling of amines to an acid fluoride-modified surface,[23] the stamp-induced catalytic deprotection of a surface that exposed a Boc-protected amine,[24] and local thiol-ene click chemistry onto alkene-terminated monolayers.[25] While such approaches all have their benefits, direct μCP onto H-Si would still be desirable as it allows a wider flexibility. Here we report the proof-of-principle of such a method.

A number of recent developments have sparked our interest in direct μCP onto silicon. First, recent studies have shown that 1-alkynes can already form well-packed monolayers on H-Si at room temperature,[26,27] i.e. under conditions in which PDMS is stable. Second, the rate of monolayer formation at low temperatures can be enhanced by illumination with visible light.[27,28] This, combined with the transparency of the PDMS stamps, motivated us to investigate a process to which we refer as light-enhanced microcontact printing (LE-μCP). In this process, a stamp with pillar-like features was inked with 1-alkyne, placed into contact with a freshly etched H-Si surface, and subsequently the silicon is illuminated *through* the stamp (**Figure 2.1**).

Monolayer formation only occurred where reagent was available, i.e. where the stamp was in contact with the substrate, and this resulted in a patterned silicon surface. These surfaces were characterized with atomic force microscopy (AFM), and with scanning electron microscopy (SEM). The latter has been shown to be a sensitive instrument for the imaging of chemically heterogeneous surfaces.[29-34] Surfaces obtained after LE-μCP with featureless (i.e. "flat") stamps were characterized with water contact angle measurements, ellipsometry and X-ray photoelectron spectroscopy (XPS), which showed that a 1-alkenyl monolayer was formed onto the Si surface. Control experiments showed the enhancement effect of illumination, as

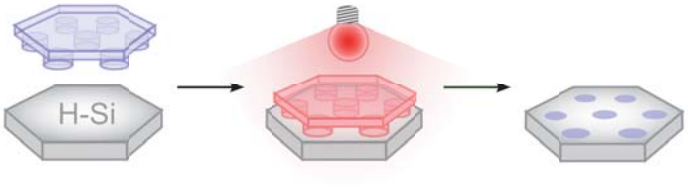

Figure 2.1. In LE-μCP, a 1-alkyne-inked PDMS stamp is contacted with a freshly etched H-Si surface and subsequently illuminated, resulting in monolayer formation on the contacted areas.

well as the need to keep the stamp into contact during the illumination process. The influence of illumination wavelength, contact time, and inking conditions on the LE-μCP process were studied. Finally, the non-contacted areas were backfilled to create chemically heterogeneous, oxide-free silicon surfaces.

2.3 Experimental

Materials. De-ionized water (with a resistivity of 18.3 MΩ cm) was used for sample cleaning. Acetone (semiconductor grade, Riedel de Haen), cyclohexane (anhydrous, Sigma-Aldrich), 40% NH_4F solution (semiconductor grade, Honeywell), sulfuric acid (95-97 %, Sigma-Aldrich), hydrogen peroxide (30 %, Sigma-Aldrich) and PDMS precursors (Sylgard 184, Dow Corning) were used as received. EtOH and CH_2Cl_2 were distilled prior to use. 1-Octadecyne was synthesized from 1-bromohexadecane and lithium acetylide ethylene diamine complex as described elsewhere,[35] and purified by column chromatography, recrystallization and vacuum distillation. 2,2,2-Trifluoroethyl undec-10-ynoate was synthesized from 2,2,2-trifluoroethanol and 10-undecynoic acid as described elsewhere,[36] and purified by flash column chromatography. Silicon wafers were (111)-oriented single-side and double polished, 475-550 μm thick, n-type, P-doped samples, with a resistivity 1.0-5.0 Ω cm (Siltronix, France).

Stamp fabrication. Stamps were made by casting a PDMS prepolymer mixture onto a patterned silicon master. The stamps were cast from a silicon master with a hexagonal pattern of 4 μm wide wells, with a period of 8 μm. After degassing the mixture for 60 min under vacuum, the polymer-covered master was annealed at 60 °C

for > 48 h. The polymer was removed from the master and subsequently cut into stamps of 1 × 1 cm. These were extracted with ethanol by overnight Soxhlet extraction, dried at 50 °C under vacuum, and stored. Prior to use, stamps were cleaned by 5 min ultrasonication in ethanol.

Light-enhanced microcontact printing. A piece of n-type Si(111) was cleaned by wiping with an acetone-soaked piece of cotton, followed by ultrasonication for 5 min in acetone, and then in water. The sample was subsequently immersed into a freshly prepared piranha solution (7 parts H_2SO_4 mixed with three parts 30 % H_2O_2. *Caution: Piranha is a very strong oxidizer and can react explosively with organic compounds*). After 15 min, the sample was rinsed copiously with degassed, de-ionized water and was then etched for 15 min in an argon-saturated aqueous solution of 40 % NH_4F. Afterwards, the sample was rinsed with water, shortly ultrasonicated with water, and dried in a stream of argon. It was mounted on a magnetic base and transferred into a glovebox with O_2 and H_2O levels typically below 1 ppm.

Simultaneously to sample cleaning and etching, a stamp was immersed in a solution of alkyne in ethanol (typically 2 min in 100 mM 1-octadecyne), blown dry with argon and then further dried under vacuum for 30 min. It was transferred to the glovebox, where it was contacted to the etched silicon sample. A thin metal frame was carefully placed on top, which ensures contact throughout illumination, because of the attractive force of the magnetic base. The sample was covered with a long pass filter, and then illuminated with a phosphor-coated, low-pressure mercury lamp (Jelight, Irvine, CA). In a typical experiment, illumination was performed for 3 h with a lamp designed to emit at 658 nm, in combination with a 395 nm long pass filter. After illumination, the sample was taken from the glovebox and cleaned by ultrasonication in ethanol, and in dichloromethane (5 min each). It was further cleaned by Soxhlet extraction in cyclohexane (> 30 min), shortly ultrasonicated with ethanol and water, and etched in an argon-saturated 40 % NH_4F solution for 1 min. Finally, the sample was rinsed and ultrasonicated with water, dried with argon and taken to the AFM or further modified in a backfilling step.

Monolayer backfilling. Backfilling of patterned samples was performed using the modification procedure reported by Scheres et al.[26] Briefly, the etched sample was transferred to a three-neck flask charged with neat, deoxygenated alkyne under argon

overflow. The flask was equipped with a capillary argon inlet and with a condenser connected to a Schlenk line. The flask was closed, its pressure was reduced to approximately 10 mbar (the inert atmosphere being maintained by argon flowing through the capillary), and it was immersed in an oil bath at 80 °C. After 16 h, the flask was backfilled with argon until atmospheric pressure was attained, and the sample was taken out. After rinsing excessively with ethanol and CH_2Cl_2 and sonication in CH_2Cl_2 for 5 min to remove physisorbed molecules, the sample was blown dry with a stream of dry nitrogen.

Atomic Force Microscopy. AFM images were obtained in tapping mode (AC-AFM) with an MFP3D instrument (Asylum Research, Santa Barbara, CA) using NSC35 3-lever probes (MikroMasch, Estonia). Usually, the A-type cantilever (210 kHz, 7.5 N/m) was used, except for imaging the backfilled samples, when the C-type cantilever (150 kHz, 4.5 N/m) was used. Images were flattened with the MFP3D software.

Scanning Electron Microscopy. Scanning electron micrographs were obtained with a JEOL JCM-5000 NeoScope using the secondary electron detector. The electron acceleration voltage was 5 kV. For the backfilled samples, the image contrast was enhanced using ImageJ 1.43u.

X-ray Photoelectron Spectroscopy. XPS analysis was performed with a JPS-9200 Photoelectron Spectrometer (JEOL, Japan). High-resolution spectra were obtained under UHV conditions using monochromatic Al Kα X-ray radiation at 12 kV and 25 mA, using an analyzer pass energy of 10 eV. The X-ray incidence angle and the electron acceptance angle were 80º and 10º with respect to the surface normal, respectively. Spectra were corrected with a linear background subtraction before quantification and any peak deconvolution.

Ellipsometry. Ellipsometric measurements were performed with a Sentech Instruments (Type SE-400) ellipsometer, operating at 632.8 nm (He-Ne-laser) and an angle of incidence of 70°. The optical constants of the substrate were determined with a piece of freshly etched n-Si(111) (n = 3.713 and k = 0.088). The thickness of the monolayer was determined with a planar three-layer (ambient, monolayer, substrate) isotropic model with refractive index of 1.46 for the organic monolayer. The reported value is the average of 20 measurements taken at multiple locations on the sample.

Water contact angle measurements. Static contact angles were measured using a Krüss DSA-100 goniometer. Droplets of 3 µl were dispensed on the surface and contact angles were measured with a CCD camera using a tangential method. The reported value is the average of 5 droplets measured on different positions on the surface.

2.4 Results and discussion

2.4.1 LE-µCP

In a typical experiment, a stamp with pillar-like features (4 µm wide with an 8 µm period) was inked with 1-octadecyne and contacted to freshly etched H-Si, after which it was illuminated for 3 h with a 658 nm lamp. Contacting and illumination took place in the dry nitrogen atmosphere of a glovebox to prevent oxidation. After illumination, the sample was thoroughly cleaned with organic solvents, etched for 1 min in 40% NH_4F and directly imaged with AC-mode atomic force microscopy (AC-AFM). From the resulting height and phase images (Figure 2.2) it follows that the pattern is well-transferred to the Si(111) surface. The lateral dimensions of the transferred pattern are slightly different from those of the original master: the feature size is 4.2 µm, whereas the period is 7.6 µm. The latter can be attributed to deformation of the stamp due to cleaning and aging, whereas ink spreading and/or stamp deformation during contact can explain the increased feature size.[15]

The height image reveals that the features are uniform and have an average feature height of 1.4 nm, while the phase image shows a clear contrast between the contacted and non-contacted areas. These observations point to the selective formation of an organic 1-alkenyl monolayer onto the contacted areas. The pattern's ability to withstand NH_4F etching reveals the quality of the monolayer. The observed feature height (1.4 nm) is similar to that reported for catalytic µCP on silicon.[20] Comparison of this height with the known thickness of a well-ordered 1-octadecenyl monolayer on H-Si (2.2 nm, obtained thermally[21]) shows that the resulting monolayer is only moderately packed.

Further characterization by Scanning Electron Microscopy (SEM) showed a clear contrast between the contacted and non-contacted areas, confirming that these are

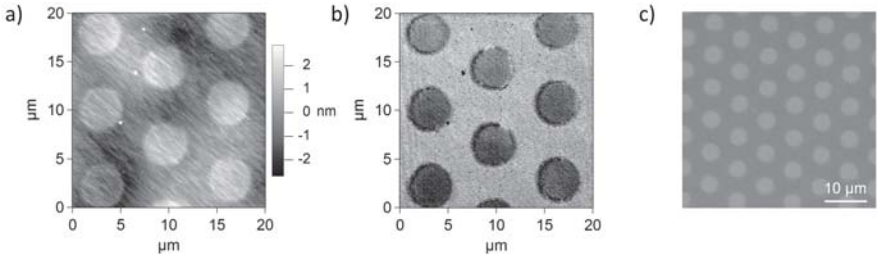

Figure 2.2. Si(111) sample patterned with 1-octadecyne by LE-μCP (λ = 658 nm, t = 3 h): a) AC-AFM height image; b) AC-AFM phase image; c) SEM image.

chemically distinct (Figure 2.2c).[30-32] In addition, it showed that the pattern was uniformly transferred to the whole light-illuminated printing area, thus revealing the power of LE-μCP.

To allow macroscopic investigations of the surface by water contact angle measurements, ellipsometry, and X-ray photoelectron spectroscopy (XPS), LE-μCP was applied with a flat (i.e. featureless) stamp under similar conditions. This yielded a hydrophobic surface with a contact angle of 101°. Ellipsometry measurements on this surface gave an adsorbed layer thickness of 1.2 ± 0.1 nm. This value is slightly lower than the feature height derived from AFM images, since the latter also includes height differences in the Si substrate that are introduced by the second etching step. By contrast, ellipsometry only measures the thickness of the organic layer, which can explain the difference. The wide-area XPS scan (Figure 2.3a) only shows the presence of Si, C and a trace amount of O (at 532.3 eV) due to airborne organic contaminants, as follows from the position of the O peak and the absence of an Si-O peak in the high-resolution Si spectrum. The latter (Fig. 2a) also shows that contamination with siloxane oligomers (which can result from the use of PDMS stamps), or reaction with ethanol (the inking solvent) are not a significant issue here. Instead, the adsorbed layer merely consists of hydrocarbons, which is indicative of the formation of an alkenyl monolayer. The C_{1s} spectrum (Figure 2.3c) displays both the C-C (285.0 eV) and C=C-Si (283.5 eV) peaks in the ratio (17:1) and at the positions characteristic for an octadecenyl monolayer,[21] while the small shoulder at 286.5 eV reveals the presence of some adventitious carbon contamination. The C/Si ratio is somewhat lower than

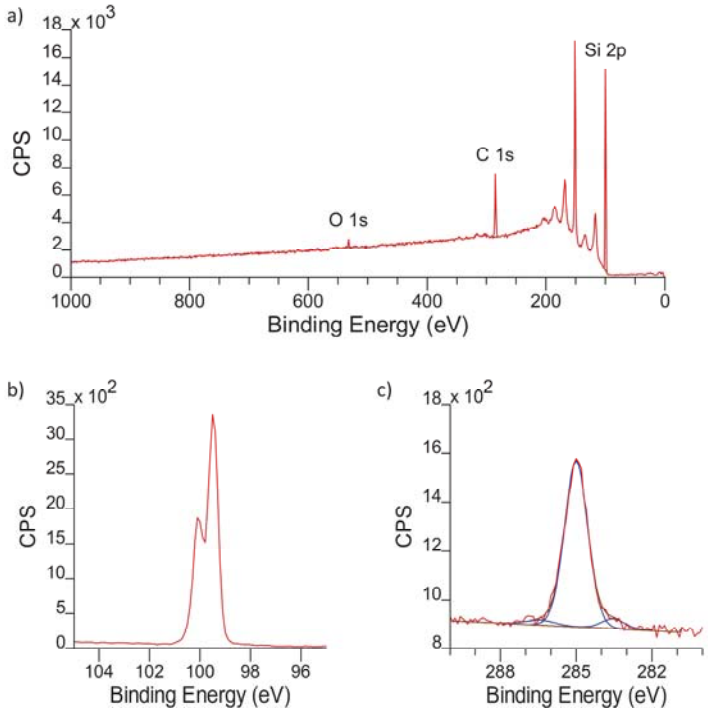

Figure 2.3. XPS characterization of a sample that was obtained by LE-mCP (3 h, 658 nm) with 1-octadecyne using a flat stamp: a) Surface composition; b) Si_{2p} spectrum; c) C_{1s} spectrum.

obtainable for such a monolayer from solution,[21] indicating that the 1-alkenyl monolayer formed during LE-µCP has significant surface coverage, but is not densely packed.

2.4.2 Control experiments

A set of three control experiments outlines the importance of the various factors involved in LE-µCP. First, the effect of illumination was studied by blocking the incoming light with a filter (contact time (t) = 3 h). The use of a filter was selected over performing the experiment without illumination, because it has less effect on the temperature at the stamp-substrate interface. The AFM height image of these samples showed the hexagonal pattern, but with feature heights of only 0.8 nm. From this we

can conclude that: 1) monolayers of alkynes on H-Si can form under the mild conditions employed in microcontact printing, and 2) there is a distinct effect of illumination, to which we refer as light enhancement.

Second, performing LE-μCP with uninked stamps (λ = 658 nm, t = 3 h) did not result in an observable topographical pattern, even prior to etching. The AFM phase image, however, did show the hexagonal pattern, but the contrast was minimal and disappeared after etching. This indicates that if any PDMS-based contaminants were transferred to the surface, these were removed in the subsequent cleaning steps. Such contaminants are notoriously associated with the use of PDMS, but their transfer may have been reduced by oligomer-reducing measures taken during preparation of the stamps (long curing time, Soxhlet extraction with ethanol). In addition, PDMS transfer to H-Si may be inherently limited due to the relatively low surface free energy of H-Si compared to Au.[37]

Third, an inked stamp was contacted to H-Si for 2 min, but was removed before illumination (λ = 658 nm, t = 3 h). AFM showed that the pattern was transferred, but that the feature height was minimal: $\sim$ 0.2 nm. This is a significant reduction compared to regular LE-μCP experiments, and shows that the presence of the stamp is required for proper monolayer formation in μCP on H-Si. This contrasts to μCP on other substrates, e.g. thiols on Au or silanes on SiO_2, where short contact times are sufficient for the formation of well-defined monolayers. However, monolayer formation on H-Si is a slow process, requiring high local concentrations,[38] which - in combination with limited ink transfer from the stamp to the surface - can explain the minimal feature size in this experiment: As the initially transferred ink is used in monolayer formation, the local concentration decreases, which may eventually hamper the reaction. The presence of the stamp can prevent this reactant exhaustion, since PDMS is not only known to adsorb ink on the surface, but also to absorb hydrophobic inks (up to several hundred mM)[39] in the stamp. This absorbed ink can then diffuse to the surface during reaction. Thus, in μCP on H-Si the stamp does not only function as a template, but also as an ink reservoir.

2.4.3 Influence of reaction parameters

We investigated the influence of several parameters on the LE-μCP process, starting with the illumination wavelength. It is known that light in the UV and visible range can induce monolayer formation on Si,[40] involving excitation of Si electrons to the conduction band[28] and/or direct homolytic Si-H bond cleavage. As the bandgap of Si is only 1.1 eV, excitation from the valence band to the conduction band can be achieved with any visible light wavelength. Indeed, it was observed that, after performing LE-μCP with either 447 or 658 nm light, patterns were well transferred and the feature height was not significantly different, ~ 1.4 nm. Illuminating with 254 nm, however, only resulted in a faint pattern in the phase image. These results cannot be sufficiently explained the lower intensity of UV light at the Si surface compared to visible light (caused by decreased transmission of UV light) since the experiment without illumination did in fact show a more distinct pattern in the AFM height image. Instead, it may be the UV light absorption of the stamp that induces a side reaction. This was supported by AFM imaging of the printed samples prior to etching, which showed the formation of ring-shaped structures of several nanometers in height (Figure 2.4). These structures could withstand ultrasonication and Soxhlet extraction, but could be removed by etching with NH_4F solution. Therefore, it is likely that they are chemisorbed, and contain siloxane fragments originating from the stamp, such as the alkene-terminated PDMS fragments that function as crosslinking agents in commercial PDMS kits.[41] Presumably, the side reaction in the stamp and/or the formation of ring-shaped structures competes effectively with monolayer formation, since no monolayer formation is observed at all. For the formation of similar ring-shaped structures upon long-contact printing, it has been proposed that this originates from migration of PDMS residues from the vertical walls of the stamp, resulting in accumulation at the stamp/surface/air interface.[42] In addition, alkenes are photoreactive under UV illumination, and thus may initiate side reactions, at the surface, but also within the stamp, resulting in decreased diffusion of alkyne to the surface. To prevent these side reactions, 658 nm light was selected for further experiments.

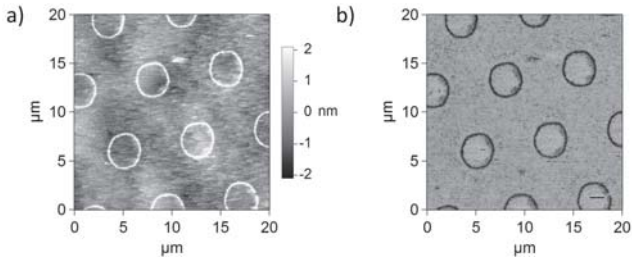

Figure 2.4. AFM images of a patterned Si(111) sample obtained by LE-µCP (254 nm, 3 h) with 1-octadecyne: a) height image before etching; b) corresponding phase image.

Next, the influence of stamp contact time on the monolayer formation was studied. Decreasing the contact time to 1 h resulted in decreased feature height: 0.9 instead of 1.4 nm (as measured with AFM). Increasing the contact time to 7 h, however, did not increase the feature height above the latter value, yet it did result in slight pattern broadening. In contrast to µCP of alkyl thiols on gold, where pattern broadening is a major issue (with reported smearing rates of up to several µm/s),[41,43], the pattern broadening in LE-µCP of alkynes on H-Si remains limited. Figure 2.5 shows an AFM height image of a single feature formed by illuminating for 7 h. Comparison with Figure 2.2 shows that: 1) the features only slightly broaden with contact time, and 2) the edge resolution of ~500 nm is hardly affected. This attractive feature of LE-µCP can be attributed to the low sticking factor of alkynes-on-Si versus the high sticking factor of thiols-on-Au. In the latter case, any lateral diffusion of excessive thiol-ink on the surface will result in monolayer formation. By contrast, monolayer formation of alkynes on H-Si is slow and requires high local concentrations due to its radical propagation.[1,44] Thus, broadening and edge resolution may relate to the shifting concentration profile of alkyne on the surface.

Third, the effect of different inking parameters on the LE-µCP process was investigated. In regular experiments, stamps were inked in a 100 mM 1-octadecyne solution. Inking the stamp in a 10 mM solution resulted in decreasing feature heights: the pattern was barely visible by AFM. This shows that at these low concentrations, the amount of available ink is limiting the monolayer formation. However, increasing the inking concentration to 500 mM did not result in higher features. In addition, practical difficulties (e.g. crystallization) were encountered due to saturation

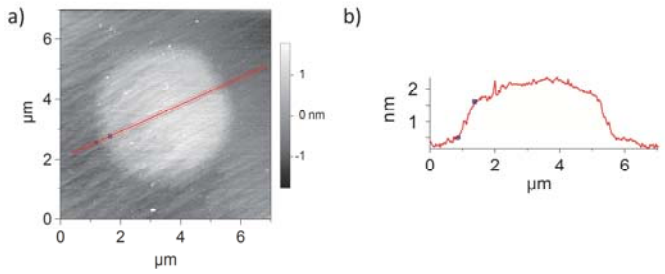

Figure 2.5. a) AC-AFM height image of a feature obtained after LE-µCP with 1-octadecyne for 7 h; b) corresponding cross section.

of the solution. Therefore, increasing the inking concentration above 100 mM is not recommended.

Likewise, the stamp immersion time was varied. Whereas prolongation of the immersion time from 2 to 10 min in a solution of 10 mM alkyne resulted in slight improvement of the feature height, this was not the case for the 100 mM solution. Moreover, printing with a stamp that had been immersed overnight in 100 mM inking solution could not be performed due to the lack of interaction between stamp and surface, which prevented conformal contact. Thus, we were unable to further improve the feature height by changing the inking parameters, indicating that the amount of available ink is not the limiting step in LE-µCP.

Alternatively, the feature height may be limited by undesired reaction of the solvent with the surface. Ethanol was selected as a solvent because it hardly swells PDMS and can dissolve apolar compounds such as alkynes, but it is also known to react with Si-H. Thus, LE-µCP using an ethanolic inking solution could lead to the formation of a mixed monolayer, which would have a limited thickness due to ethanol's short chain length. Even though no direct evidence of ethoxysilyl formation was found (e.g. Si-O peaks in the XPS Si_{2p} spectrum), a reaction with ethanol cannot be fully excluded. Thus, the monolayer quality in LE-µCP may be improved by using a non-reactive inking solvent. Alternatively, the use of solvents can be abandoned by using backside inking.[39] Here, an ink reservoir is placed on the backside of the stamp, which induces ink diffusion through the stamp towards the molded side. Further investigation is necessary to combine this inking strategy with backside illumination.

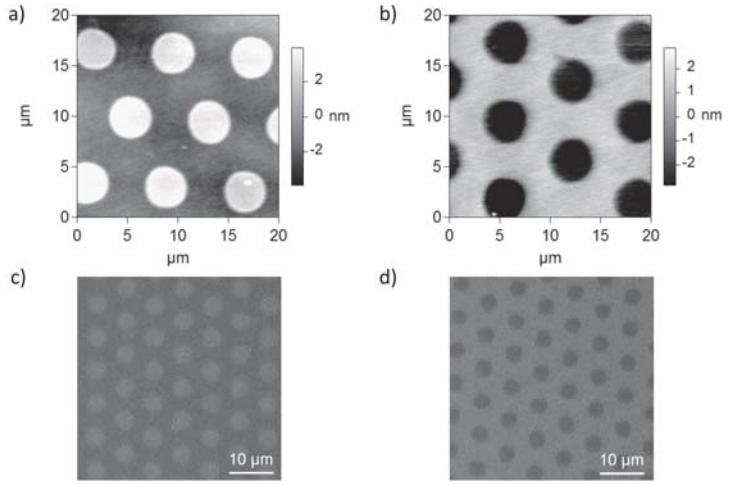

Figure 2.6. AC-AFM artificial height images (a, b) and SEM images (c, d) of backfilled samples. Left (a, c): LE-µCP with 1-octadecyne and backfilling with TFEE (C18/TFEE). Right (b, d): LE-µCP with TFEE and backfilling with 1-octadecyne (TFEE/C18).

2.4.4 Heterogeneous monolayers

Finally, heterogeneously functionalized surfaces were obtained via LE-µCP. For this purpose 1-octadecyne and 2,2,2-trifluoro-ethyl undec-10-ynoate (a mildly activated ester, TFEE) were used, since the resulting TFEE monolayer can be easily further functionalized.[45] To this aim the H-Si surface was patterned by LE-µCP with either 1-octadecyne or TFEE, and the remaining part of the surface was subsequently backfilled with the other component following the procedure of Scheres et al.[26] The resulting samples were named C18/TFEE and TFEE/C18, respectively.

AC-AFM images did not show distinct height differences between the contacted and backfilled areas on the C18/TFEE surfaces, whereas a faint height difference (~0.2 nm higher in the C18 backfilled area) was observed on the TFEE/C18 surfaces. This apparent contrast can be explained by: 1) the larger molecule size of 1-octadecyne compared to TFEE and 2) the relatively denser monolayer in the backfilled area compared to the printed area. Interestingly, a large contrast could be observed in the AC-AFM height image upon imaging with a weak cantilever in the non-contact regime (phase signal > 90°; Figure 2.6). The C18/TFEE sample gave the inverse contrast of

the TFEE/C18 sample. Even though the height features are artificial, they reveal that the AFM tip interacts differently with both areas. This can be explained by the lower surface energy of the TFEE areas compared to the C18 areas, as a result of which the AFM tip approaches the former more closely than the latter.

SEM imaging also showed a significant contrast between the different areas, confirming they are chemically heterogeneous (Figure 2.6). The octadecenyl monolayer presented brighter areas in SEM images than the TFEE–terminated areas due to its higher yield of secondary electrons, in line with previously reported results.[30,32] These experiments demonstrate that by combining LE-μCP with subsequent backfilling, oxide-free silicon can be patterned with chemically heterogeneous, functional monolayers.

2.5 Conclusions

This study shows that patterned monolayers of 1-alkynes can be directly formed onto H-Si surfaces by means of light-enhanced microcontact printing (LE-μCP) using visible light (658 nm). The features of the stamp are well-transferred to the surface, and unlike e.g. thiols on gold, pattern broadening remains limited. Extended contact times (~3 h) are required for optimal results, yielding moderately packed monolayers. Chemically heterogeneous surfaces were prepared by backfilling the uncontacted areas with a functional second ink, as visualized with AFM and SEM. Interchanging the inks resulted in contrast inversion, showing that LE-μCP is also compatible with functional inks.

2.6 References

(1) Linford, M. R.; Fenter, P.; Eisenberger, P. M.; Chidsey, C. E. D. *J. Am. Chem. Soc.* **1995**, *117*, 3145-3155.

(2) Sung, M. M.; Kluth, G. J.; Yauw, O. W.; Maboudian, R. *Langmuir* **1997**, *13*, 6164-6168.

(3) Aswal, D. K.; Lenfant, S.; Guerin, D.; Yakhmi, J. V.; Vuillaume, D. *Anal. Chim. Acta* **2006**, *568*, 84-108.

(4) Salomon, A.; Böcking, T.; Gooding, J.; Cahen, D. *Nano Lett.* **2006**, *6*, 2873-2876.

(5) Vilan, A.; Yaffe, O.; Biller, A.; Salomon, A.; Kahn, A.; Cahen, D. *Adv. Mater.* **2010**, *22*, 140-159.

(6) Boukherroub, R. *Curr. Opin. Solid State Mater. Sci.* **2005**, *9*, 66-72.

(7) Buriak, J. M. *Chem. Rev.* **2002**, *102*, 1271-1308.

(8) Hamers, R. J. *Annu. Rev. Anal. Chem.* **2008**, *1*, 707-736.

(9) Wayner, D. D. M.; Wolkow, R. A. *J. Chem. Soc. Perk. Trans. 2* **2002**, 23-34.

(10) Kumar, A.; Biebuyck, H. A.; Whitesides, G. M. *Langmuir* **1994**, *10*, 1498-1511.

(11) Kumar, A.; Whitesides, G. M. *Appl. Phys. Lett.* **1993**, *63*, 2002-2004.

(12) Woodson, M.; Liu, J. *Phys. Chem. Chem. Phys.* **2007**, *9*, 207-225.

(13) Gates, B. D.; Xu, Q. B.; Stewart, M.; Ryan, D.; Willson, C. G.; Whitesides, G. M. *Chem. Rev.* **2005**, *105*, 1171-1196.

(14) Ravoo, B. J. *J. Mater. Chem.* **2009**, *19*, 8902-8906.

(15) Perl, A.; Reinhoudt, D. N.; Huskens, J. *Adv. Mater.* **2009**, *21*, 2257-2268.

(16) Quist, A. P.; Pavlovic, E.; Oscarsson, S. *Anal. Bioanal. Chem.* **2005**, *381*, 591-600.

(17) Delamarche, E.; Schmid, H.; Bietsch, A.; Larsen, N. B.; Rothuizen, H.; Michel, B.; Biebuyck, H. *J. Phys. Chem. B* **1998**, *102*, 3324-3334.

(18) Sharpe, R. B. A.; Burdinski, D.; Huskens, J.; Zandvliet, H. J. W.; Reinhoudt, D. N.; Poelsema, B. *Langmuir* **2004**, *20*, 8646-8651.

(19) Jun, Y.; Le, D.; Zhu, X. Y. *Langmuir* **2002**, *18*, 3415-3417.

(20) Mizuno, H.; Buriak, J. M. *J. Am. Chem. Soc.* **2008**, *130*, 17656-17657.

(21) Scheres, L.; Giesbers, M.; Zuilhof, H. *Langmuir* **2010**, *26*, 4790-4795.

(22) Arafat, S. N.; Dutta, S.; Perring, M.; Mitchell, M.; Kenis, P. J. A.; Bowden, N. B. *Chem. Commun.* **2005**, 3198-3200.

(23) Scheres, L.; ter Maat, J.; Giesbers, M.; Zuilhof, H. *Small* **2010**, *6*, 642-650.

(24) Shestopalov, A. A.; Clark, R. L.; Toone, E. J. *Langmuir* **2010**, *26*, 1449-1451.

(25) Campos, M. A. C.; Paulusse, J. M. J.; Zuilhof, H. *Chem. Commun.* **2010**, *46*, 5512-5514.

(26) Scheres, L.; Arafat, A.; Zuilhof, H. *Langmuir* **2007**, *23*, 8343-8346.

(27) Scheres, L.; Giesbers, M.; Zuilhof, H. *Langmuir* **2010**, *26*, 10924-10929.

(28) Sun, Q. Y.; de Smet, L. C. P. M.; van Lagen, B.; Giesbers, M.; Thune, P. C.; van Engelenburg, J.; de Wolf, F. A.; Zuilhof, H.; Sudhölter, E. J. R. *J. Am. Chem. Soc.* **2005**, *127*, 2514-2523.

(29) Bittermann, A. G.; Jacobi, S.; Chi, L. F.; Fuchs, H.; Reichelt, R. *Langmuir* **2001**, *17*, 1872-1877.

(30) Lopez, G. P.; Biebuyck, H. A.; Whitesides, G. M. *Langmuir* **1993**, *9*, 1513-1516.

(31) Mack, N. H.; Dong, R.; Nuzzo, R. G. *J. Am. Chem. Soc.* **2006**, *128*, 7871-7881.

(32) Saito, N.; Wu, Y.; Hayashi, K.; Sugimura, H.; Takai, O. *J. Phys. Chem. B* **2003**, *107*, 664-667.

(33) Srinivasan, C.; Mullen, T. J.; Hohman, J. N.; Anderson, M. E.; Dameron, A. A.; Andrews, A. M.; Dickey, E. C.; Horn, M. W.; Weiss, P. S. *Acs Nano* **2007**, *1*, 191-201.

(34) Wang, X.; Colavita, P. E.; Metz, K. M.; Butler, J. E.; Hamers, R. J. *Langmuir* **2007**, *23*, 11623-11630.

(35) Smith, W. N.; Beumel, O. F. *Synthesis-Stuttgart* **1974**, 441.

(36) Scheres, L.; Klingebiel, B.; ter Maat, J.; Giesbers, M.; de Jong, H.; Hartmann, N.; Zuilhof, H. *Small* **2010**, *6*, 1918-1926.

(37) Yang, L.; Shirahata, N.; Saini, G.; Zhang, F.; Pei, L.; Asplund, M. C.; Kurth, D. G.; Ariga, K.; Sautter, K.; Nakanishi, T.; Smentkowski, V.; Linford, M. R. *Langmuir* **2009**, *25*, 5674-5683.

(38) Sieval, A. B.; Vleeming, V.; Zuilhof, H.; Sudhölter, E. J. R. *Langmuir* **1999**, *15*, 8288-8291.

(39) Balmer, T. E.; Schmid, H.; Stutz, R.; Delamarche, E.; Michel, B.; Spencer, N. D.; Wolf, H. *Langmuir* **2005**, *21*, 622-632.

(40) Sun, Q. Y.; de Smet, L. C. P. M.; van Lagen, B.; Wright, A.; Zuilhof, H.; Sudhölter, E. J. R. *Angew. Chem. Int. Ed.* **2004**, *43*, 1352-1355.

(41) Sharpe, R. B. A.; Burdinski, D.; van der Marel, C.; Jansen, J. A. J.; Huskens, J.; Zandvliet, H. J. W.; Reinhoudt, D. N.; Poelsema, B. *Langmuir* **2006**, *22*, 5945-5951.

(42) Wigenius, J. A.; Hamedi, M.; Inganas, O. *Adv. Funct. Mater.* **2008**, *18*, 2563- 2571.

(43) Gannon, G.; Larsson, J. A.; Greer, J. C.; Thompson, D. *Langmuir* **2009**, *25*, 242-247.

(44) de Smet, L. C. P. M.; Pukin, A. V.; Sun, Q. Y.; Eves, B. J.; Lopinski, G. P.; Visser, G. M.; Zuilhof, H.; Sudhölter, E. J. R. *Appl. Surf. Sci.* **2005**, *252*, 24-30.

(45) Rosso, M.; Giesbers, M.; Arafat, A.; Schroën, K.; Zuilhof, H. *Langmuir* **2009**, *25*, 2172-2180.

Chapter 3

Photochemical Covalent Attachment of Alkene-Derived Monolayers onto Hydroxyl-Terminated Silica

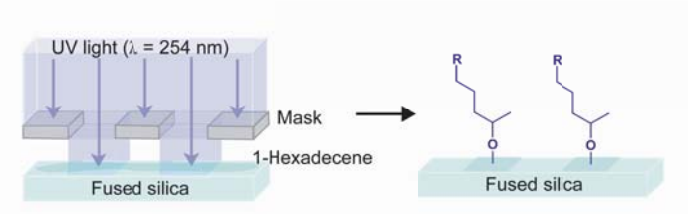

This chapter was published as:

ter Maat, J.; Regeling, R.; Yang, M.; Mullings, M. N.; Bent, S. F.; Zuilhof, H. "Photochemical covalent attachment of alkene-derived monolayers onto hydroxyl-terminated silica", *Langmuir* **2009**, *25*, 11592-11597.

3.1 Abstract

The functionalization of optically transparent substrates is of importance for example in the field of biosensing. In this article, a new method for modification of silica surfaces is presented that is based on a photochemical reaction of terminal alkenes with the surface. This yields highly hydrophobic surfaces, which are thermally stable up to at least 400 ºC. The formed monolayer provides chemical passivation of the underlying surface, according to studies showing successful blocking of platinum atomic layer deposition (ALD). The reaction is photochemically initiated, requiring light with a wavelength below 275 nm. X-ray photoelectron spectroscopy and infrared spectroscopy studies show that the alkenes initially bind to the surface hydroxyl groups in Markovnikov fashion. At prolonged reaction times (> 5h), however, oligomerization occurs, resulting in layer growth normal to the surface. The photochemical nature of the reaction enables the use of photolithography as a tool to constructively pattern silica surfaces. Atomic force microscopy showed that the features of the photomask were well transferred. The newly developed method can complement existing patterning methods on silica that are based on soft lithography.

3.2 Introduction

Silica glasses are an important class of materials because of their excellent optical properties. The specific properties of a silica glass depend on its composition and fabrication method.[1] Whereas silica glasses made from natural quartz show considerable absorption above 200 nm, synthetic fused silica is transparent at wavelengths down to 180 nm. Optical transparency is a desired property in the field of biosensing, where techniques of fluorescent labeling are well-developed.[2] For biosensing, the material of choice should also be easily functionalizable. For silica, a number of functionalization methods have been developed. Esterification of silica surface hydroxyl groups with alcohols is known since the 1950s,[3] however, the resulting monolayers are easily hydrolyzed.[4] The currently prevailing method makes use of organosilanes,[5] which can react with surface hydroxyl groups to yield a closely packed monolayer.[6,7] The modification is rapid, is usually performed in dilute solutions, and several functional groups are compatible with the procedure. Patterned functionalization of silica surfaces is e.g. possible using soft lithographic techniques.[7]

However, the reaction is notoriously difficult to control due to the tendency of silanes to condense in solution.[8,9] In addition, the high reactivity of organotrichlorosilanes requires careful handling and limits their use in an industrial environment. Thirdly, the monolayer is prone to hydrolysis under certain conditions. Finally, the excellent optical properties of silica are currently not exploited by using photolithography to locally absorb the monolayer.

In this paper we demonstrate a novel and mild method for surface modification of silica surfaces, synthetic fused silica in particular, based on a photochemical reaction of terminal alkenes with the glass surface. A first indication for the occurrence of this reaction was given by Mischki et al., who reported that oxidized silicon surfaces that were immersed in 1-alkenes became slightly more hydrophobic upon illumination with UV light (> 300 nm).[10] They concluded that 1-alkenes can bind to the silicon oxide in a Markovnikov fashion, but that the extent to which this reaction occurs under photochemical conditions is small. Here, we show that monolayers of 1-alkenes can be formed photochemically on fused silica surfaces, resulting in very hydrophobic surfaces. We characterized the modified surfaces with water contact angle measurements, infrared spectroscopy and X-ray photoelectron spectroscopy, and

using thermogravimetric mass spectroscopy, we show that the modified surfaces are thermally stable. Atomic layer deposition (ALD) experiments are further used to show that the monolayers are chemically passivating, indicative of a well-packed layer. Finally, we demonstrate that silica surfaces can be constructively patterned with photolithography, and characterize the resulting pattern with atomic force microscopy.

3.3 Materials and methods

Materials. Glassware used for surface modification was cleaned with organic solvents and etched overnight in basic detergent solution. Prior to use, it was rinsed with ultrapure water and dried at 120 ºC. 1-Hexadecene (98 %, Sigma-Aldrich) was purified by column chromatography and vacuum distillation. 11-Fluoroundec-1-ene was synthesized as described elsewhere.[11] Solvents used were either of analytical grade or distilled prior to use.

Surface modification. A specially designed quartz flask was filled with 1-hexadecene (~2 ml). This was degassed using three consecutive freeze-pump-thaw cycles. Liquid N_2 was used as cooling agent. Prior to sample immersion, the 1-hexadecene was frozen again by short immersion in liquid N_2 and the flask was filled with argon.

A synthetic fused silica slide (15×25 mm, Praezisions Glas & Optik, Iserlohn, Germany) was cleaned by sonication in acetone for 5 min. After drying with argon, the slide was immersed in a freshly made 1:1 (v:v) mixture of hydrochloric acid (37%, analytical grade, Acros) and methanol for at least 30 min. The slide was rinsed with ultrapure water, dried with argon and inserted into the flask containing frozen 1-alkene. Vacuum was applied again until the 1-alkene was molten completely and the slide was immersed, after which the flask was filled with argon and kept under a slight overpressure. Two low-pressure mercury lamps (6.0 mW/cm^2, Jelight, Irvine CA, USA) were placed at a fixed distance (~ 0.5 cm) from the fused silica slide. For some experiments, a longpass filter (cut-on wavelength 275 nm, Asahi Spectra, Torrance CA, USA) was placed in between the lamps and the flask. The setup was packed in aluminum foil and the slide was illuminated for a specified time. After illumination, the slide was removed from the flask, rinsed with petroleum ether 40/60 and ethanol,

sonicated in ethanol and dichloromethane for 5 min per solvent, rinsed with dichloromethane and finally dried with argon.

Photolithography. Photolithography was performed with cleaned slides and degassed 1-hexadecene in a glove box. An electron microscope grid (T2000-Cu or SEM F1 (Au), Gilder Grids) was placed on top of the fused silica slide, onto which the 1-alkene was dropped. A fused quartz microscope slide (Alfa Aesar) was used as a cover, onto which a mercury capillary lamp (Jelight) was pointed. Samples were irradiated for 10 h, then removed from the glove box and cleaned as described above.

Water contact angle measurements. Static contact angles were measured using a Krüss DSA-100 goniometer. Droplets of 3 μl were dispensed on the surface and contact angles were measured with a CCD camera using a tangential method. The reported value is the average of at least 5 droplets and has an error of ± 1º.

Infrared reflectance absorbance spectroscopy. IRRA spectra were obtained with a Bruker Tensor 27 FT-IR spectrometer, using a commercial variable-angle reflection unit (Auto Seagull, Harrick Scientific). A Harrick grid polarizer was installed in front of the detector and was used for measuring spectra with s-polarized radiation with respect to the plane of incidence at the sample surface. Single channel transmittance spectra were collected at an angle of 75º using a spectral resolution of 4 cm^{-1} and 2048 scans in each measurement. The raw data were divided by the data recorded on a freshly cleaned reference fused silica slide, after which a baseline correction was applied to give the reported spectra.

X-ray Photoelectron Spectroscopy. XPS analyses of the substrates following reaction with the alkene were performed using a JPS-9200 photoelectron spectrometer (JEOL). The spectra were obtained under ultrahigh vacuum (UHV) conditions using monochromatic Al Kα X-ray radiation at 12 kV and 25 mA, with an analyzer pass energy of 30 eV. The X-ray incidence angle and the electron acceptance angle were 80º and 10º with respect to the surface normal, respectively. To prevent surface charging during measurements, samples were irradiated with electrons with a kinetic energy of 3.8 eV. Post-ALD XPS analyses were performed using a PHI VersaProbe Scanning XPS. The C_{1s} peak at 285.0 eV was used as a reference for both systems. Spectra were corrected using a linear background subtraction before quantification and any peak deconvolution.

Determination of attenuation lengths. Electron attenuation lengths (EALs) were determined using the NIST Electron Effective-Attenuation-Length database.[12] In this program, electron inelastic mean free paths (IMFPs) were determined using the TPP-2M equation.[13] This required input of the density as well as the bandgap of the 1-hexadecene adlayer. For both parameters, the values of (low-density) polyethylene, 0.92 g/cm^3 and 8.8 eV, respectively, were used. The uncertainty in the attenuation length is mainly dependent on the uncertainties in the calculated IMFP, the transport mean free path and the transport approximation,[12] and amounts to ca. 20 %.

X-ray Reflectivity. X-ray reflectivity measurements were performed on a Panalytical X'Pert Pro diffractometer using nickel-filtered Cu Kα radiation (tube settings 40 kV and 50 mA). The data were collected using a fixed divergence slit of 1/32° and a parallel plate collimator on the diffracted beam side. The layer thickness is calculated from the interference fringes.

Fluorescence spectroscopy. Steady-state fluorescence excitation and emission measurements were performed on a time-correlating single photon counting F900 spectrometer (Edinburgh Instruments). For emission measurements λ_{exc} = 254 nm, for fluorescence excitation measurements λ_{em} = 387 nm. To allow for comparison, the measured spectra have been normalized.

ThermoGravimetric-Mass Spectrometry. TG-MS analyses were carried out in a TGA/SDTA851e instrument (Mettler-Toledo GmbH, Switzerland), coupled to a Thermostar GSD 301 T2 quadrupole mass spectrometer (Pfeiffer Vacuum GMBH, Asslar). Samples were weighed into 100 µL aluminum crucibles and sealed. The seals were pin-holed and the crucibles were heated in the TGA from 25 to 400 °C at 10 °C min^{-1}. Dry N_2 gas was used for purging. The detection limit of the MS for release gases was 10^{-14} mbar. A Multiple Ion Detection (MID) measurement was performed with a channeltron voltage of 950 V. The scan measurements were performed over a mass range 0 - 130 amu.

Atomic Force Microscopy. AFM images (512 × 512 pixels) were obtained with an MFP3D AFM (Asylum Research, Santa Barbara, CA). The imaging was performed in contact mode in air using NP silicon nitride cantilevers with a stiffness of 0.58 N/m (Veeco Metrology, Santa Barbara, CA) at a scan speed of 18.75 µm/s. The scan angle was 90º with respect to the cantilever axis, which allowed the simultaneous recording

of lateral force images. Images were flattened with a 0th order flattening procedure using the MFP3D software.

Atomic Layer Deposition. ALD of Pt was carried out in a custom-built reactor. The ALD process consisted of 2 s pulses of high-purity methylcyclopentadienyl trimethyl platinum [$CH_3C_5H_4Pt(CH_3)_3$] and dry air, each separated by 30 s nitrogen purges, carried out for 100 cycles with the substrate at 300 ºC.

3.4 Results and discussion

Cleaned synthetic fused silica slides were modified with 1-hexadecene by illumination with a low-pressure mercury lamp under an argon atmosphere. After cleaning, the degree of modification was initially assessed by determining the surface wettability with static contact angle measurements. Figure 3.1 shows the influence of the modification time on the surface wettability. The contact angle increases steadily with modification time, reaching a maximum value of 109 ± 1° after 8 h. As the surface wettability does not change upon sonication in organic solvents, this shows that a tightly bound hydrophobic layer is formed on the surface.

To confirm the presence of a hydrophobic layer, the samples were studied with infrared reflection-absorption spectroscopy (IRRAS). The obtained spectra display an increased intensity of the C-H stretching vibrations with modification time (Figure 3.2a). This implies that the absorbed layer is steadily growing, even after 8 h of modification, after which no further change in the contact angle is observed. After 8 h of illumination, the positions of the symmetric and antisymmetric methylene stretching peaks are at 2854 and 2924 cm^{-1}, respectively, and do not shift upon prolonged modification. This indicates that the adsorbed layer is disordered.[14] These observations contrast with the monolayer formation of thiols on gold, silanes on silicon oxide and alkenes on silicon, where the position of the methylene stretching peaks shifts to lower values with increasing packing density.[15-18] The increased peak intensity at prolonged modification times is therefore likely to be caused by on-going growth normal to the surface.

Another feature in the IRRA spectra is the sharp negative peak at the Christiansen frequency (1374 cm^{-1}), named the substrate band,[19,20] which becomes more negative with prolonged modification time (Figure 3.2b). At this frequency the refractive index

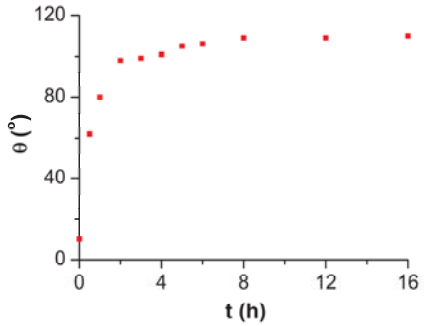

Figure 3.1. Static water contact angle of fused silica slides modified with 1-hexadecene after different modification times.

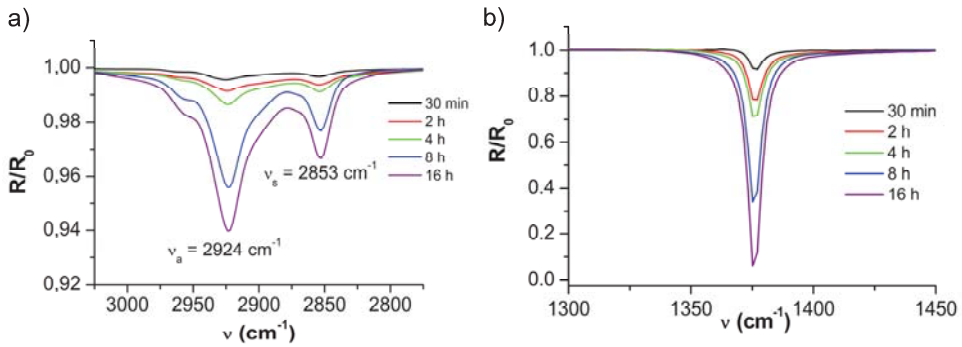

Figure 3.2. IRRA spectra of fused silica modified with 1-hexadecene for different modification times a) methylene stretching region b) substrate band region.

of fused silica passes from a value above 1.0 to a value below 1.0. Because its absorbance coefficient is also very small, fused silica optically resembles air at the Christiansen frequency. The substrate with adsorbed film can therefore be modeled as a freestanding film.[21] Figure 3.2b shows that the intensity of the peak at 1374 cm^{-1} correlates well with the intensity of the C-H stretching peaks. This is in accordance with previous reports, where it was shown that the peak intensity at the Christiansen frequency is very sensitive to layer thickness.[20]

Compared to the unmodified sample, all modified samples show decreased absorptions in the OH region. The two main features have maximum intensities at 3720 and 3550 cm^{-1}, which can be attributed to free and hydrogen-bonded Si-OH,

respectively.[6,22] In addition, loss of physisorbed water is also contributing to the signal. The intensity of these peaks is similar for all modified samples.

XPS analysis of the modified samples shows the presence of three elements only: Si, O and C. Figure 3.3 shows that the C atomic ratio increases with modification time. By plotting atomic ratios, two effects are combined: the increase of the C_{1s} signal and the decrease of the Si_{2p} and O_{1s} signals. Both effects are the result of growth of the adsorbed hydrocarbon layer.

From Figure 3.3 it can be seen that the increase in C atomic ratio is gradual for small modification times, but after 5 h the relative C signal rises rapidly, giving rise to a sigmoidal curve. At high modification times, the absolute O_{1s} and Si_{2p} signals are < 20 % of those of the unmodified samples, measured under the same conditions. The thickness of the growing hydrocarbon layer can be calculated using:

$$I_{Si} = I_{Si}^{\infty} \exp\left(\frac{-d}{\lambda_{Si,C} \cos\theta}\right) \qquad (1)$$

with I_{Si} = absolute silicon peak intensity, I_{Si}^{∞} = absolute silicon peak intensity of unmodified, cleaned fused silica, d = thickness of the adsorbed layer, $\lambda_{Si,C}$ = attenuation length of Si_{2p} electrons in the hydrocarbon layer, and θ = electron take-off angle. $\lambda_{Si,C}$ was calculated to be 4.9 nm using the NIST Electron Effective-Attenuation-Length database.[12] Similarly, the adlayer thickness can be calculated from the oxygen peak intensities using the attenuation length of O_{1s} electrons in the hydrocarbon layer (3.6 nm). Using both these methods, the thickness of the hydrocarbon layer was, after 5 h of modification, calculated to be 1.7 nm. This is slightly less than the length of a 1-hexadecene molecule (1.9 nm, as determined with Chem3D), indicating that the layer formed is still a monolayer, most likely with tilted alkyl chains. After 16 h of modification, the layer thickness was calculated to be 10 nm for various samples (estimated experimental uncertainty: ~2 nm, due to assumptions; see Exp. Section). This evidence shows that after long modification times the attached coating layer is significantly thicker than a monolayer.

To evaluate the accuracy of these calculations, X-ray reflectivity was performed. With this method, the thickness of the adsorbed layer can be directly determined, provided that it is larger than 2 nm. Reflectivity measurements on a sample modified

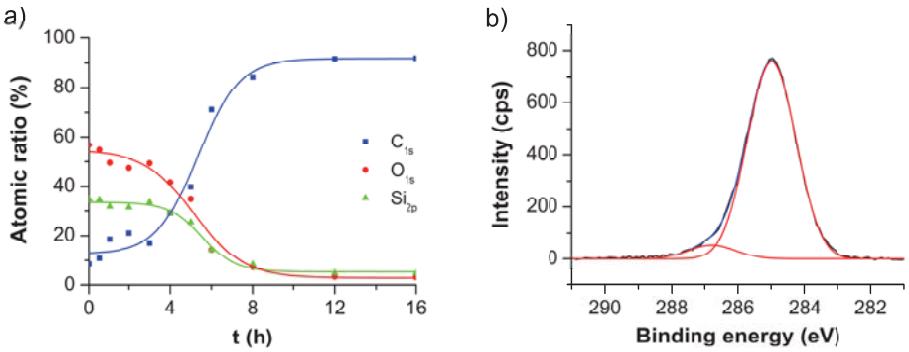

Figure 3.3. a) Ratios of elements present on the surface of fused silica plotted against modification time. Ratios were determined by integrating the XPS C_{1s}, O_{1s} and Si_{2p} signals. Lines were added as a guide to the eye. b) C_{1s} spectrum with curve fitting for fused silica modified with 1-hexadecene for 5 h.

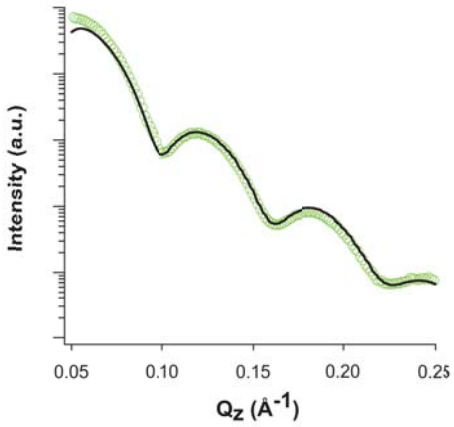

Figure 3.4. X-Ray reflectivity profile of fused silica that was modified for 16 h with 1-hexadecene (green circles) and the calculated profile for a layer of 9.9 nm thickness (black line).

for 5 h did not result in any interference fringes, indicating that the layer thickness is indeed below 2 nm. Conversely, an adsorbed layer thickness of 9.9 ± 0.2 nm was derived. from measurements on a sample after 16 h of modification (Figure 3.4). This agrees well with the XPS-derived value, and thus shows the validity of XPS attenuation length calculations for such layer thickness estimations.

The thermal stability of the modified samples was studied using thermogravimetry-mass spectroscopy (TG-MS). No hydrocarbon fragments could be detected by MS when modified samples were heated up to 400 °C in a nitrogen atmosphere. This contrasts with the unmodified samples, which showed desorption of physically adsorbed hydrocarbon fragments between 70 and 160 °C. The absence of physisorbed material on the modified surface may be explained by its lower surface energy compared to cleaned fused silica.[23] In addition to the TG-MS measurements, samples were heated to 200 °C in an argon-purged vacuum oven and cooled down again. Because of the slow heating and cooling rate of the oven, the samples were exposed to a temperature of at least 185 °C for more than 60 min. Prior to and after this thermal treatment, XPS spectra were taken. No significant changes (> 2% in relative C_{1s} intensities) could be observed. This is in agreement with the TG-MS results, supporting the conclusion that the modified surfaces are thermally stable.

ALD of Pt was used to test the quality of the 1-hexadecene monolayer and its ability to passivate the underlying substrate. It has been shown that high-quality organic monolayers (such as highly hydrophobic organosilane self-assembled monolayers on silica) can resist ALD growth, whereas less well-packed monolayers lead to deposition by ALD.[24,25] Fused silica samples with and without the 1-hexadecene monolayer were subjected to Pt ALD and then characterized by XPS. Figure 5 shows that after 100 cycles of Pt ALD carried out 300 ºC, all Pt XPS peaks were completely absent on the modified silica sample, compared to significant Pt (22.8 at. %) for the unmodified sample. The ability to block the Pt ALD reactions indicates that the monolayers are dense and hydrophobic, and confirms their stability at these elevated temperatures.

It has recently been reported that illumination of silicon oxide-covered silicon in the presence of 1-decene with 300 nm light yielded a water contact angle of 59°.[10] Low-pressure mercury lamps mainly emit at 254 nm, but spectral lines are also present at 296 and 312 nm. When the emission at 254 nm was blocked using a 275 nm longpass filter, prolonged illumination of fused silica indeed yielded a contact angle of only 60°. Using a phosphor-coated low-pressure mercury lamp, designed to emit at 285 nm, in combination with the 275 nm long-pass filter, similarly low contact angles were measured. This implies that the additional modification is caused by the 254 nm radiation.

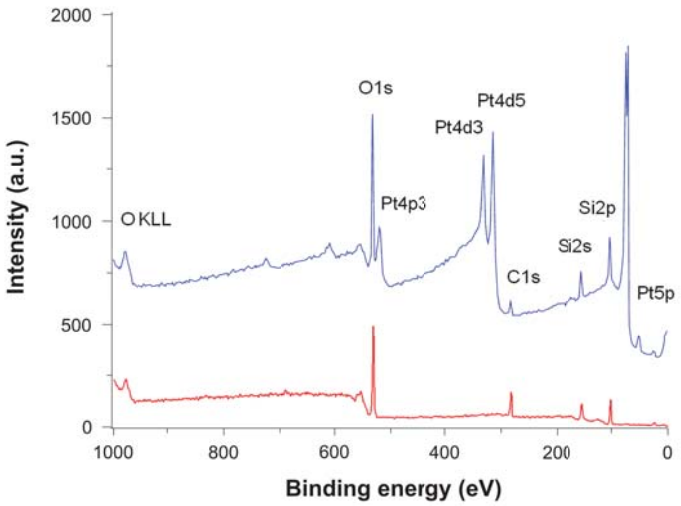

Figure 3.5. XP spectra after 100 cycles of Pt of ALD onto unmodified fused silica (top) and onto fused silica that was modified with 1-hexadecene (bottom).

To investigate the origin of the reaction, the absorption and emission spectrum of fused silica were measured. UV/Vis absorption spectroscopy is excluded, due to the very limited absorptivity of fused silica at the relevant wavelengths. Interestingly, exciting a fused silica slide at 254 nm in a fluorescence spectrometer gives rise to an emission at 387 nm (Figure 6). The corresponding fluorescence excitation spectrum shows a weak but distinct absorption peak at 253 nm. The origin of these photophysical properties lies in the presence of a small fraction of defects.[26] It has been reported that photoluminescent bands observed in silica around 400 nm are caused by oxygen-deficient Ge and Sn impurities (at levels too low to be detected by XPS).[27,28] These bands could be excited at 248 nm. The same bands were also found in oxygen-deficient high purity silica and attributed to an oxygen deficiency-associated defect center.[29] In addition to the emission at 387 nm, a very weak emission at 452 nm is observed. This emission can be attributed to dicoordinated silicon, another oxygen deficiency-related defect center.[26]

The oxygen deficiency of the surface can be determined by calculating the XPS O_{1s}/Si_{2p} ratio. For cleaned, unmodified silica this ratio was found to be 1.7 ± 0.1 (rather than 2.0, expected for SiO_2), thereby implicitly confirming the presence of

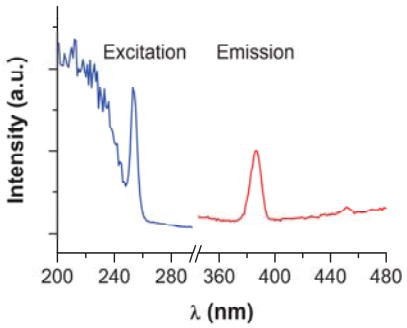

Figure 3.6. Excitation and emission spectra of fused silica. Emission was measured upon irradiation at 254 nm, while excitation was measured by monitoring the emission at 387 nm.

oxygen-deficient centers. To investigate whether these defects play a role in the photochemical reaction on the surface, the XPS C_{1s} spectrum of a modified sample was further examined. Deconvolution of the high-resolution C_{1s} spectrum for a sample that was modified for 5 h shows two contributions (Figure 3.3b). The major contribution is from C atoms solely bound to C or H atoms, which was set to 285.0 eV. The other contribution is found at 286.8 eV. A similar shift was observed for long-chain alcohols absorbed on glass and was attributed to the carbon atoms bound to oxygen in a C-O bond.[30] The ratio of the peak area at 286.8 eV to the total carbon peak area is 1 to 15.2, which would correspond to one C-O bond per molecule of 1-hexadecene. Thus, we can conclude that 1-hexadecene binds covalently to the surface hydroxyl groups. Oxygen-deficient surface defects therefore do not necessarily play a stoichiometric role in the reaction. Deconvolution of XPS spectra of samples that were modified for more than 5 h show a reduced contribution of oxygen-bound C atoms to a level where they become indiscernible, indicating that at prolonged reaction times another mechanism comes into play. This is in agreement with Figure 3.3, which shows a sharp increase of the C_{1s} signal after 5 h of modification.

The reaction of 1-decene with surface hydroxyl groups of oxidized silicon upon irradiation with 300 nm light was proposed to proceed via Markovnikov addition.[10] The same type of addition was also found when 1-alkenes were thermally[31] or photochemically[32] reacted with hydroxyl-terminated silicon carbide. To check the mechanism of the photochemical attachment of alkenes onto silica at λ = 254 nm,

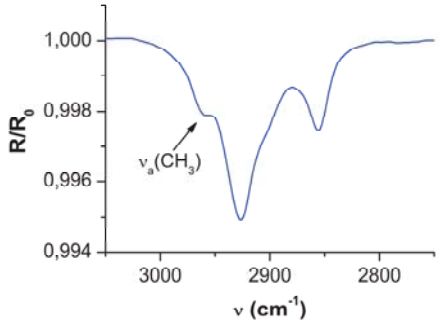

Figure 3.7. IRRA spectrum of a sample modified with 11-fluoro-undec-1-ene. The peak at 2960 cm^{-1} is attributed to the asymmetric methyl stretch vibration; this CH_3 group is introduced by the surface reaction.

samples were modified with 11-fluoro-undecene, and studied with IRRAS. The attachment of this molecule via a Markovnikov addition should introduce a methyl group to the surface that is not present in the alkene. The presence of a methyl stretching signal was indeed confirmed in the IRRA spectrum (Figure 7), thereby confirming Markovnikov addition. This type of addition also explains why the monolayers remain disordered, since the presence of a methyl group close to the surface does not allow the hydrocarbon chains to closely pack together.

The exact nature of the photochemical reaction is still unclear. Modification may be caused by direct excitation of the 1-alkene. Even though the absorption maximum of e.g. 1-hexadecene lies around 193 nm in dilute solutions, the absorption edge of the pure compound stretches out to over 260 nm. The excited alkene may then be prone to addition to surface hydroxyl groups. On the other hand, excited surface defects may initiate a radical surface reaction, which then propagates laterally over the surface until a certain surface coverage is reached. Further studies are necessary to get a better understanding of the reaction mechanism.

The oligomerization we observed at prolonged reaction times may be initiated by the excitation of the alkene into its triplet state. The importance of the triplet excited state in the photopolymerization of ethylene has been pointed out by Hagiwara et al.[33] For ethylene, the transition from the singlet ground state to the triplet excited state occurs upon absorption of UV light in the range of 260 - 350 nm, and it is promoted by

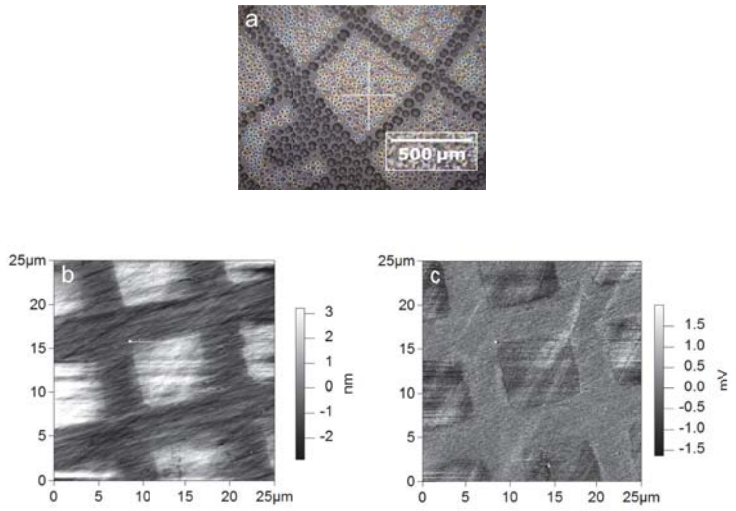

Figure 3.8. a) Micrograph of a hydrophobically patterned sample exposed to water vapor. b) Topography of a patterned sample, measured with contact-mode AFM. c) Corresponding lateral force image.

oxygen.[34] The corresponding absorption coefficient of $\sim 10^{-4}$ shows that this transition occurs with very low probability.[35] As oxygen is involved in the initiation, the oxygen concentration strongly influences the rate of reaction, with an optimum concentration of around 100 ppm.[33] In our case, the oxygen level was minimized by extensive degassing, but this was limited by an oxygen contamination (<5 ppm) in the argon that was used. Therefore, photopolymerization at prolonged reaction times cannot be excluded and is indeed observed on the surface.

As the reaction of 1-hexadecene with fused silica is clearly photochemical in nature, photolithography can be used to constructively create a pattern on fused silica surfaces. Photolithography was performed using contact masks in the inert atmosphere of a glovebox. After illumination, the sample was cleaned and exposed to water vapor. Condensation of water on the surface led to visualization of the pattern (Figure 8). The droplets formed on the illuminated, hydrophobic parts of the surface are small and appear colored, while droplets formed on the masked area are bigger and appear dark. The different appearance is caused by differences in hydrophilicity, introduced by the photochemical reaction.

AFM was used to study modified samples with smaller feature sizes (obtained using a 2000 mesh electron microscope grid). Contact mode measurements clearly reveal 7.5 × 7.5 um squares with a spacing of 5 um, both in topography and in lateral mode (Figure 8). The underlying texture of the polished slides can also be distinguished. The height difference between the patterned and unpatterned area is at least 3 nm (not corrected for differences in elasticity). This value is bigger than the maximum chain length of 1-hexadecene (1.9 nm), again confirming the growth of an oligomeric multilayer. The data in Figure 7 and 8 provide the first examples of photolithography onto glass, and reveal the power of this mild method of surface modification. The local modification of the inside of microchannels with DNA oligomers provides an example of the extension that this reaction yields over contact-requiring soft lithographic techniques.[36]

3.5 Conclusions

We have developed a mild, room-temperature photochemical procedure by which 1-alkenes can bind covalently to the surface of hydroxyl-terminated fused silica. The resulting functionalized surfaces can be prepared reproducibly, are highly hydrophobic but disordered, and are thermally stable up to at least 400 °C. The 1-hexadecene monolayer was shown to act as a resist against Pt ALD, which indicates its high quality. The grafting reaction is photochemically initiated, requiring light with a wavelength below 275 nm, and occurs via Markovnikov addition of surface hydroxyl groups to the double bond of the alkene. However, after 5 h of modification, oligomerization normal to the surface is also observed. Using photolithography, it was possible to constructively pattern the fused silica surface with 1-hexadecene. This can complement currently existing (soft lithographic) patterning methods, specifically since without the light source none of the reactants involved displays any significant reactivity.

3.6 References

(1) Brückner, R. *J. Non-Cryst. Solids* **1970**, *5*, 123-175.

(2) Altschuh, D.; Oncul, S.; Demchenko, A. P. *J. Mol. Recognit.* **2006**, *19*, 459-477.

(3) Iler, R. K.; E. I. du Pont de Nemours & Co., I., Ed. U.S., 1953.

(4) Pesek, J. J.; Matyska, M. T. *Interface Sci.* **1997**, *5*, 103-117.

(5) Sagiv, J. *J. Am. Chem. Soc.* **1980**, *102*, 92-98.

(6) Vansant, E. F.; Van Der Voort, P.; Vrancken, K. C. *Characterization and chemical modification of the silica surface*; 1st ed.; Elsevier: Amsterdam, 1995.

(7) Onclin, S.; Ravoo, B. J.; Reinhoudt, D. N. *Angew. Chem. Int. Edit.* **2005**, *44*, 6282-6304.

(8) Vallant, T.; Brunner, H.; Mayer, U.; Hoffmann, H.; Leitner, T.; Resch, R.; Friedbacher, G. *J. Phys. Chem. B* **1998**, *102*, 7190-7197.

(9) Silberzan, P.; Leger, L.; Ausserre, D.; Benattar, J. J. *Langmuir* **1991**, *7*, 1647-1651.

(10) Mischki, T. K.; Donkers, R. L.; Eves, B. J.; Lopinski, G. P.; Wayner, D. D. M. *Langmuir* **2006**, *22*, 8359-8365.

(11) Sun, Q. Y.; de Smet, L. C. P. M.; van Lagen, B.; Giesbers, M.; Thune, P. C.; van Engelenburg, J.; de Wolf, F. A.; Zuilhof, H.; Sudholter, E. J. R. *J. Am. Chem. Soc.* **2005**, *127*, 2514-2523.

(12) Powell, C. J.; Jablonski, A. *NIST Electron Effective-Attenuation-Length Database - Version 1.1*; National Institute of Standards and Technology: Gaithersburg, MD, 2003.

(13) Tanuma, S.; Powell, C. J.; Penn, D. R. *Surf. Interface Anal.* **1994**, *21*, 165-176.

(14) Porter, M. D.; Bright, T. B.; Allara, D. L.; Chidsey, C. E. D. *J. Am. Chem. Soc.* **1987**, *109*, 3559-3568.

(15) Ulman, A. *An introduction to Ultrathin Organic Films: From Langmuir-Blodgett to Self-Assembly*; Academic Press: Boston, 1991.

(16) Scheres, L.; Arafat, A.; Zuilhof, H. *Langmuir* **2007**, *23*, 8343-8346.

(17) Buriak, J. M. *Chem. Rev.* **2002**, *102*, 1271-1308.

(18) Sondag, A. H. M.; Raas, M. C. *J. Chem. Phys.* **1989**, *91*, 4926-4931.

(19) Tolstoy, V. P.; Chernyshova, I. V.; Skryshvsky, V. A. *Handbook of infrared spectroscopy of ultrathin films*; Wiley-VCH: Hoboken, NJ, 2003.

(20) Mielczarski, E.; Duval, Y. B.; Mielczarski, J. A. *J. Phys. Chem. B* **2002**, *106*, 11985-11992.

(21) Roseler, A.; Korte, E. H. *Vib. Spectrosc* **2007**, *43*, 111-115.

(22) Inaki, Y.; Yoshida, H.; Yoshida, T.; Hattori, T. *J. Phys. Chem. B* **2002**, *106*, 9098-9106.

(23) Cong, P.; Kubo, T.; Nanao, H.; Minami, I.; Mori, S. *Tribol. Lett.* **2007**, *27*, 137-143.

(24) Jiang, X. R.; Chen, R.; Bent, S. F. *Surf. Coat. Tech.* **2007**, *201*, 8799-8807.

(25) Chen, R.; Kim, H.; McIntyre, P. C.; Bent, S. F. *Chem. Mater.* **2005**, *17*, 536-544.

(26) Skuja, L. *J. Non-Cryst. Solids* **1998**, *239*, 16-48.
(27) Skuja, L. N.; Trukhin, A. N. *Phys. Rev. B* **1989**, *39*, 3909-3911.
(28) Skuja, L. *J. Non-Cryst. Solids* **1992**, *149*, 77-95.
(29) Sakurai, Y. *J. Non-Cryst. Solids* **2000**, *271*, 218-223.
(30) Fagerholm, H. M.; Rosenholm, J. B.; Horr, T. J.; Smart, R. S. *Colloid Surface A* **1996**, *110*, 11-22.
(31) Rosso, M.; Arafat, A.; Schroën, K.; Giesbers, M.; Roper, C. S.; Maboudian, R.; Zuilhof, H. *Langmuir* **2008**, *24*, 4007-4012.
(32) Rosso, M.; Giesbers, M.; Arafat, A.; Schroën, K.; Zuilhof, H. *Langmuir* **2009**, *25*, 2172-2180.
(33) Hagiwara, M.; Okamoto, H.; Kagiya, T. *J. Polym. Sci. Pol. Chem.* **1970**, *8*, 3295-3301.
(34) Evans, D. F. *J. Chem. Soc.* **1960**, 1735-1745.
(35) Reid, C. *J. Chem. Phys.* **1950**, *18*, 1299-1300.
(36) Vong, T. H.; ter Maat, J.; van Beek, T. A.; van Lagen, B.; Giesbers, M.; van Hest, J. C. M.; Zuilhof, H. *Langmuir* **2009**, *25*, 13952-13958.

Chapter 4

Site-Specific Immobilization of DNA in Glass Microchannels via Photolithography

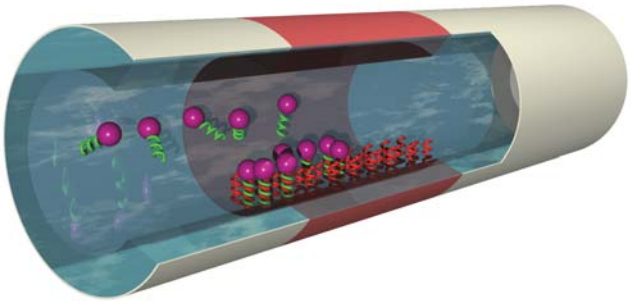

This chapter was published as:

Vong, T. H.; ter Maat, J.; van Beek, T. A.; van Lagen, B.; Giesbers, M.; van Hest, J. C. M.; Zuilhof, H. "Site-Specific Immobilization of DNA in Glass Microchannels via Photolithography", *Langmuir* **2009**, *25*, 13952-13958.

4.1 Abstract

In this chapter, the photochemical patterning of silicon oxide surfaces with a functional linker is demonstrated. This allowed the site-specific attachment of single-stranded DNA onto plain surfaces, as well as onto curved, enclosed surfaces. The latter was visualized by functionalization of the inner surface of a fused silica microchannel, which is hard to access using other patterning methods. Sharp, µm-range boundaries between modified and unmodified zones were demonstrated by attachment of fluorescently labeled DNA oligomers. The modified surfaces were characterized with XPS, IR, water contact angle measurements and confocal laser scanning microscopy. Moreover, studies of repeated hybridization-dehybridization cycles revealed selective and reversible binding of complementary DNA strands at the explicit locations. By performing these experiments in microchannels coupled to a fluorescence detector, it was determined that $\sim 7 \times 10^{11}$ fluorescently labeled DNA molecules were hybridized per cm^2. By furnishing target compounds with the complementary DNA strand, this hybridization approach may be applied for the selective, localized binding of proteins, antibodies and other biomolecules to the surface.

4.2 Introduction

Immobilization of DNA is widely used in microchip technology for applications including medical diagnostics, genetic analysis and hybridization studies. The ability of DNA to reversibly hybridize is utilized for DNA amplification and for studying binding interactions.[1,2] Even though still under development, this technology has proven to be robust, which makes it interesting for the reversible anchoring of e.g. protein-DNA conjugates.[3] Although DNA microarray devices allow multiple parallel analyses, operations such as regeneration and binding need to be performed in a step-by-step fashion, which is a consequence of using open, flat surfaces. By contrast, immobilizing the DNA into a microchannel facilitates the study of flow-through processes and enables continuous reloading of the microfluidic device. This allows re-using of the device and, as a result, minimizes the required amount of the protein-DNA conjugates.

Glass substrates are particularly popular for DNA microchips due their low cost, thermal stability, chemical inertness, optical transparency and low fluorescence.[4] The last two characteristics are especially important, because they result in a high signal-to-noise ratio in fluorescence detection, which is the prevailing method for monitoring hybridization efficiency.

In order to attach the DNA to the surface, it is necessary to modify the glass substrates. This is currently almost exclusively done with organosilanes. These silanes may contain reactive functionalities, such as amine, epoxide, aldehyde and poly-lysine, which allow the subsequent mild coupling of DNA and other bio-organic moieties to the surface.[5-8] Moreover, silane modification is easy and has been reported to require only several minutes.[9] Organosilane chemistry is compatible with several soft lithographic techniques, including microcontact printing, that allow the fabrication of chemically patterned surfaces.[10,11] However, as these techniques require mechanical contact with the substrate, they cannot be used to pattern enclosed surfaces, such as the inner surface of a microchannel. Photolithography-based techniques would be better suitable to pattern these surfaces. However, silane chemistry is not compatible with constructive photolithography, and photopatterning of a silane monolayer could only be achieved by its local photochemical degradation.[12] Patterning of microchannels has therefore been achieved by local heating-induced[13] or electro-

induced deposition.[14] Alternatively, in the case of in-situ microchannel formation, patterning can be performed using soft lithography prior to surface bonding.[15,16]

Very recently, an alternative method was developed, which does allow the covalent modification of glass surfaces by photolithography.[17] This method is based on a photochemical reaction of 1-alkenes with the silica surface, and is applied in this chapter to provide a proof-of-principle for the local patterning of a microchannel. To this extent, the tailor-made linker 2,2,2-trifluoroethyl undec-10-enoate is photochemically coupled to the microchannel surface. Subsequently, this modified surface is further functionalized with short DNA oligomers, and its stability under hybridization and dehybridization conditions is investigated. Finally, the DNA surface coverage is quantified by measuring the fluorescence emission of hybridization and dehybridization experiments.

4.3 Materials and methods

Chemicals and materials. All chemicals and solvents were purchased from Sigma-Aldrich (the Netherlands) and used without additional purification unless stated otherwise. The chemicals involved for coupling and hybridization experiments were dilutions of 20 × SSC buffer, pH 7 (= 3 M NaCl in 3 M sodium citrate; molecular biological grade, VWR; note: 2 × SSC is a 10 × dilution of this 20 × stock buffer, etc.), Tween-20 and sodium dodecyl sulphate (SDS, Fluka). Dichloromethane (DCM, Fisher) and petroleum ether 40/60 were distilled prior to use. Other used solvents were methanol (HPLC-grade, BioSolve), hydrochloric acid (p.a. 37%, Riedel de Haën), absolute ethanol (Merck), acetone (semiconductor grade, Riedel de Haën) and ultrapure water (18.3 MΩ cm). Synthetic fused silica substrates (10 × 20 mm) used for surface modification were purchased from Praezisions Glas & Optik GmbH (Germany), large diameter synthetic fused silica capillaries (ID = 1 mm, 100 mm length) were obtained from Vitrocom (USA) and fused silica capillaries (ID = 100 μm) with a Teflon® AF fluoro-polymer external coating, TSU100375 were purchased from Polymicro (USA). 2,2,2-Trifluoroethyl undec-10-enoate (TFEE) was synthesized as described elsewhere.[18,19]

DNA probes and targets. The end-modified DNA oligonucleotides used as probes and targets were purchased from IBA GmbH (Germany) and consisted of twenty-one

bases with the following sequence: H2N-(CH2)6-5'- CCA CGG ACT ACT TCA AAA CTA-3'-Cy3. Two targets were used, both were modified at the 5'-end with an amine group, and one was additionally labeled at the 3'-end with Cy3. They are further denoted as "A-NH2" and "ANH2-Cy3". Also two probes were used, one as a positive and the other as a negative control, both labeled at the 3'-end position with Cy5 and Atto488 respectively, referred as "AC-Cy5" and "NC-Atto488". The sequence for the complementary strand "AC-Cy5" was: 5'- TAG TTT TGA AGT AGT CCG TGG-3'-Cy5 and for the non-complementary strand "NC-Atto488": 5'-AGT ATT GAC CTA AGT ATT GAC-3'-Atto 488 was used.

Pretreatment reaction vessels. Prior to use, glassware used for surface modification was cleaned and etched overnight in basic detergent, followed by thorough rinsing with ultrapure water and drying for ≥ 2 hrs at 120 ºC.

Cleaning and hydroxyl formation. A fused silica slide was cleaned by sonication in acetone for 5 min. After drying with argon, the slide was immersed in a freshly prepared 1:1 (v:v) mixture of HCl and methanol for 45 min. The cleaned slide was ready for modification after rinsing with ultrapure water and drying with argon.

The same cleaning procedure was applied for the large diameter fused silica capillaries, but these were additionally dried at 120 ºC for 30 min. Cleaning of small diameter fused silica capillaries was performed by flushing for 20 min at 20 µL/min with the following solvents: acetone, ultrapure water, 1 M NaOH (1 hr), ultrapure water, 1 M HCl, ultrapure water, and acetone, respectively. Afterwards the capillaries were dried with argon.

Surface modification. The modification of a fused silica slide was performed in a specially designed quartz flask as described previously.[17] Neat TFEE (1.5 - 2 ml) was deoxygenated by three consecutive freeze-pump-thaw cycles, after which the liquid was frozen again under argon. The cleaned fused silica sample was immersed, and vacuum was applied again until the TFEE had molten completely and the slide could be immersed. Two low-pressure mercury lamps (254 nm, 6.0 mW/cm2, Jelight, USA) were placed in front of the fused silica slide at a distance of approximately 0.5 cm, and the sample was irradiated for 10 hrs. The setup was wrapped in aluminum foil and kept under a slight argon overpressure during the entire process. After illumination, the sample was removed from the reaction flask and cleaned by rinsing with

petroleum ether 40/60, dichloromethane, and ethanol, respectively. Subsequently, it was sonicated in ethanol and dichloromethane (5 min per solvent), and then finally dried with argon.

The modification of cleaned and dried large diameter capillaries were performed in a glovebox (MBraun MB20G, <0.1 ppm H2O, <0.1 ppm O2) under an argon atmosphere. The capillaries were immersed in 1-hexadecene and covered with a fused quartz microscope slide (Alfa Aesar), followed by irradiation for 10 hrs using two low-pressure UV lamps. Afterwards, the capillaries were cleaned as described above.

Patterning. Patterning experiments of both glass slides as capillaries were performed in a glovebox using degassed TFEE. For patterning of a fused silica slide, the neat alkene was carefully dropped on the surface, until the surface was completely covered with a thin liquid film. Then the mask, an electron microscopy grid (SEM F1, Au, Gilder Grids) was carefully placed on top, followed by a fused quartz cover, which was used to reduce evaporation of the alkene and to absorb any 185 nm light emitted by the mercury lamp. Black paper was put underneath the substrate to minimize light scattering and reflection. A mercury lamp (Jelight) was placed directly above the cover. After irradiation for 10 hrs, the samples were taken out of the glovebox and cleaned as described above.

Patterning of the fused silica capillary was done by filling the capillary with TFEE and capping it on both ends with gas chromatography septa. The capillary was secured with black tape between a support that was covered with black paper and a mask with a window of ~0.5 × 0.5 cm. The fused quartz cover, lamp and illumination time were the same as used in the modification of the silica slides.

Attachment of the oligonucleotides. The DNA oligomers used for the attachment were dissolved in 3 × SSC buffer to a concentration of 5 μM. The modified surface was submerged in the DNA-probe solution for at least 12 h at RT or 24 h at 4 ºC. The solution was refreshed every 4 h in case of the attachment in the capillary or shaken gently in case of attachment on the slide. After modification the samples were rinsed thoroughly with 0.2 × SSC buffer with 0.1% SDS and stored in 3 × SSC buffer at 4 ºC until use. Probe "ANH2-Cy3" was used to visualize the patterning on the surfaces, and the label-free probe was used for hybridization experiments.

Hybridization and dehybridization. ssDNA modified surfaces were pretreated with 3 × SSC buffer prior to hybridization. Hybridization was performed by exposing the surface to a 0.05 μM solution of the complementary probe AC-Cy5 in 3 × SSC buffer. Hybridization inside the modified capillaries was performed by infusing this solution at 1 μl/min for at least 30 min. For control experiments, a 0.05 μM solution of the non-complementary probe NC-Atto488 in 3 × SSC buffer was used instead. After hybridization, the surfaces were washed with 0.1 % SDS in 2 × SSC (wash buffer) to remove any non-specifically bound DNA. Dehybridization was performed by exposing the hybridized surfaces to a solution of 0.1 % Tween 20 in 0.2 × SSC at 65 °C.

Water contact angle measurements. Static contact angle measurements on the TFEE modified surfaces were performed using a Krüss DSA-100 goniometer. 4 μL droplets were dispensed on the surface and the contact angle was determined with a CCD camera using a tangential method.

X-ray Photoelectron Spectroscopy (XPS). XPS analyses were performed using a JPS-9200 photoelectron spectrometer (JEOL). The spectra were obtained under ultrahigh vacuum (UHV) conditions using monochromatic Al Kα X-ray radiation at 12 kV and 25 mA, using an analyzer pass energy of 10 eV. To prevent surface charging during measurements, samples were neutralized with electrons with a kinetic energy of 3.8 eV. Peaks were calibrated using the C1s peak at 285.0 eV as a reference. Spectra were corrected using a linear background subtraction before data analysis.

IR measurements. IR measurements were performed in a nitrogen atmosphere with a Bruker Tensor 27 FT-IR spectrometer equipped with a Bruker Hyperion 1000 FT-IR microscope. The spectra were measured in transmission mode using a spectral resolution of 4 cm-1 and 4096 scans in each measurement. The raw data were divided by the data recorded on a freshly cleaned reference fused silica slide, after which a baseline correction was applied to give the reported spectra.

Density Functional Theory (DFT) Calculations. All calculations were done with the GAUSSIAN03 program.[20] The geometries of the different systems were optimized at the B3LYP/6-311G(d,p) level of theory. Natural bond orbital (NBO) analysis[21] was employed to obtain the core orbital energies.

Confocal Laser Scanning Microscopy. The samples were measured dry or in ultrapure water with a TCS SP2 AOBS Leica confocal laser scanning microscope (Leica

Microsystems, Mannheim, Germany) mounted on an inverted DM IRE2 microscope, using an HC PL FLUOTAR 10.0× objective. The focus median was kept at its maximum for all samples and transmission images were also made for orientation in the fluorescent images. The following settings were kept constant for all measurements, unless stated otherwise: laser intensity (50%), pinhole (200 μm), photomultiplier (600 V), box size (512 × 512 μm), number of scans (8 averaged), scan speed (400 Hz) and zoom factor 1. The argon and He/Ne lasers were utilized to excite the three employed probes at 488 nm (Atto488), 514 nm (Cy3) and 633 nm (Cy5), with an emission range of 500 - 580 nm, 530 - 600 nm, and 640 - 750 nm, respectively. Sequential imaging was applied when necessary. The intensity profiles were made with the ImageJ program after background subtraction.

Fluorescence detection. Hybridization and dehybridization experiments were done online with a Jasco FP-1520 intelligent fluorescence detector equipped with a capillary flow cell (75 μm ID). The time profiles were recorded with a Shimadzu C-R6A Chromatopac integrator. The complementary strand AC-Cy5 was excited at λ = 633 nm and its emission was measured at λ_{max} = 670 nm. The non-complementary strand NC-Atto488 was excited at λ = 488 nm and its emission was measured at λ_{max} = 520 nm.

4.4 Results and discussion

4.4.1 Modification of flat fused silica surface

Figure 4.1 illustrates the chemistry employed for the functionalization of the fused silica surface. Trifluoroethyl undec-10-enoate (TFEE) was used as a linker for several reasons: First, the protected ester group is sufficiently UV-resistant[19] and was not expected to react with the silica surface, which should result in exclusive reaction of the molecule to the surface via its alkene moiety. Second, the trifluoroethyl group is not sterically demanding, which may result in a high surface coverage. In addition, the molecule contains carbon atoms in different chemical environments that can easily be distinguished by XPS after adsorption. Moreover, the fluorine atoms give a strong F_{1s} signal that should disappear after deprotection or nucleophilic reactivity. Finally, the

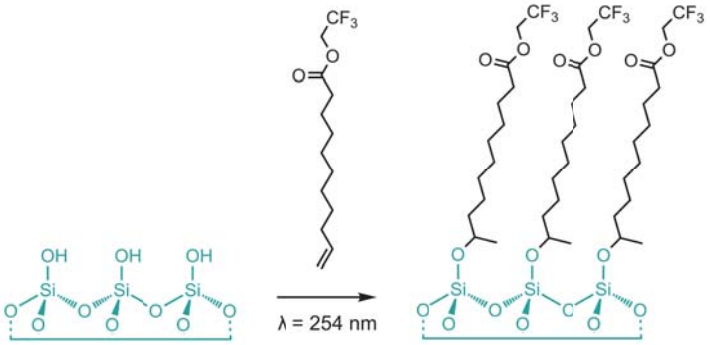

Figure 4.1. Schematic illustration of photochemistry employed for surface modification with TFEE on glass.

trifluoroethyl ester can readily undergo nucleophilic attack by primary amines,[19,22] which gives various opportunities for further surface coupling.

Hydroxyl-terminated fused silica samples were reacted with TFEE by immersion in the neat compound and subsequent UV irradiation at 254 nm for 10 hrs. After cleaning, the modified surfaces were characterized using static water contact angle measurements. A contact angle of 85 ± 1° was measured, which is clearly higher than the contact angle of hydroxyl-terminated silica (<10°), and which is in accordance with previously reported values for TFEE-derived monolayers on Si(111) surfaces.[23] Shorter reaction times resulted in increased variation in the observed contact angles, indicating that the absorbed layer is less homogeneous and that the monolayer formation is incomplete. XPS measurements on the modified samples showed that the elements Si, O, C and F were present at the surface. Together, F and C contributed for 21.0 % to the total signal (see Table 4.1). When compared to a 1-hexadecene monolayer (which also has 16 atoms per adsorbed molecule, but gives a relative contribution of to the XPS signal of 40 %), it seems that this contribution is rather low.[17] While a quantitative comparison would require a proper account of differences in attenuation of the XPS signal,[24] it can qualitatively be stated that the surface coverage of a 2,2,2-trifluoroethyl undec-10-enoate monolayer is somewhat smaller than that of a non-functionalized 1-alkene. Similar observations have been done on silicon, where it was shown that the surface coverage of unprotected carboxylic acid

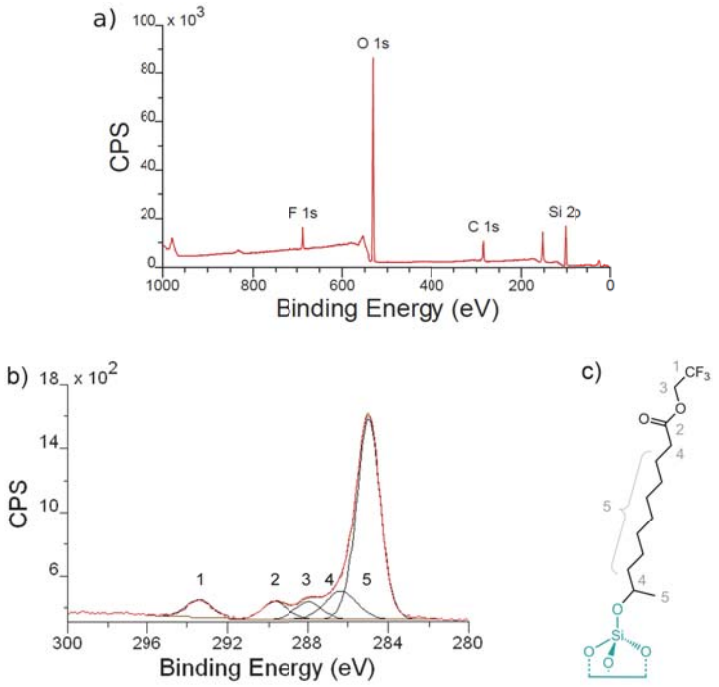

Figure 4.2. XPS analysis of TFEE-modified fused silica. a) Wide area spectrum, b) high-resolution C_{1s} spectrum, c) assignment to the corresponding carbon atoms.

monolayers is maximally 35-40 %,[25] whereas that of alkyl-terminated monolayers can get to 50-55 %.[26]

The F/C ratio on the surface was determined to be 19.3 % (theoretical: 23.1 %), indicating that the trifluoroethyl ester group remains intact after reaction. Further evidence for the intactness of the TFEE comes from the high-resolution C_{1s} spectrum (which resembles that measured for TFEE-modified silicon carbide[27]), which could be fitted with five contributions (Figure 4.2b). These contributions were attributed to the different types of carbon in the trifluoroethyl ester, as shown in Figure 4.2c. DFT calculations (B3LYP/6-311G(d,p) level of theory) on a model of the TFEE-modified surface were performed to qualitatively verify the observed chemical shifts (see Appendix A). The ratios of the carbon contributions (see Table 4.2) accurately match those in the molecule, with the exception of the main contribution at 285.0 eV, which is overrepresented on the surface. Since the ratio between **C**=O and **C**F_3 is 1.0, it

Table 4.1. XPS-based surface composition of trifluoroethyl ester-modified fused silica.

Position (eV)	Assignment	Atom %
523.0	O_s	48.5
285.0	C_{1s}	17.6
688.0	F_{1s}	3.4
102.0	Si_{2p}	30.4

Table 4.2. Deconvolution parameters of the C_{1s} XPS data of trifluoroethyl ester-modified fused silica.

Peak	Position (eV)	Assignment	Intensity ratio	
			Exp.	Theory
1	293.4	CF_3	1.0	1
2	289.7	O-C=O	1.0	1
3	288.0	O-C*H_2-CF_3	1.0	1
4	286.3	C-O-Si + C*H_2-C=O	2.0	2
5	285.0	Alkyl chain	11.1	8

follows that the trifluoroethyl ester remains intact upon attachment to the surface, and thus that the overrepresentation of alkyl carbon atoms cannot be explained by hydrolysis of the TFEE. Therefore, it is most probably caused by adsorption of hydrocarbon contaminants after modification.

Further characterization of the modified surfaces was performed by infrared spectroscopy. As it was not possible to obtain a proper signal with infrared reflection-absorption spectroscopy, measurements were performed in transmission mode. This has the disadvantage that absorptions below 2000 cm^{-1} cannot be observed, due to strong absorption of fused silica in that region and the low signal-to-noise ratio of the available equipment. Therefore, this technique does not allow the observation of the C=O stretching vibration of the ester. Nevertheless, increased CH_2 stretching absorptions could be observed for a TFEE-modified fused silica sample compared to an unmodified reference sample (Figure 4.3), which is in line with adsorption of TFEE. Based on previous studies, in which unfunctionalized 1-alkenes were suggested to be

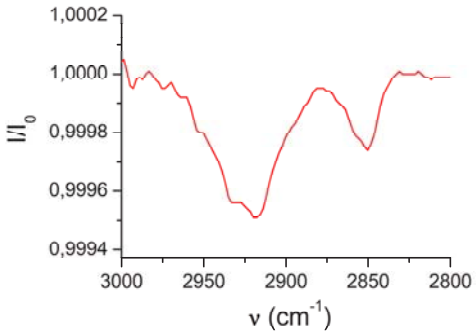

Figure 4.3. CH_2 stretching region of the infrared spectrum of a TFEE-modified fused silica sample.

coupled to the glass surface via Markovnikov addition,[17,28] we would expect to see CH_3 stretching absorptions as well, but we did not observe these clearly, probably due to the low signal-to-noise ratio. The latter also hampers determination of the exact frequency of the CH_2 stretching vibrations, which limits us to draw conclusions on the packing density of the monolayer. However, these positions could be estimated by taking the center of each peak at 75% of its maximum, resulting in values of 2924 and 2855 cm^{-1}, which are indicative for disordered monolayers.[29,30]

In addition to fused silica, we have also performed preliminary experiments on the modification with TFEE of borosilicate glass. UV irradiation of the immersed borosilicate (4 h) resulted in the covalent attachment of TFEE to the surface, as was confirmed with XPS. The XPS spectrum showed the presence of the elements F, C, O, N, Si, and B. Although the F/C ratios were slightly lower than observed for the fused silica surfaces, the high-resolution C_{1s} spectrum could be deconvoluted into five contributions that indicated only marginal hydrolysis (Appendix A). The chemical shifts of these contributions were comparable to those obtained from DFT calculations on the isolated TFEE molecule, with the exception of the carbon atom that is bound to the surface oxygen atom. The reduced F/C ratio is therefore attributed to airborne contaminants. It thus follows that the photochemical method can also be used to modify borosilicate surfaces with ω-functionalized-1-alkenes via concomitant C-O bond formation. Optimization of the reaction conditions may further improve the resulting monolayer quality / packing density on these substrates.

The successful modification of silica surfaces with TFEE allowed further surface functionalization with DNA oligomers. We used single-stranded DNA with a length of 21 bases that was amine-functionalized at the 5'-end and fluorescently labeled with Cy3 at the 3'- end. Adsorption of the DNA was confirmed with fluorescence microscopy, which clearly showed increased fluorescence of DNA-treated surfaces compared to TFEE-modified samples. Extensive rinsing with buffer, at elevated temperatures, in presence of 1 - 10% SDS, 8 M urea, or combinations thereof did not result in removal of the adsorbed species, indicating that the DNA was firmly coupled to the surface. These observations provided a firm basis for the patterning experiments.

4.4.2 Patterning

All patterning experiments were carried out in the dry nitrogen atmosphere of a glovebox. There, the surfaces were covered with a layer of neat TFEE, followed by a mask (Figure 4.4a) and finally by a fused quartz cover. The surface was subsequently illuminated for 10 h with a UV lamp (254 nm), after which the sample was cleaned and immersed into a solution containing the amine-terminated, fluorescently-labeled, single-stranded DNA. After additional cleaning the pattern was visualized with confocal microscopy. The confocal fluorescence image clearly displays the features of the applied mask (Figure 4.4b), and provides a proof-of-principle for the local DNA attachment. The non-negligible background is probably caused by diffraction, scattering and/or internal reflection of the UV light during illumination, which exposes the covered areas of the sample to some UV-light. Nevertheless, the profile histogram (Figure 2c) shows that the fluorescence increases from 20 to 95% over a distance of about 20 μm, confirming that detailed photopatterning of DNA oligomers can be achieved with this reaction.

4.4.3 Modification of fused silica microchannels

To investigate whether the photochemical attachment of 1-alkenes can also be performed on enclosed surfaces, the modification of the inside of a fused silica capillary with 1-hexadecene was studied. This compound was chosen as it enables

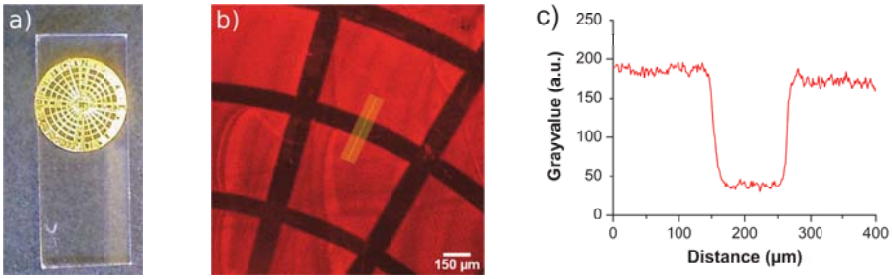

Figure 4.4. (a) Photograph of a fused silica slide that is partially covered with a mask. (b) Fluorescence microscope image of a patterned fused silica surface, after covalent binding of a Cy3-labeled DNA oligomer. (c) The corresponding profile histogram depicts the transition distance between modified and non-modified surface.

evaluation of the degree of modification by determining the corresponding change in contact angle. The latter can be derived from the capillary rise in equilibrium, described by:

$$h = \frac{2\gamma\cos\theta}{(\rho_2-\rho_1)gR} \qquad (1)$$

in which γ = interfacial tension, θ = contact angle between the rising liquid and the capillary, ρ_2 = density of the rising liquid, ρ_1 = density of the surrounding medium, g = gravitational constant and R = inner radius of the capillary. For systems where ρ_1 is negligible, this static height difference h is often referred to as Jurin's height.[31]

The static height difference was studied for both freshly cleaned and modified capillaries (R = 0.5 mm) in a hexane-water system. This system was chosen because the expected height differences are smaller than the length of the capillary (100 mm) and because data on the interfacial tension are available. A freshly cleaned capillary gave a static height difference of 61.0 ± 1.0 mm, which is within experimental error of the calculated value of 60.4 mm for a fully wettable capillary. A modified capillary gave a static height difference of -13.5 ± 1.0 mm, from which a contact angle of 103 º can be calculated. This value is only slightly less than the contact angle of a monolayer

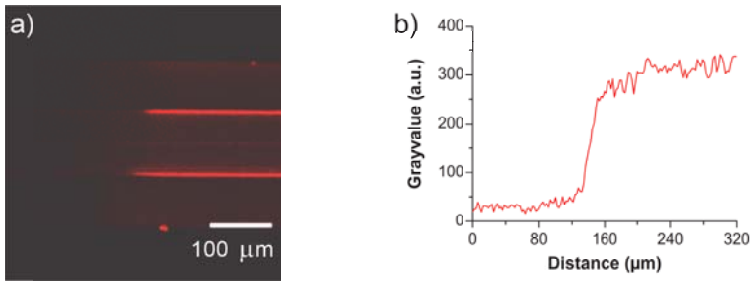

Figure 4.5. a) Confocal image of a patterned capillary with an inner diameter of 100 µm, which was subsequently modified with ANH_2-Cy3 to visualize the transition distance. b) Profile histogram of the boundary of the modified and non-modified capillary surface.

of 1-hexadecene on an exposed surface (105 °),[17] thereby showing the applicability of the photochemical modification method to enclosed surfaces.

As both the capillary modification and the patterning of flat fused silica surfaces were successful, we investigated the patterning of fused silica capillaries with TFEE and the subsequent DNA attachment. Cleaned capillaries were filled with TFEE in the dry nitrogen atmosphere of a glovebox, after which the ends were capped and the capillary was illuminated for 10 h with UV light. This has the evident advantages that 1) this closed system cannot be influenced by possible changes in the surroundings and 2) no reagent can evaporate during the reaction. After extensive cleaning, the capillaries were filled with a buffer containing ANH_2-Cy3 for further coupling. The use of fluorescently labeled DNA was required to allow characterization of the modified capillaries by fluorescence imaging, since these surfaces were unsuitable for characterization with XPS.

As can be clearly seen from Figure 5, this procedure allowed the photochemical patterning of the inner surface of the microchannel, which is (to the best of our knowledge) the first reported site-specific modification and biofunctionalization of such surfaces. The transition distance of the pattern in the capillary (50 µm, Figure 4.5) is less defined than that on the flat surface (20 µm, Figure 4.4), which is probably related to the following geometrical causes: 1) the curvature of the capillary surface, and 2) the presence of a 15 µm thick UV-transparent coating on the outer capillary surface (which is present on commercial capillaries to maintain flexibility and easy

handling). These properties can enhance the scattering of UV-light due to irregularities, and therefore broaden the light-dark transition. Furthermore, the mask used for this proof-of-principle microchannel patterning was not as well-defined as the grid used on the flat surfaces, as it consisted of a piece of black tape manually wrapped around the capillary. Obviously, a less defined mask will also result in a less defined transition. Nevertheless, most of these causes are due to technological rather than chemical flaws, and should be avoidable with more advanced equipment. But even with this simple set-up, the low background fluorescence indicates minimal undesired adsorption of DNA to the unmodified surface. Thus, it was shown that the amino-terminated DNA can be selectively bound to modified capillary wall.

4.4.4 Hybridization and dehybridization experiments

For hybridization and dehybridization experiments, TFEE-modified capillaries were reacted with non-labeled amino-terminated ssDNA. This was done to prevent false fluorescence detection and dye-induced steric hindrance during hybridization. The complementary strain used for hybridization was furnished with a Cy5 label (Figure 4.6), which enabled visualization of hybridization by confocal microscopy and quantification of the amount of dehybridized DNA by fluorescence detection.

By monitoring the hybridization process with confocal microscopy, it was revealed that hybridization mainly took place in the first 30 min of exposure. Therefore, hybridization was performed by infusing AC-Cy5 solution for at least 30 min. The capillary was subsequently washed with washing buffer to remove any non-specifically bound DNA. Finally, hybridized capillaries were dehybridized by eluting detergent solution at elevated temperature. This resulted in a peak in the fluorescence graph (Figure 4.7), from which an average surface coverage of 6.8×10^{11} molecules of DNA/cm^2 was calculated using a calibration curve (see Appendix A). This is similar to the average reported literature values of $\sim 10^{12}$ molecules/cm^2 for DNA microchip technology.[7] Nevertheless, it should be noted that in our set-up, hybridization was performed in just 30 min, whereas other reports required overnight hybridization at elevated temperatures.[2,32,33] As a control, the hybridization cycle was also performed with a non-complementary, fluorescently labeled DNA strand (NC-Atto488), which did

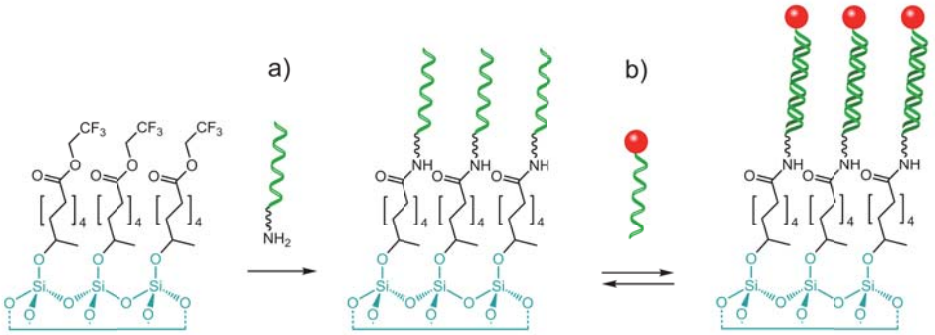

Figure 4.6. DNA coupling and hybridization onto TFEE-modified silica surfaces. a) Coupling of the amine-terminated ss-DNA oligomer to the surface. b) Hybridization and dehybridization with complementary, fluorescently labeled ss-DNA oligomer.

not result in a peak in the fluorescence graph under dehybridization conditions (Figure 4.7). This shows that hybridization is specific for the complementary strand, and that non-specific absorption is negligible.

The hybridization cycle was repeated two times with a recovery time of 30 min between the cycles, after which hybridization was still 78 % of the initial hybridization. Using a prolonged recovery time (12 h in 3 x SSC solution), the hybridization efficiency could be improved to 88%. This diminished hybridization may be explained by several factors. First, the loose packing of DNA at the surface may result in non-specific interactions of the DNA with the surface, especially during dehybridization, which takes place at low salt concentrations.[34] Second, deamination or depurination of the DNA may have taken place.[35] Third, the bond coupling the ssDNA to the surface may have been hydrolyzed.

The latter was investigated by coupling fluorescently labeled ANH2-Cy3 to the capillary inner surface and exposing this to 10 hybridization cycles. Confocal imaging did not show any decrease in fluorescence intensity, thereby confirming that the ssDNA stays firmly bound to the surface under hybridization and dehybridization conditions.

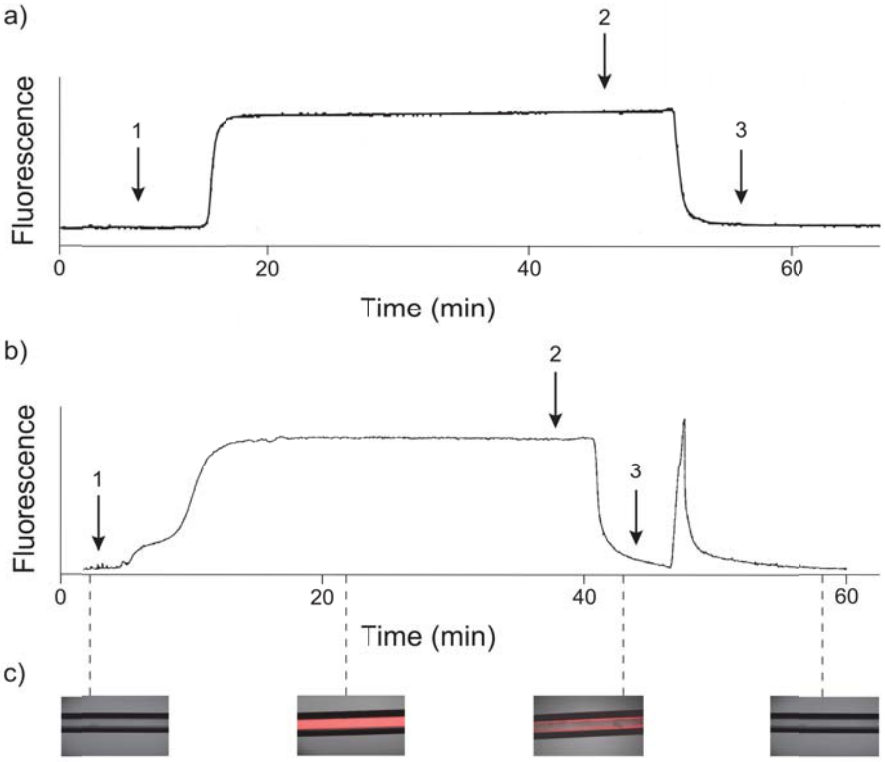

Figure 4.7. Frontal affinity chromatography with online fluorescence detection of a hybridization cycle. a) after infusion of a non-complementary strand, b) after infusion of a complementary strand, and c) corresponding fluorescence overlays. Arrows indicate changes in buffer composition: 1) Addition of fluorescently-labeled DNA, 2) wash buffer, and 3) elution buffer.

4.5 Conclusions

Trifluoroethyl ester-terminated 1-alkenes were covalently coupled to silicon oxide surfaces by UV illumination. These molecules were selectively coupled via their alkene terminus, whereas degradation of the trifluoroethyl ester moiety was negligible under the applied conditions. The photochemical nature of this reaction allowed patterning by means of constructive photolithography. Such site-specific attachment of ω-functionalized-1-alkenes was demonstrated on flat silica substrates, but also on the inner surface of silica microchannels. The resulting activated ester monolayer allows

the mild and localized coupling of primary amines, which was demonstrated by coupling an amine-terminated ssDNA oligomer to the surface. In addition, the selective and reversible hybridization of a complementary DNA strand was demonstrated within a microchannel. The surface coverage of the hybridized complementary DNA was ~7 x 10^{11} molecules/cm^2, which is comparable to other methods. By furnishing target compounds with complementary DNA strands, this method may be used to locally bind proteins, antibodies and other biomolecules to the otherwise inaccessible surfaces.

4.6 References

(1) Ramsay, G. *Nat. Biotechnol.* **1998**, *16*, 40-44.

(2) Seela, F.; Budow, S. *Mol Biosyst.* **2008**, *4*, 232-245.

(3) Schweller, R. M.; Constantinou, P. E.; Frankel, N. W.; Narayan, P.; Diehl, M. R. *Bioconjugate Chem.* **2008**, *19*, 2304-2307.

(4) Zammatteo, N.; Jeanmart, L.; Hamels, S.; Courtois, S.; Louette, P.; Hevesi, L.; Remacle, J. *Anal. Biochem.* **2000**, *280*, 143-150.

(5) Grainger, D. W.; Greef, C. H.; Gong, P.; Lochead, M. J. In *Microarrays Volume 1: Synthesis Methods*; 2nd ed.; Rampal, J. B., Ed.; Humana Press Inc.: Towata, New Jersey, 2007, Chapter 2.

(6) Miyazaki, M.; Kaneno, J.; Kohama, R.; Uehara, M.; Kanno, K.; Fujii, M.; Shimizu, H.; Maeda, H. *Chem. Eng. J.* **2004**, *101*, 277-284.

(7) Pirrung, M. C. *Angew. Chem. Int. Edit.* **2002**, *41*, 1276-1289.

(8) Rusmini, F.; Zhong, Z.; Feijen, J. *Biomacromolecules* **2007**, *8*, 1775-1789.

(9) Jang, L.-S.; Liu, H.-J. *Biomed. Microdevices* **2009**, *11*, 331-338.

(10) Gates, B. D.; Xu, Q. B.; Stewart, M.; Ryan, D.; Willson, C. G.; Whitesides, G. M. *Chem. Rev.* **2005**, *105*, 1171-1196.

(11) Onclin, S.; Ravoo, B. J.; Reinhoudt, D. N. *Angew. Chem. Int. Edit.* **2005**, *44*, 6282-6304.

(12) Sugimura, H.; Nakagiri, N. *Appl. Phys. A-Mater.* **1998**, *66*, S427-S430.

(13) Yamamoto, M.; Yamada, M.; Nonaka, N.; Fukushima, S.; Yasuda, M.; Seki, M. *J. Am. Chem. Soc.* **2008**, *130*, 14044-14045.

(14) Kaji, H.; Hashimoto, M.; Nishizawa, M. *Anal. Chem.* **2006**, *78*, 5469-5473.

(15) Goto, M.; Tsukahara, T.; Sato, K.; Kitamori, T. *Anal. Bioanal. Chem.* **2008**, *390*, 817-823.

(16) Martin, C. R.; Aksay, I. A. *J. Mater. Res.* **2005**, *20*, 1995-2003.

(17) ter Maat, J.; Regeling, R.; Yang, M.; Mullings, M. N.; Bent, S. F.; Zuilhof, H. *Langmuir* **2009**, *25*, 11592-11597.

(18) de Smet, L. C. P. M.; Pukin, A. V.; Sun, Q. Y.; Eves, B. J.; Lopinski, G. P.; Visser, G. M.; Zuilhof, H.; Sudhölter, E. J. R. *Appl. Surf. Sci.* **2005**, *252*, 24-30.

(19) Rosso, M.; Giesbers, M.; Arafat, A.; Schroën, K.; Zuilhof, H. *Langmuir* **2009**, *25*, 2172-2180.

(20) Frisch, M. J.et al. *Gaussian 03,* Revision D.01, **2004**; Gaussian, Inc.: Wallingford, CT.

(21) Glendening, E. D.; Reed, A. E.; Carpenter, J. E.; Weinhold, F. *NBO,* Version 3.1.

(22) Latham, A. H.; Williams, M. E. *Langmuir* **2006**, *22*, 4319-4326.

(23) Strother, T.; Cai, W.; Zhao, X. S.; Hamers, R. J.; Smith, L. M. *J. Am. Chem. Soc.* **2000**, *122*, 1205-1209.

(24) Wallart, X.; de Villeneuve, C. H.; Allongue, P. *J. Am. Chem. Soc.* **2005**, *127*, 7871-7878.

(25) Faucheux, A.; Gouget-Laemmel, A. C.; de Villeneuve, C. H.; Boukherroub, R.; Ozanam, F.; Allongue, P.; Chazalviel, J. N. *Langmuir* **2006**, *22*, 153-162.

(26) Sieval, A. B.; van den Hout, B.; Zuilhof, H.; Sudholter, E. J. R. *Langmuir* **2001**, *17*, 2172-2181.

(27) Rosso, M.; Arafat, A.; Schroën, K.; Giesbers, M.; Roper, C. S.; Maboudian, R.; Zuilhof, H. *Langmuir* **2008**, *24*, 4007-4012.

(28) Mischki, T. K.; Donkers, R. L.; Eves, B. J.; Lopinski, G. P.; Wayner, D. D. M. *Langmuir* **2006**, *22*, 8359-8365.

(29) Porter, M. D.; Bright, T. B.; Allara, D. L.; Chidsey, C. E. D. *J. Am. Chem. Soc.* **1987**, *109*, 3559-3568.

(30) Scheres, L.; Arafat, A.; Zuilhof, H. *Langmuir* **2007**, *23*, 8343-8346.

(31) Jurin, J. *Phil. Trans.* **1717**, *30*, 739-747.

(32) Gong, P.; Grainger, D. W. *Surf. Sci.* **2004**, *570*, 67-77.

(33) Zhang, G. J.; Tanii, T.; Zako, T.; Funatsu, T.; Ohdomari, I. *Sensor Actuat. B-Chem.* **2004**, *97*, 243-248.

(34) Gorodetsky, A. A.; Buzzeo, M. C.; Barton, J. K. *Bioconjugate Chem.* **2008**, *19*, 2285-2296.

(35) Lindahl, T. *Nature* **1993**, *362*, 709-715.

Chapter 5

Organic Modification of Porous Anodic Alumina using Terminal Alkynes

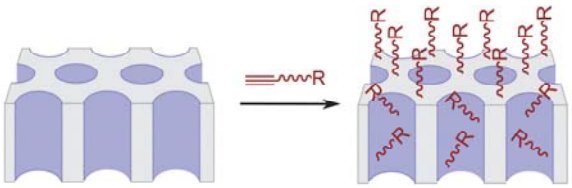

This chapter was published as part of:

ter Maat, J.; Regeling, R.; Ingham, C.J.; Weijers, C.A.G.M.; Giesbers, M.; de Vos, W.M.; Zuilhof, H. "Organic Modification and Subsequent Biofunctionalization of Porous Anodic Alumina Using Terminal Alkynes", *Langmuir* **2011**, *27*, 13606-13617.

5.1 Abstract

Porous anodic alumina (PAA) is a well-defined material that has found many applications. The range of applications towards sensing and recognition can be greatly expanded if the alumina surface is covalently modified with an organic monolayer. Here, we present a new method for the organic modification of PAA, based on the reaction of terminal alkynes with the alumina surface. The reaction results in the formation of a monolayer within several hours at 80 °C and is dependent on both oxygen and light. Characterization with X-ray photoelectron spectroscopy and infrared spectroscopy indicates the formation of a well-defined monolayer, in which the adsorbed species is an oxidation product of the 1-alkyne, namely its α-hydroxy carboxylate. The obtained monolayers are fairly stable in water and at elevated temperatures, as was shown by monitoring of the water contact angle. Modification with 1,15-hexadecadiyne resulted in a surface that has alkyne endgroups available for further reaction, as was demonstrated by the subsequent reaction of 11-azido-3,6,9-trioxaundecyl-trifluoro-acetamide with the modified surface. This shows that the newly developed method is capable of providing the PAA surface with different functionalities, which may be further exploited for sensing and recognition purposes.

5.2 Introduction

Porous anodic alumina (PAA, also referred to as anodic aluminum oxide (AAO) or porous aluminum oxide (PAO)) is an interesting nanostructured material. It is formed upon anodic oxidation of aluminum as an oxide layer that has a well-defined porous structure, in which parallel pores of uniform diameter run perpendicularly to the surface. By optimizing the anodization conditions, the pore diameter can be tuned in the range of 10 to 450 nm. Because of its well-ordered structure, ease of fabrication and good mechanical properties, PAA has found applications in many fields.[1] It has been used as a structural template in the fabrication of carbon nanotubes[2-4] and metal nanowires,[5,6] and as a mold for self-assembly[7] and nanoimprinting.[8] It has also been applied as a membrane for the filtration of proteins[9,10] and in fuel cells,[11] and it has been used as a substrate for cell cultivation.[12] Moreover, PAA has found use as a substrate material in biosensor systems, based on optical waveguide sensing,[13,14] surface plasmon resonance[15] and surface-enhanced Raman spectroscopy.[16,17]

Selective membrane transport and specific detection in biosensors require a robust and flexible functionalization of the PAA. This can be achieved by modifying the alumina surface with an organic monolayer. In recent years, there have been reports on the surface modification of alumina using organosilanes,[18-24] carboxylic acids,[25-30] and phosphonic acids[31-33] as anchoring groups. While all these methods modify the surface properties effectively, each of these surface chemistries has its own disadvantages. Organosilanes do not form high-quality monolayers on alumina, i.e. the packing density and stability of these monolayers is limited compared to those of organosilane monolayers on other substrates, such as silica.[28,34,35] Carboxylic acids do form densely packed monolayers on alumina, but their dynamic nature results in relatively easy desorption and exchange.[25] Monolayers of phosphonic acids on alumina are promising, as these are densely packed and highly stable.[34] However, reports on this type of modification are limited and are usually restricted to alkyl-terminated surfaces, although recently also carbohydrate-terminated phosphonate monolayers have been reported.[36] Therefore, unlike on other substrates, it seems that there is currently no generally preferred monolayer chemistry on alumina.

The limited progress in the surface modification of alumina may primarily be due to the lack of compatible functional groups, precisely owing to the high reactivity of the

alumina surface. Alumina has surface sites of different character, including Brønsted acid, base, nucleophilic and Lewis acid sites. These form the basis of its use as a catalyst in many reactions, such as elimination, addition and condensation reactions.[37,38] In a typical catalytic cycle, compounds are first adsorbed onto the alumina, then converted into the reaction product, and finally desorbed. Detailed studies of the adsorption of numerous compounds have been performed in the past, with the aim of understanding the catalytic behavior of alumina. Yet in the current study we aimed for stable monolayer formation, by using materials that could perhaps be transformed in a well-defined manner upon adsorption, but which would not be released afterwards.

In view of our recent success in the modification of silica with 1-alkenes,[39-41] we became interested in the adsorption of unsaturated hydrocarbons onto alumina. It has been reported that ethene can adsorb onto η-alumina, thereby forming surface ethyl groups.[42] Alternatively, longer 1-alkenes were shown to bind to plasma-grown alumina via a Lewis base interaction with the surface aluminum cations.[43] This seemingly contrasting behavior may result from the use of different types of alumina, which may expose different surface sites. This also applies to the chemisorption of alkynes. Acetylene was found to interact strongly with basic Al-OH groups, resulting in an adsorbed species that is attached perpendicularly to the surface plane.[44,45] Weaker adsorption was also observed, resulting in a species that is bound parallel to the surface.[43,44] Furthermore, acetylene and 1-alkynes was shown to form reduced and even polymerized species on the alumina surface.[43,46,47] Finally, acetylene and ethene were found to form multiwalled carbon nanotubes inside porous alumina at high temperatures.[3,48]

Despite all these studies, the adsorption of unsaturated hydrocarbons onto alumina has not been investigated in relation to surface modification of the PAA. In this proof-of-principle study, we report on the modification of porous alumina surfaces with 1-alkynes, and characterize the modified surfaces using static water contact angle measurements, infrared spectroscopy and X-ray photoelectron spectroscopy (XPS). We show that this class of compounds can form a monolayer onto the alumina (Figure 5.1), we investigate the structure of the adsorbate, and study the hydrolytic stability of

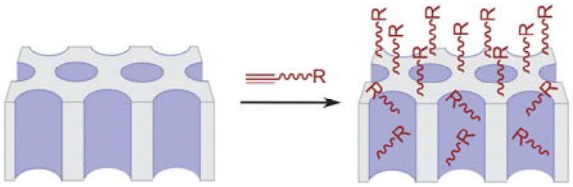

Figure 5.1. Covalent attachment of 1-alkynes onto porous alumina.

the modified surfaces by immersing them in de-ionized water. Finally, using 1,15-hexadecadiyne as a reagent, we demonstrate that functional surfaces can be obtained which are reactive towards azides.

5.3 Materials and methods

Materials. Glassware used for surface modification was cleaned with organic solvents and etched overnight in 10 % KOH solution. Before use, it was rinsed with ultrapure water and dried at 120 ºC. Chemicals were obtained from Sigma-Aldrich unless stated otherwise. Porous anodic alumina samples (36 × 8 mm, Anopore™) with an average pore size of 200 nm, were obtained from Whatman Scientific. 1-Hexadecyne was synthesized from 1-bromotetradecane and lithium acetylide ethylene diamine complex as described elsewhere,[49] and purified by column chromatography and vacuum distillation. 1,15-Hexadecadiyne was synthesized similarly from 1,12-dibromododecane and was purified by recrystallization and vacuum distillation. Hydrochloric acid (37 %, analytical grade) was obtained from Acros. Solvents used were either of analytical grade or distilled prior to use. NMR spectra were recorded on a Bruker Avance III 400 spectrometer. HRMS data were collected on an Exactive high resolution MS (Thermo Scientific) equipped with an ESI probe.

Synthesis of 11-azido-3,6,9-trioxaundecyl-trifluoro-acetamide (1). 11-Azido-3,6,9-trioxaundecan-1-amine (1.16 g, 5.3 mmol) and triethylamine (0.61 g, 6.1 mmol) were dissolved in dry dichloromethane. The solution was cooled to 0 °C and trifluoroacetic anhydride (0.81 ml, 5.8 mmol) was added. The solution was stirred for 2 h at 0 °C, allowed to attain room temperature and stirred for 1 h. The mixture was concentrated under reduced pressure and purified by column chromatography

(eluens: ethyl acetate) to afford **1** as a pale yellow liquid (0.79 g, 2.5 mmol, 48% yield). ^{1}H NMR (400 MHz, $CDCl_3$): δ 7.20 (broad, 1H, NH), 3.69 (m, 12H, CH_2O), 3.54 (m, 2H, $C\underline{H}_2NH$), 3.37 (t, 2H, CH_2N_3, *J* = 5.2 Hz). ^{13}C NMR (100 MHz, $CDCl_3$): δ 157.2 (q, *J* = 37 Hz), 115.9 (q, *J* = 286 Hz), 70.7, 70.6, 70.5, 70.3, 70.0, 68.6, 50.7, 39.7. HRMS: *m/z* 313.1122, calculated for $C_{10}H_{16}F_3N_4O_4$ ($[M-H]^-$): 313.1118.

Surface modification. The neat modifying agent (~2 ml) was added to the reaction flask and was subsequently frozen with liquid N_2. A porous anodic alumina substrate was cleaned by sonication in acetone (5 min) and ultrapure water (5 min). The substrate was then immersed for 30 min in a freshly made 1:1 (v:v) mixture of 37% hydrochloric acid and methanol. Afterwards, it was rinsed and sonicated (5 min) with ultrapure water and then with methanol. The cleaned substrate was transferred to the flask containing frozen modifying agent. In order to dry the sample, the pressure was decreased to ~ 15 mbar until the modifying agent was molten completely and the substrate was immersed, after which the flask was filled with argon and kept under a slight overpressure at the desired temperature for the desired reaction time. Following the reaction, the substrate was removed from the flask, rinsed copiously with dichloromethane, sonicated in ethanol and dichloromethane (5 min per solvent), and finally dried in air.

2-Hydroxy hexadecanoic acid-modified surfaces were prepared similarly, but were rinsed in ethanol instead of methanol, and immersed in a (non-frozen) 1 mM solution of 2-hydroxy hexadecanoic acid in ethanol at 65 °C for 16 h.

Secondary modification. Reactions on the 1,15-hexadecadiyne-modified substrates were performed with 11-azido-3,6,9-trioxaundecyl-trifluoro-acetamide using the Cu(I)-catalyzed azide-alkyne cycloaddition (CuAAC). Two equivalents of copper sulfate were added to a reaction tube containing a solution of the azide in water (1 eq). The tube was also equipped with a stirring bar and a platform. The alkyne-terminated substrate was immersed and placed onto the platform, which protected the fragile PAA from the stirring bar. Adsorbed air bubbles were removed by sonication. To generate Cu(I), two equivalents of sodium ascorbate were added, resulting in a final azide concentration of 0.1 mM. The reaction tube was then placed in a microwave oven (CEM Discover), set to operate at 70 ºC for 30 min under

continuous stirring. Following the reaction, the substrate was copiously rinsed with water, then sonicated in water, ethanol and dichloromethane (5 min per solvent), and finally dried in air. Modified samples were cut into four pieces, thereby reducing the sample size to ~ 9 × 8 mm.

Water contact angle measurements. Static contact angles were measured using a Krüss DSA-100 goniometer. Droplets of 3 µl were dispensed on the surface and contact angles were measured with a CCD camera using a tangential method. The reported value is the average of at least 5 droplets and has a standard deviation typically smaller than ± 2º.

Infrared spectroscopy. IR spectra were obtained with a Bruker Tensor 27 FT-IR spectrometer in transmission mode. Spectra were collected using a spectral resolution of 2 cm^{-1} and 256 scans in each measurement. The raw data were divided by the data recorded on a freshly cleaned reference substrate.

X-ray Photoelectron Spectroscopy. XPS analyses were performed using a JPS-9200 photoelectron spectrometer (JEOL). The spectra were obtained under ultrahigh vacuum (UHV) conditions using monochromatic Al Kα X-ray radiation at 12 kV and 25 mA, with an analyzer pass energy of 10 eV for narrow scans and 50 eV for wide area scans. The X-ray incidence angle and the electron acceptance angle were 80º and 10º to the surface normal, respectively. To prevent surface charging during measurements, samples were irradiated with electrons with a kinetic energy of 3.0 eV. Peaks were shifted using the C_{1s} peak at 285.0 eV as a reference. Spectra were corrected using background subtraction (linear or Tougaard) before quantification and any peak deconvolution. Peaks were deconvoluted using GL(30) line shapes (Gaussian/Lorentzian product formulas with 30 % of Lorentzian weight).

Determination of attenuation lengths. Electron attenuation lengths (EALs) were determined using the NIST Electron Effective-Attenuation-Length database.[50] In this program, electron inelastic mean free paths (IMFPs) were determined using the TPP-2M equation.[51] This required input of the density as well as of the bandgap of the 1-hexadecyne adlayer. For both parameters, the values of (low-density) polyethylene, 0.92 g/cm^3 and 8.8 eV, respectively, were used. The uncertainty in the attenuation length is mainly dependent on the uncertainties in the calculated IMFP, the transport mean free path and the transport approximation,[50] amounts to ca. 20 %.

5.4 Results and discussion

When a cleaned PAA substrate was immersed in neat 1-hexadecyne, it became increasingly hydrophobic. The hydrophobic properties were retained after sonication in several organic solvents and after extensive Soxhlet extraction in 1,2-dichloroethane. This indicates that the 1-hexadecyne chemically adsorbs to the alumina, forming a hydrophobic layer.

5.4.1 Temperature dependence

The influence of temperature on the chemisorption process was studied by varying the reaction temperature from 20 to 120 °C. The temperature was not increased further, since at 120 °C slight coloration of the 1-hexadecyne was observed, indicating the occurrence of side reactions. After 16 h of immersion in 1-hexadecyne at the desired temperature, the surface hydrophobicity was assessed by means of static water contact angle measurements. Since the two sides of the PAA differ in pore size and surface roughness, both sides were measured. These measurements showed that 1-hexadecyne readily reacts with porous alumina, as the initially hydrophilic alumina surface became hydrophobic already after immersion at room temperature. Performing the reaction at elevated temperatures (≥ 60 °C) yielded even more hydrophobic surfaces, with a maximum contact angle of 139° for the rough side and 137° for the smooth side of the PAA substrates, respectively (Figure 5.2a). These high contact angles are typically found for nanostructured, hydrophobic surfaces and correspond to values reported for self-assembled monolayers of hexadecanoic acid on porous alumina.[29]

The same set of samples was characterized with infrared spectroscopy (IR, Figure 5.2b). While the IR spectra showed several features (vide infra), the main absorption was due to C-H stretching vibrations. In this region, the spectra of samples modified at 20 and 40 °C were practically overlapping. Raising the reaction temperature to 60 °C led to increased absorption, showing that more 1-hexadecyne had reacted with the surface. Further increase of the reaction temperature only slightly increased the C-H absorption and the maximum absorption was obtained at 80 °C, with identical intensities as obtained at 100 and 120 °C (data not shown).

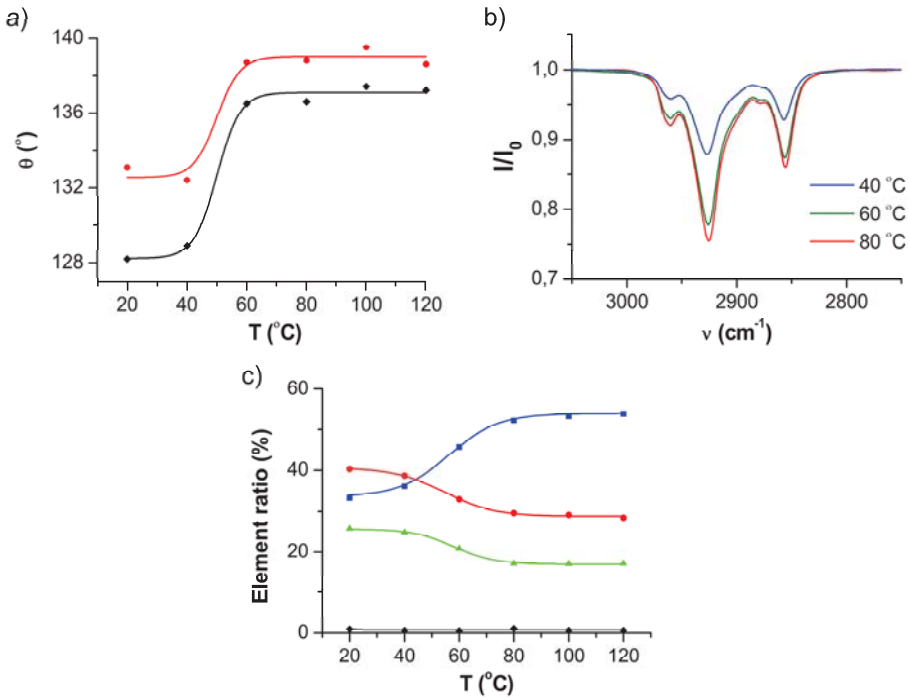

Figure 5.2. Characterization of porous alumina modified with 1-hexadecyne for 16 h at different temperatures: (a) Static water contact angle measured on both smooth (◆) and rough (●) side of PAA, (b) Infrared C-H stretch region and (c) Surface composition determined from XPS C_{1s} (■), O_{1s} (●), Al_{2p} (▲) and P_{2s} (◆) signals. The lines in (a) and (c) serve as a guide to the eye.

In addition, the surface composition of the modified samples was studied with XPS. Electron emissions due to C, O, Al and P atoms could be detected. Phosphorus was only present at small concentrations (~1 %), and has likely been introduced during the anodization process, which is usually performed in phosphoric acid solution. In all samples, the ratio of O to Al was somewhat larger than 1.5, as was expected for the non-stoichiometric PAA used. Furthermore, all modified samples contained significantly more carbon than unmodified samples, which confirms the hydrocarbon adsorption. On the surface of the unmodified samples ≤ 10 % of the total signal was due to carbon, likely originating from contaminations introduced during PAA

fabrication. In modified samples, the amount of carbon at the surface was found to increase with reaction temperature, from 33 % at 20 °C to 53 % at temperatures of 80 °C and higher (Figure 5.2c).

The data obtained by the different characterization techniques are in agreement and show that 1-hexadecyne already reacts with porous alumina at room temperature, and that maximum adsorption is obtained at temperatures of 80 °C and higher. Based on the attenuation of the XPS O_{1s} signal, information can be derived on the adsorbed layer thickness. For a flat oxide surface with a single hydrocarbon adlayer, the thickness of this layer can be calculated using:

$$I_O = I_O^{\infty} exp\left(\frac{-d}{\lambda_{O,C}\cos\theta}\right) \quad (1)$$

with I_O = absolute oxygen peak intensity, I_O^{∞} = absolute oxygen peak intensity of an unmodified, cleaned substrate, d = thickness of the adsorbed layer, $\lambda_{O,C}$ = attenuation length of O_{1s} electrons in the hydrocarbon layer, and θ = electron take-off angle. However, from geometrical considerations following from the porosity of the PAA, as well as from our experimental setup, it follows that calculated values for d using equation 1 will only yield an upper limit for the true layer thickness (see Appendix B). We calculated $\lambda_{0,C}$ to be 3.5 nm using the NIST Electron Effective-Attenuation-Length database.[50] Based on this value and the O_{1s} intensities of the different samples, equation 1 yielded an adlayer thickness of 2.6 nm after 16 h of modification at 80 °C. Since this is only slightly higher than the length of a 1-hexadecyne molecule (1.9 nm, as determined with Chem3D), and as we indicated that the layer thicknesses obtained from equation 1 are overestimated, the adsorbed layer is at least predominantly a monolayer.

5.4.2 Progress of the attachment reaction

The reaction progress at 80 °C was studied with the same set of techniques (Figure 5.3). Hydrophobic samples were already obtained within 5 min of reaction, as was shown by the rise of the water contact angle from < 10° to 130° and 135° for the smooth and rough side, respectively. After this initial steep increase, the contact angle

increased only slightly with time. This is most obvious from the contact angle data measured on the smooth side, which is best defined and therefore shows less variation. These data also show that after 4 h the reaction is not yet complete, as the contact angle is still slightly lower than after 16 h of reaction. This is in accordance with the self-assembled monolayer formation of e.g. thiols on gold or alkynes on hydrogen-terminated silicon,[52] which is initially very fast, but then requires several hours to complete.[53]

The XPS data (Figure 5.3c) are in excellent agreement with the contact angle data: The relative C_{1s} ratio shows an initial steep rise and then slowly increases with reaction time. Similarly, the relative C_{1s} signal after 4 h of adsorption is still smaller than after 16 h of adsorption. Infrared spectroscopy (Figure 5.3b) also confirms that the majority of the hydrocarbon adsorption takes place within the first hour. On the other hand, it shows that the methylene stretching absorptions after 4 and 16 h have similar intensities, which contrasts with the contact angle and XPS results. Yet this may be explained by the lack of surface sensitivity of transmission IR measurements compared to XPS and contact angle measurements. Thus, the results indicate that after 4 h the reaction is complete within the pores, but still proceeds at the outer surface of the PAA. While this may reflect differences in the chemical structure of the outer versus the inner surface, the limited data available does not allow us to draw any definitive conclusions.

The precise position of the CH_2 stretching vibrations provides information on the order in the obtained monolayer. With increasing reaction time ν_{as} decreases, but only slightly: from 2927 to 2925 cm^{-1}; similarly, ν_s decreases from 2857 to 2856 cm^{-1}. Both shifts are in line with the increase in packing density concomitant with monolayer formation, while the end values clearly indicate the formation of a disordered monolayer.[54,55]

5.4.3 Investigation of surface structure

In addition to the methyl and methylene C-H stretching absorptions, the infrared spectrum of modified porous alumina shows several other features (Figure 5.4). Superimposed to these features is an oscillation that is attributed to internal reflections and/or optical effects caused by the well-aligned nanopores.

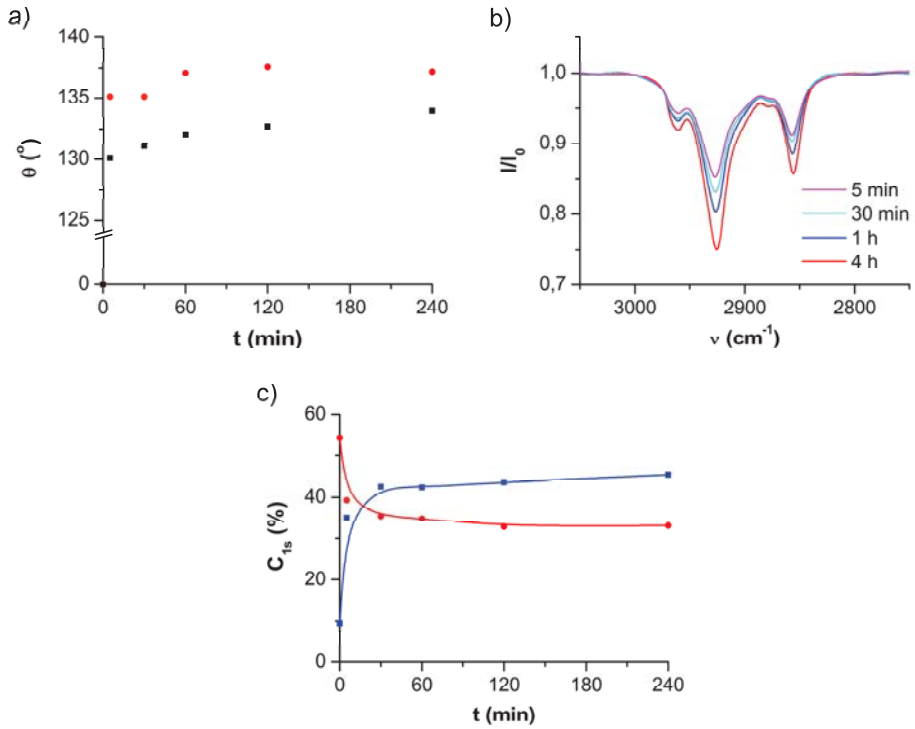

Figure 5.3. Characterization of PAA modified with 1-hexadecyne at 80 °C and varying reaction times: a) Static water contact angle measured on smooth (◆) and rough (●) side of PAA, b) Infrared ν_{CH2} region, and c) Surface composition determined from XPS C_{1s} (■), O_{1s} (●), Al_{2p} and P_{2s} signals. The continuous lines in c) serve as a guide to the eye.

The methylene C-H bending absorption at 1465 cm^{-1} can clearly be observed. Furthermore, there is a broad negative absorption in the range of 3750 – 3000 cm^{-1}, i.e. the O-H stretching region. This can partially be attributed to reduced absorption of surface hydroxyl groups on the modified surface, which are known to absorb at 3800 – 3590 cm^{-1},[56] thereby indicating that these bonds were consumed in the reaction. In addition, the negative absorption in the O-H stretching region shows that the 1-hexadecyne-modified alumina contains less adsorbed water than the unmodified reference sample, which can be explained by its hydrophobic nature. The intensity of the absorption in this region showed sample-to-sample variation, presumably due to slight differences in sample thickness. The most striking feature in the IR spectrum,

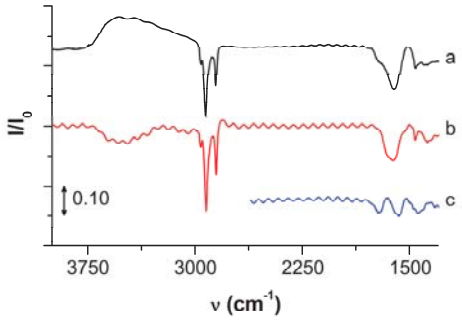

Figure 5.4. Infrared spectra of PAA after modification with 1-hexadecyne (a), 2-hydroxy hexadecanoic acid (b), and the residual spectrum obtained by subtracting (b) from a (c).

however, is the strong and broad absorption peak at 1610 cm^{-1}, which also shows a shoulder at 1720 cm^{-1}. As this absorption is not present in the IR spectrum of 1-hexadecyne, it must result from the surface coupling. Finally, there is another absorption near 1400 cm^{-1}.

Additional information was obtained from high-resolution XPS measurements. These show that the 1-hexadecyne-modified alumina contains three types of carbon, with binding energies of 285.0, 287.0 and 289.1 eV, respectively (Figure 5.5). The ratio between these three contributions is 14 : 1 : 1, which implies that per adsorbed 1-hexadecyne molecule, two carbon atoms display an increased oxidation level. Additionally, the highly reproducible observed stoichiometry indicates that the surfaces are modified with a single surface species only.

While several options can be considered for the nature of the adsorbed species, the IR and XPS data set is most consistent with an alkyl carboxylate with a hydroxy functionality at its α-position (R-CHOH-COO(-)) that is coordinatively bound to the alumina surface. This becomes most evident from comparison with the XPS spectra of poly-L-lactic acid,[57] and the IR spectrum of aluminum lactate.[58] In addition, the C_{1s} XPS spectrum can be simulated using a B3LYP/6-311G(d,p)-derived method[59] on simplified structure models (Figure 6b). These predict that C_{1s} electrons arising from the hydroxylated and carboxylated carbon show up at 287.6 and 289.4 eV, respectively, which is in good agreement with the experimental data of 287.0 and 289.1 eV (see Appendix B).

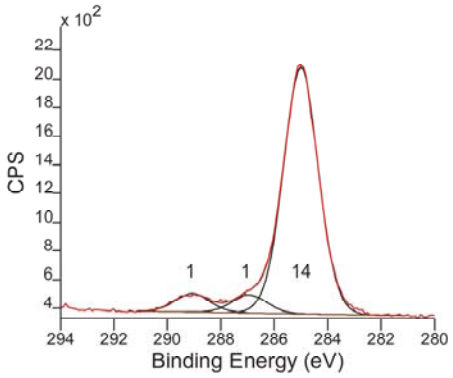

Figure 5.5. X-ray photoelectron spectrum of the C_{1s} region of 1-hexadecyne-modified PAA and its deconvolution.

Further support comes from experiments in which 2-hydroxy hexadecanoic acid (2-HHA) was directly adsorbed onto the alumina. This compound was shown to self-assemble onto platinum and pyrex as early as in 1946,[60] but its self-assembly on inorganic surfaces has not been systematically studied afterwards. Adsorption of 2-HHA onto PAA from ethanolic solution yields a hydrophobic surface (contact angle 137°). The IR spectrum of this modified surface is given in Figure 5.4b and shows strong resemblance to that of 1-hexadecyne-modified PAA (Figure 5.4a). The broad bands at 1620 and 1375 cm^{-1} can be attributed to asymmetric and symmetric stretching vibrations of the surface-bound α-hydroxy carboxylate. Interestingly, the absorption of the 1-hexadecyne-modified surface exceeds that of the 2-HHA-modified surface everywhere in the region of 2000-1300 cm^{-1}, i.e. the region that harbors the surface bond-related bands. Subtraction of the former from the latter yields a residual spectrum with absorptions at 1720, 1580 and 1450 cm^{-1} (Figure 5.4c). These absorptions can be attributed to the C=O stretching vibrations of the undissociated acid, and to the symmetric and asymmetric stretching vibrations of a surface-bound carboxylate (without α-hydroxyl participation), respectively. Although several interpretations are possible, such absorptions can arise from (partially) desorbed α-hydroxy carboxylate, and their presence may therefore support the proposed structure.

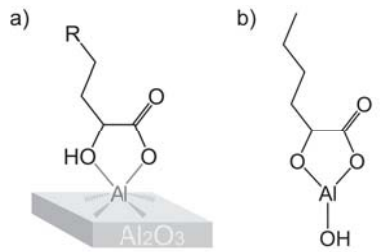

Figure 5.6. (a) Schematic representation of the binding of an α-hydroxy-carboxylate to the alumina surface, resulting from the oxidative adsorption of a terminal alkyne, and (b) simplified model used for the theoretical calculation of XPS data.

The IR spectrum can also provide information on the surface binding mode. For metal carboxylates, Deacon has shown that there is a correlation between the difference in symmetric and asymmetric CO_2^- stretching frequencies Δ and the bond type.[61] For Δ > 170 cm^{-1}, this correlation predicts that the carboxylate forms a covalent monodentate with the metal ion. For aluminum lactate, in which the carboxylate is known to bind as a covalent monodentate,[58] Δ = 210 cm^{-1}, which is in accordance with the correlation. In the spectrum of 2-HHA-modified PAA, Δ is found to be even higher: 245 cm^{-1}. This strongly indicates that the carboxylate binds to the surface as a covalent monodentate. Since the IR spectrum of the 1-hexadecyne-modified PAA is highly similar to that of the 2-HHA-modified surface, it follows that this monolayer is predominantly bound by covalent interactions as well.

Further support on the proposed structures arises from the XPS spectrum of the 2-HHA-modified surface (see Appendix B), which is also very similar to that of the 1-hexadecyne-modified surface. The wide area spectrum shows the same elements (C, O, Al and P), with a similar relative carbon concentration (53 %, compare with Figure 5.2c). Moreover, the high-resolution C_{1s} spectrum can also be deconvoluted in three components. These have a relative ratio of 1 : 1 : 19, and are positioned at 289.2, 286.8 and 285.0 eV, respectively (the overexpression of the 285.0 eV component is likely due to contamination of the XPS system). This deconvolution is nearly identical to that of Figure 5.5, and thus further supports the formation of adsorbed α-hydroxy carboxylate species during the modification of PAA in 1-hexadecyne.

While the route towards formation of such oxidized species derived from terminal alkynes does not seem straightforward, oxidation of such electron-rich compounds on PAA is not only well-known, but also highly likely in the presence of oxygen and light. In fact, the rigorous exclusion of either oxygen or light results in surfaces that display incompletely oxidized species. It may indeed well be that more than one type of oxidation product is formed: the oxidation of 1-alkynes has been shown to form α,β-unsaturated aldehydes, α-oxo-aldehydes and carboxylic acids, amongst others.[62-65] However, as most of these products will desorb from the surface again (either spontaneously or by competition), the species that can form stable interactions with the alumina are likely to accumulate. This will eventually yield a well-defined monolayer of a single species, the α-hydroxy carboxylate.

5.4.4 Influence of oxidation parameters

As it is likely that the mechanism involves oxidation, the question is raised whether dissolved oxygen and/or surface oxygen play a role in this process. Therefore, we first performed the surface modification under oxygen-free conditions, by rigorously degassing the 1-hexadecyne with three freeze-pump-thaw cycles and working in an argon atmosphere. This still resulted in monolayer formation, but the XPS high-resolution C_{1s} spectrum could not be properly deconvoluted into three contributions in a 1 : 1 : 14 ratio anymore, indicating the presence of multiple species. This suggests that the oxidation was incomplete in this case, underlining a crucial role for dissolved oxygen species in the oxidation of 1-alkynes. Second, the role of surface oxygen atoms was investigated by performing the reaction on a different alumina substrate. α-Alumina is the most stable form of alumina and it has a defined stoichiometry (Al_2O_3). This differs from porous anodic alumina, which is partially hydroxylated and thus is relatively oxygen-rich. The reactivity of α-alumina is dependent on the exposed face, as this determines the amount of hydroxyl groups on the surface. Modification on the least reactive <0001> face with 1-hexadecyne resulted in a contact angle of 78º, while on the more reactive <1$\dot{1}$02> face a contact angle of 92º was measured. Thus, modification of α-alumina did not yield highly hydrophobic surfaces, indicating a reduced reactivity of α-alumina compared to PAA. The observed difference may relate

to differences in surface hydroxylation. As PAA is relatively oxygen-rich and shows increased hydrocarbon adsorption, this supports the role of surface oxygen in the adsorption and oxidation of alkynes on alumina. In short: both dissolved O_2 and surface-bound oxygen are important.

In addition to oxygen, the reaction was also found to be dependent on the presence of light. When a porous alumina surface was modified in the dark, the corresponding IR spectrum showed decreased absorptions intensities, together with an additional absorption at 1508 cm^{-1}. In addition, the sample became slightly colored during modification. Such features have been explained by the formation of alkenyl carbenium ions.[66] Light-induced oxidation is therefore likely a predominant reaction step in the formation of these stable monolayers.

5.4.5 Stability of modified alumina

The stability of modified surfaces is dependent on both the stability of the surface bond as well as on the stability of the substrate itself.[67,68] Since alumina is stable under strong acidic and basic conditions, even up to high temperatures, the stability of the surface bond is likely to be limiting. The stability was tested in two ways: First, the modified surfaces were exposed to condensing 1,2-dichloroethane (b. p. 84 °C) in a Soxhlet extraction setup. No deterioration of the adsorbed layer could be observed after 3 h, showing that the monolayers are stable in the mild temperature regime. Secondly, hydrolytic stability was tested by immersion of 1-hexadecyne-modified surfaces in water and monitoring their water contact angle with immersion time. Under these conditions, the adsorbed layer did deteriorate, but the rate was slow: after 2 h of immersion, the contact angle on the rough side decreased from 139 to 125° (Figure 5.7). After this initial decrease, the contact angle did not further change even up to 24 h of immersion, i.e. the surface remained hydrophobic. For comparison, porous anodic alumina was also modified with 1-hexadecene. This resulted in hydrophobic surfaces with similar contact angle (138°) and relative XPS carbon content (49 %) as 1-hexadecyne-modified surfaces. However, the 1-alkene-modified surfaces were completely hydrolyzed within 90 min after immersion in water, which shows that 1-alkenes and 1-alkynes yield surface-bound species that are structurally

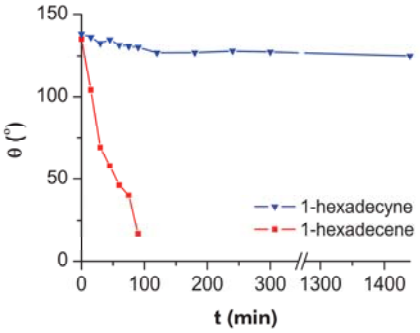

Figure 5.7. Stability of modified PAA upon immersion in water as measured by its water contact angle.

different. The relatively high stability of 1-alkyne-modified surfaces confirms alkyne chemisorption, whereas 1-alkenes may either only physisorb or form less and/or less stable bonds to the alumina surface.

5.4.6 Functionalization of modified porous alumina.

Alumina surfaces with a wide range of functionalities may be obtained using ω-functionalized 1-alkynes as a reactant. By studying the adsorption of several ω-functionalized alkanes, we pursued to find compatible functional groups. However, many functional groups (e.g. alkenes, aldehydes, alcohols, thiols) are reactive towards the porous alumina surface, as was indicated by IR and contact angle measurements. From these initial tests, it followed that 1-alkylamines hardly chemisorb to the alumina surface. Unfortunately, the reaction of 10-undecyn-1-amine with porous alumina did only proceed to a very small extent. This can be explained by the reversible adsorption of amines onto alumina surfaces. If this process is kinetically favored over the adsorption of alkynes, the reactive sites will be blocked, preventing the latter reaction to occur. During washing steps, the amine will desorb from the surface again, leaving most surface sites unreacted.

An approach to prevent the reactive amine groups from adsorbing is to protect them. Many protective groups are available, which usually contain an oxycarbonyl compound, that can be removed hydrolytically in a later stage. However, as alumina is

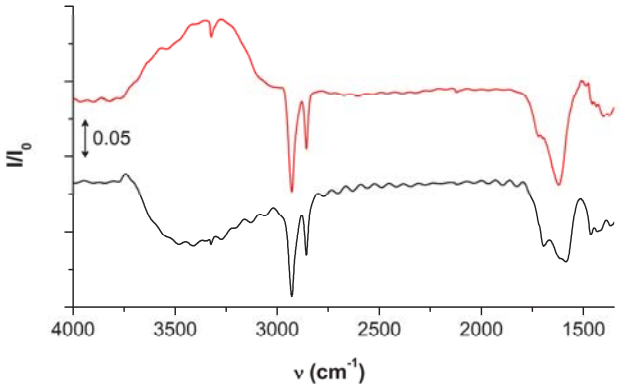

Figure 5.8. Infrared spectrum of PAA modified with 1,15-hexadecadiyne (top) and after subsequent reaction with 11-azido-3,6,9-trioxaundecyl-trifluoro-acetamide (bottom).

known to catalyze transesterifications, we avoided these compounds and decided for phthalimide protection instead. The formation of undecynyl phthalimide-derived monolayers was successful, but deprotection proved repeatedly troublesome, as the reductive deprotection conditions (due to the use of hydrazine or $NaBH_4$) resulted in partial desorption.

Therefore we decided to use α,ω-dialkynes instead. 1,15-Hexadecadiyne was synthesized and used to modify the porous alumina surface. Characterization with XPS showed that the relative contribution of carbon to the spectrum was 50 % on these surfaces, which was somewhat less than on surfaces modified with 1-hexadecyne (53 %). However, no significant backfolding of the hydrocarbon chains could be detected, as the high resolution C_{1s} spectrum still showed three contributions with a 14 : 1 : 1 ratio. Moreover, characterization by IR spectroscopy revealed absorptions due to C≡C stretching (2120 cm^{-1}) and alkyne C–H stretching (3320 cm^{-1}), while methyl stretching absorptions were absent (Figure 5.8). This shows that the reaction was successful, and that the terminal alkyne functionality was maintained.

To investigate whether these alkyne-terminated surfaces were suitable for further surface modification, they were reacted with 11-azido-3,6,9-trioxaundecyl-trifluoro-acetamide (**1**) using the Cu(I)-catalyzed alkyne-azide cycloaddition. Compound **1** was prepared because it contains an amide group, which is a good marker in IR

spectroscopy, as well as fluorine, which is a good marker in XPS. Thus, the reacted surfaces could be easily characterized with these two techniques.

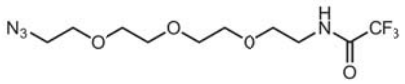

(1)

After reaction, the absorptions due to C≡C stretching (2120 cm^{-1}) and alkyne C–H stretching (3320 cm^{-1}) almost disappeared, indicating that the majority of alkyne groups has reacted. The intensity of the absorption around 1610 cm^{-1} - which we attributed to vibrations of the surface bond - decreased somewhat as well, implying that some desorption took place during the reaction, which is presumably induced by the reductive coupling conditions. Partial desorption also follows from the ν_{CH2} absorptions, which decreased in spite of coupling of the methylene-containing compound **1**. On the other hand, additional absorptions at 1690 cm^{-1} and 1580 cm^{-1} appeared, which can be attributed to amide C=O stretching and N-H bending vibrations. The presence of an amide group at the surface shows that the coupling reaction has been successful. This is supported by increased absorption in the ν_{OH} region (3750 - 3000 cm^{-1}), which is likely caused by water adsorbed to the hydrophilic oligoethylene glycol chains.

Comparison of the XPS spectra prior to and after reaction with the azide showed that the C/Al ratio increased upon reaction. This shows that the thickness of the organic layer has increased, as could be expected for a cycloaddition reaction. These results seem to contrast the IR data, but can be explained by the limited analysis depth of XPS, as discussed before. This indicates that the coupling reaction mainly takes place on the outer surface, whereas desorption likely occurs evenly on the outer surface and within the pores.

More interestingly, the XPS spectrum of the azide-reacted alumina shows that fluorine and nitrogen have been introduced to the surface (Table 5-1). In addition, it shows a trace amount of copper, which was used to catalyze the reaction. The ratio of F/N signals is 0.81, which is close to the F/N ratio in the azide (0.75). Since the difference can be interpreted in terms of attenuation effects (F only present on top of

Table 5-1. XPS element ratios of alkyne-terminated porous alumina before and after reaction with azide **1**.

Ratio	Alkyne-terminated alumina	Azide-reacted alumina
C/Al	2.25	3.69
O/Al	1.47	1.82
F/Al	-	0.24
N/Al	-	0.30
P/Al	0.05	0.06
Cu/Al	-	< 0.01

the monolayer, while N is predominantly found in the triazole ring), these results confirm that the amide bond stays intact upon reaction.

If every molecule of 1,15-hexadecadiyne on the surface would have been coupled to the azide, one would expect N/C and F/C ratios of 0.154 and 0.115, respectively. The XPS data show N/C and F/C ratios of 0.080 and 0.065, respectively, which means that roughly 40% of all hydrocarbon chains have reacted with the azide (note that the surface reaction yield and these element ratios are not linearly related). This somewhat limited reaction yield is likely due to the formation of sterically demanding triazole groups at the hydrocarbon interface, thereby reducing the number of available alkyne groups on the surface. In addition, the adsorption of adventitious carbon to the modified surface may have further decreased the N/C and F/C ratios.

Knowledge of the surface reaction yield is helpful in predicting the high-resolution C_{1s} spectrum of the azide-reacted surface. This spectrum could be well-described with four components (Figure 5.9). The relative intensities of these components match well with predictions based on the determined reaction yield (Table 5-2).

These experiments show that 1,15-hexadecadiyne-modified porous alumina is a suitable substrate for the subsequent surface reaction with organic azides. The widespread use of the alkyne-azide cycloaddition reaction has resulted in the availability of various azido-terminated biomolecules. These may be easily attached to the PAA surface using the presented method, thereby creating biofunctional surfaces that can be used for e.g. sensing and recognition purposes.

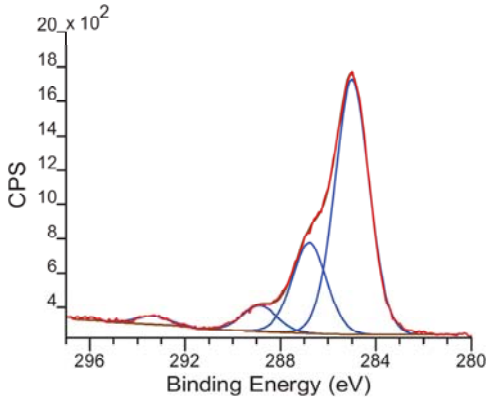

Figure 5.9. High-resolution C_{1s} spectrum of an alkyne-terminated surface that was reacted with azide **1**,

Table 5-2. Deconvolution parameters of the spectrum displayed in Figure 5.9, and predicted intensities based on a surface reaction yield of 40 %.

Position (eV)	Assigned to	Rel. intensity (%)	
		Experimental	Predicted
285.0	C-C	67.4	66.0
286.8	C-O, C-N	23.9	25.0
288.9	C=O	6.7	7.0
293.4	CF_3	2.0	2.0

5.5 Conclusions

We have presented a new method to modify the surface of porous anodic alumina. 1-Alkynes have been shown to react with the surface, resulting in the formation of an organic monolayer. Surface modification already occurs at room temperature, and proceeds to completion within a few hours at 80 °C. The resulting modified surfaces show good stability in water and at elevated temperatures. Detailed characterization of these surfaces showed that the chemisorbed species is an oxidation product of the 1-alkyne, namely its α-hydroxy carboxylate. Functional surfaces have been obtained by reaction of 1,15-hexadecadiyne with porous alumina, resulting in alkyne-terminated surfaces that can be further functionalized, e.g. using the Cu(I)-catalyzed

alkyne-azide cycloaddition reaction. This can provide the PAA surface with different (bio)functionalities, which may be further exploited for sensing and recognition purposes.

The surface modification method demonstrated here provides a valuable alternative to existing methods because of 1) the stability of the modified surfaces and 2) the ease of further (bio)functionalization. Even though this study was only concerned with PAA, the method may also be applicable to other types of alumina, such as γ-alumina.

5.6 References

(1) Ingham, C. J.; ter Maat, J.; de Vos, W. M. *Biotechnol. Adv.* **2011**, doi:10.1016/j.biotechadv.2011.1008.1005.

(2) Yu, G. J.; Wang, S.; Gong, J. L.; Zhu, D. Z.; He, S. X.; Li, Y. L.; Zhu, Z. Y. *Chin. Sci. Bull.* **2005**, *50*, 1097-1100.

(3) Ciambelli, P.; Sannino, D.; Sarno, M.; Fonseca, A.; Nagy, J. B. *J. Nanosci. Nanotechno.* **2004**, *4*, 779-787.

(4) Lee, D. H.; Condrate, R. A. *Mater. Lett.* **1995**, *23*, 241-246.

(5) Matefi-Tempfli, S.; Matefi-Tempfli, M.; Vlad, A.; Antohe, V.; Piraux, L. *J. Mater. Sci.-Mater. El.* **2009**, *20*, 249-254.

(6) Borissov, D.; Isik-Uppenkamp, S.; Rohwerder, M. *J. Phys. Chem. C* **2009**, *113*, 3133-3138.

(7) Sakurai, M.; Shimojima, A.; Yantauchi, Y.; Kuroda, K. *Langmuir* **2008**, *24*, 13121-13126.

(8) Yanagishita, T.; Nishio, K.; Masuda, H. *Appl. Phys. Express* **2009**, *2*.

(9) Yeu, S.; Lunn, J. D.; Rangel, H. M.; Shantz, D. F. *J. Membr. Sci.* **2009**, *327*, 108-117.

(10) Thormann, A.; Teuscher, N.; Pfannmoller, M.; Rothe, U.; Heilmann, A. *Small* **2007**, *3*, 1032-1040.

(11) Bocchetta, P.; Ferraro, R.; Di Quarto, F. *J. Power Sources* **2009**, *187*, 49-56.

(12) Ingham, C. J.; Sprenkels, A.; Bomer, J.; Molenaar, D.; van den Berg, A.; Vlieg, J. E. T. V.; de Vos, W. M. *P. Natl. Acad. Sci. USA* **2007**, *104*, 18217-18222.

(13) Lau, K. H. A.; Tan, L. S.; Tamada, K.; Sander, M. S.; Knoll, W. *J. Phys. Chem. B* **2004**, *108*, 10812-10818.

(14) Yamaguchi, A.; Hotta, K.; Teramae, N. *Anal. Chem.* **2009**, *81*, 105-111.

(15) Koutsioubas, A. G.; Spiliopoulos, N.; Anastassopoulos, D.; Vradis, A. A.; Priftis, G. D. *J. Appl. Phys.* **2008**, *103*.

(16) Kondo, T.; Nishio, K.; Masuda, H. *Appl. Phys. Express* **2009**, *2*.

(17) Lu, Z. C.; Ruan, W. D.; Yang, J. X.; Xu, W. Q.; Zhao, C.; Zhao, B. *J. Raman Spectrosc.* **2009**, *40*, 112-116.

(18) Szczepanski, V.; Vlassiouk, I.; Smirnov, S. *J. Membr. Sci.* **2006**, *281*, 587-591.

(19) Jani, A. M. M.; Anglin, E. J.; McInnes, S. J. P.; Losic, D.; Shapter, J. G.; Voelcker, N. H. *Chem. Commun.* **2009**, 3062-3064.

(20) Sah, A.; Castricum, H. L.; Bliek, A.; Blank, D. H. A.; ten Elshof, J. E. *J. Membr. Sci.* **2004**, *243*, 125-132.

(21) Yasseri, A. A.; Kobayashi, N. P.; Kamins, T. I. *Appl. Phys. A-Mater.* **2006**, *84*, 1-5.

(22) Chehimi, M. M.; Abel, M. L.; Watts, J. F.; Digby, R. P. *J. Mater. Chem.* **2001**, *11*, 533-543.

(23) Pesek, J. J.; Matyska, M. T. *J. Chromatogr. A* **2002**, *952*, 1-11.

(24) Tseng, S. Y.; Wang, C. C.; Lin, C. W.; Chen, C. L.; Yu, W. Y.; Chen, C. H.; Wu, C. Y.; Wong, C. H. *Chem.-Asian J.* **2008**, *3*, 1395-1405.

(25) Allara, D. L.; Nuzzo, R. G. *Langmuir* **1985**, *1*, 45-52.

(26) Cheow, P. S.; Liu, L. Y.; Toh, C. S. *Surf. Interface Anal.* **2007**, *39*, 601-610.

(27) Karaman, M. E.; Antelmi, D. A.; Pashley, R. M. *Colloid Surface A* **2001**, *182*, 285-298.

(28) Oberg, K.; Persson, P.; Shchukarev, A.; Eliasson, B. *Thin Solid Films* **2001**, *397*, 102-108.

(29) Chang, C. S.; Suen, S. Y. *J. Membr. Sci.* **2006**, *275*, 70-81.

(30) Allara, D. L.; Nuzzo, R. G. *Langmuir* **1985**, *1*, 52-66.

(31) Pahnke, J.; Ruhe, J. *Macromol. Rapid Commun.* **2004**, *25*, 1396-1401.

(32) Giza, M.; Thissen, P.; Grundmeier, G. *Langmuir* **2008**, *24*, 8688-8694.

(33) Liakos, I. L.; Newman, R. C.; McAlpine, E.; Alexander, M. R. *Surf. Interface Anal.* **2004**, *36*, 347-354.

(34) Liakos, I. L.; Newman, R. C.; McAlpine, E.; Alexander, M. R. *Langmuir* **2007**, *23*, 995-999.

(35) Meng, J. C.; Averbuj, C.; Lewis, W. G.; Siuzdak, G.; Finn, M. G. *Angew. Chem. Int. Edit.* **2004**, *43*, 1255-1260.

(36) Chang, S.-H.; Han, J.-L.; Tseng, S. Y.; Lee, H.-Y.; Lin, C.-W.; Lin, Y.-C.; Jeng, W.-Y.; Wang, A. H. J.; Wu, C.-Y.; Wong, C.-H. *J. Am. Chem. Soc.* **2010**, *132*, 13371-13380.

(37) Posner, G. H. *Angew. Chem. Int. Edit.* **1978**, *17*, 487-496.

(38) Kabalka, G. W.; Pagni, R. M. *Tetrahedron* **1997**, *53*, 7999-8065.

(39) ter Maat, J.; Regeling, R.; Yang, M.; Mullings, M. N.; Bent, S. F.; Zuilhof, H. *Langmuir* **2009**, *25*, 11592-11597.

(40) Vong, T. H.; ter Maat, J.; van Beek, T. A.; van Lagen, B.; Giesbers, M.; van Hest, J. C. M.; Zuilhof, H. *Langmuir* **2009**, *25*, 13952-13958.

(41) Vong, T.; Schoffelen, S.; van Dongen, S. F. M.; van Beek, T. A.; Zuilhof, H.; van Hest, J. C. M. *Chem. Sci.* **2011**, 1278-1285.
(42) Lucchesi, P. J.; Carter, J. L.; Yates, D. J. C. *J. Phys. Chem.* **1962**, *66*, 1451-1456.
(43) Brown, N. M. D.; Timms, W. E.; Turner, R. J.; Walmsley, D. G. *J. Catal.* **1980**, *64*, 101-109.
(44) Yates, D. J.; Lucchesi, P. J. *J. Chem. Phys.* **1961**, *35*, 243-255.
(45) Ivanov, A. V.; Koklin, A. E.; Uvarova, E. B.; Kustov, L. M. *Phys. Chem. Chem. Phys.* **2003**, *5*, 4718-4723.
(46) Bhasin, M. M.; Curran, C.; John, G. S. *J. Phys. Chem.* **1970**, *74*, 3973-3980.
(47) Allenger, V. M.; Mclean, D. D.; Ternan, M. *J. Catal.* **1991**, *131*, 305-318.
(48) Lee, J. S.; Gu, G. H.; Kim, H.; Jeong, K. S.; Bae, J.; Suh, J. S. *Chem. Mater.* **2001**, *13*, 2387-2391.
(49) Smith, W. N.; Beumel, O. F. *Synthesis-Stuttgart* **1974**, 441-442.
(50) Powell, C. J.; Jablonski, A. *NIST Electron Effective-Attenuation-Length Database - Version 1.1*; National Institute of Standards and Technology: Gaithersburg, MD, 2003.
(51) Tanuma, S.; Powell, C. J.; Penn, D. R. *Surf. Interface Anal.* **1994**, *21*, 165-176.
(52) Scheres, L.; Giesbers, M.; Zuilhof, H. *Langmuir* **2010**, *26*, 10924-10929.
(53) Ulman, A. An introduction to Ultrathin Organic Films: From Langmuir-Blodgett to Self-Assembly; Academic Press: Boston, 1991.
(54) Porter, M. D.; Bright, T. B.; Allara, D. L.; Chidsey, C. E. D. *J. Am. Chem. Soc.* **1987**, *109*, 3559-3568.
(55) Sondag, A. H. M.; Raas, M. C. *J. Chem. Phys.* **1989**, *91*, 4926-4931.
(56) Morterra, C.; Magnacca, G. *Catal. Today* **1996**, *27*, 497-532.
(57) Xu, H.; Deshmukh, R.; Timmons, R.; Kytai, T. N. *Tissue Eng. Part A* **2011**, *17*, 865-876.
(58) Bombi, G. G.; Corain, B.; Sheikhosman, A. A.; Valle, G. C. *Inorg. Chim. Acta* **1990**, *171*, 79-83.
(59) Yang, M.; Teeuwen, R. L. M.; Giesbers, M.; Baggerman, J.; Arafat, A.; de Wolf, F. A.; van Hest, J. C. M.; Zuilhof, H. *Langmuir* **2008**, *24*, 7931-7938.
(60) Bigelow, W. C.; Pickett, D. L.; Zisman, W. A. *J. Coll. Sci. Imp. U. Tok.* **1946**, *1*, 513-538.
(61) Deacon, G. B.; Phillips, R. J. *Coord. Chem. Rev.* **1980**, *33*, 227-250.
(62) Curci, R.; Fiorentino, M.; Fusco, C.; Mello, R. *Tetrahedron Lett.* **1992**, *33*, 7929-7932.
(63) Ballistreri, F. P.; Failla, S.; Tomaselli, G. A. *J. Org. Chem.* **1988**, *53*, 830-831.
(64) Tiecco, M.; Testaferri, L.; Tingoli, M.; Chianelli, D.; Bartoli, D. *J. Org. Chem.* **1991**, *56*, 4529-4534.
(65) Nakajima, T.; Sonoda, T.; Miyata, H.; Kubokawa, Y. *J. Chem. Soc. Farad. T. 1* **1982**, *78*, 555-565.

(66) Davydov, A. A. D. *Molecular spectroscopy of oxide catalyst surfaces*; 1st ed.; John Wiley & Sons, Inc.: Hoboken, NJ, 2003.

(67) Yang, W. S.; Auciello, O.; Butler, J. E.; Cai, W.; Carlisle, J. A.; Gerbi, J.; Gruen, D. M.; Knickerbocker, T.; Lasseter, T. L.; Russell, J. N.; Smith, L. M.; Hamers, R. J. *Nat. Mater.* **2002**, *1*, 253-257.

(68) Rosso, M.; Arafat, A.; Schroen, K.; Giesbers, M.; Roper, C. S.; Maboudian, R.; Zuilhof, H. *Langmuir* **2008**, *24*, 4007-4012.

Chapter 6

Biofunctionalization of Porous Anodic Alumina Surfaces: Selective Adhesion of Microbial Pathogens

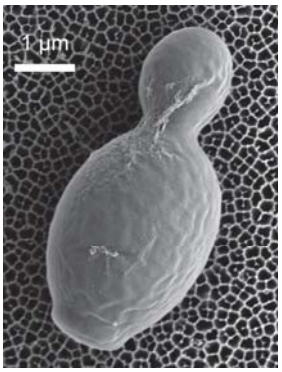

This chapter was partially published as:

ter Maat, J.; Regeling, R.; Ingham, C.J.; Weijers, C.A.G.M.; Giesbers, M.; de Vos, W.M.; Zuilhof, H. "Organic Modification and Subsequent Biofunctionalization of Porous Anodic Alumina Using Terminal Alkynes", *Langmuir* **2011**, *27*, 13606-13617.

6.1 Abstract

Selective adsorption of pathogenic micro-organisms to functionalized surfaces is potentially interesting for medical diagnostics, as it can reduce the time to diagnosis. Here, the adsorption of *Neisseria gonorrhoeae* and *Candida albicans* onto lactosylated porous anodic alumina (PAA) surfaces was investigated. Lactosylated PAA surfaces were prepared by reacting a lactosyl azide with alkyne-terminated PAA. Selective and reversible binding of the lectin peanut agglutinin (PNA) to these surfaces was demonstrated. Moreover, PNA adsorption was higher on surfaces that exposed the β-lactoside than on those that displayed the α anomer, which was attributed to surface-associated steric hindrance. *N. gonorrhoeae* was adsorbed either directly onto the lactosylated surface or subsequently to PNA adsorption. Yet in both cases, quantification of the adsorbed *N. gonorrhoeae* was hampered by high background staining. *C. albicans*, on the other hand, did show increased colonization onto lactosylated surfaces compared to unmodified surfaces, presumably due to interactions involving the cell wall β-glucan. Thus, this proof-of-principle study shows that aluminum oxide surfaces can be modified to induce selective adsorption of proteins and micro-organisms.

The electron microscopy image on page 101 shows a budding Candida Albicans cell that is adsorbed onto porous anodic alumina. (Image by Colin Ingham and Adriaan van Aelst)

6.2 Introduction

Microbial infection requires the adhesion of microorganisms to host cells. This is a complex process often involving multiple interactions, such as bacterial pili binding to mammalian cellular surfaces, other protein-based pathogen-host interactions, and also interactions between proteins and carbohydrates.[1,2] Association with epithelial cells of a mammalian host can also occur through docking of the microbe's surface proteins with host glycosphingolipids.[3] Glycosphingolipids[4] are membrane-bound glycoconjugates that expose a carbohydrate sequence. Pathogenic bacteria and fungi are capable of recognizing specific epitopes of these glycosphingolipids. In addition, the micro-organisms themselves also expose carbohydrate residues, such as lipopolysaccharides in bacteria, and structural polysaccharides in the cell wall of fungi. These compounds can also be involved in specific protein-carbohydrate interactions, for example those that induce bacterial agglutination.[5]

Diagnosis of a microbial infection usually requires isolation of the pathogen from the patient, followed by cultivation to a colony on media that may be selective or contain indicators of microbial metabolism. Subsequently, the colony is further characterized and identified. In this process, the microorganisms are transferred from their host surface to an artificial surface for cultivation, which is usually a gel such as agar. In contrast to the host surface, binding to such artificial surfaces is usually not based on specific interactions.

The need for miniaturization of the diagnosis platform has led to the development of small culture chips, such as the micro-Petri dish.[6] This particular culture chip consists of a porous anodic alumina (PAA) substrate that is divided into compartments of typically 20 to 180 μm in diameter (Figure 6.1). Since the porous substrate (when contacted to a nutrient source) can provide microorganisms with nutrients, microcolonies can grow within the compartments. The rigidity of the substrate allows it to be transferred to other environments, enabling compatibility with most identification techniques. Furthermore, it is possible to integrate multiple diagnostic tasks within the same chip. Compared to conventional methods, the smaller colonies and reduced handling can significantly reduce the required time to diagnosis.

Further reduction of diagnosis time can be foreseen when microorganisms bind selectively to the chip surface, thereby simplifying the isolation procedure. This is

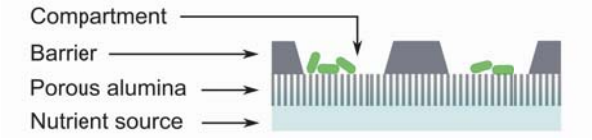

Figure 6.1. Design of the micro-Petri dish.

particularly interesting as the surface characteristics of microorganisms have specifically been adjusted to the host target cells.[7,8] Such selective binding may be achieved when the culture chip displays sugar sequences similar to those of the animal host cells. This requires surface modification of the PAA substrates, for example by forming an organic monolayer. In chapter 5, we reported on the modification of PAA with terminal alkynes. We showed that the initially modified surfaces could be further functionalized by means of the copper-catalyzed azide-alkyne cyclo-addition reaction (CuAAC). Here, we will use this procedure to covalently attach a carbohydrate moiety to the surface. By attaching a carbohydrate sequence to the surface, we aim to imitate the cell surface in order to induce specific microbial adhesion.

Lactose was selected as a model carbohydrate, as it is a simple carbohydrate that is found on human epithelial cells,[9,10] and which forms the basic building block of many of the more complex carbohydrates encountered in animal glycosphingolipids.[4] The latter, combined with the ability of bacteria to bind to internal carbohydrate structures,[3] resulted in many bacteria displaying specificity towards lactose. Even though this disqualifies the lactosyl moiety for diagnostics applications, it makes lactosyl moieties a good choice for this proof-of principle study.

One of the bacteria known to bind to lactosyl ceramide (LacCer) is *Neisseria gonorrhoeae*. This is a Gram-negative pathogen that exclusively inhabits human mucous membranes to cause the disease gonorrhea.[2] *N. gonorrhoeae* was also found to bind more complex glycosphingolipids (asialo-GM_2, asialo-GM_1), the structures of which all contain the LacCer moiety.[11] Both piliated and non-piliated variants have been shown to bind to LacCer, indicating that the corresponding receptor is located in the outer membrane.[11] An adhesin specific for glycosphingolipids has been isolated from *N. gonorrhoeae*, yet this adhesin did only bind the more complex

glycospingolipids.[9] However, the existence of more than one type of gonococcal adhesin has been suggested,[12] which may explain the specificity of *N. gonorrhoeae* for LacCer. Nonetheless, binding specificity of PAA surfaces for *N. gonorrhoeae* may be introduced by functionalizing these surfaces with lactosyl groups. In addition to binding glycosphingolipids, *N. gonorrhoeae* displays lipooligosaccharides (LOSs) that resemble human tissue antigens (i.e., which are relatively short and branched).[13] The carbohydrate sequence of one of the major gonococcal LOSs was determined to be Gal-(β1→4)-GlcNAc-(β1→3)-Gal-(β1→4)-Glc,[14] a sequence that is known to bind to human asialoglycoprotein receptor,[13] and which may be involved in bacterial auto-agglutination.[12] Such LOS sequences may also be exploited in selective bacterial adsorption on surfaces. This, however, requires the presence of receptors on the surface. Peanut agglutinin (PNA), a tetravalent lectin, may be used to provide these to a lactosyl-terminated surface, since it is known to agglutinate *N. gonorrhoeae*,[15] but to bind lactose as well.[16-18] Since PNA has four binding sites, some of these are available for interaction with gonococcal LOS, even after PNA has adsorbed to the surface. It therefore allows an alternative, indirect strategy to bind *N. gonorrhoeae* to lactosyl-terminated surfaces (Figure 6.2).

Even though the cellular organization of yeasts is remotely different from that of bacteria, they may also display specific interactions with carbohydrates. Specific interactions between LacCer and several yeasts, including *Candida albicans*, have been reported.[10] *Candida albicans* is an opportunistic pathogenic yeast that has adapted to live on the mucosal surfaces of warm-blooded animals.[19] Its cell wall comprises proteins, chitin, mannan and β-glucan.[20,21] The latter is the major constituent and accounts for 50-60 % of the cell wall dry weight.[20] This β-glucan is highly branched with mixed domains of β-(1-3) and β-(1-6) glucosidic linkages.[22,23] Branched, high molecular weight β-(1-3)-glucans have been shown to bind specifically to galactosyl-terminated glycosphingolipids (including LacCer),[24] and this binding specificity was preserved in a soluble derivative of Candida β-glucan.[25] Thus, it is likely that these interactions are involved in the observed binding of *C. albicans* cells to lactosylceramide.[10] Specific binding of *C. albicans* to PAA surfaces may therefore be realized by functionalizing the latter with lactosyl groups as well.

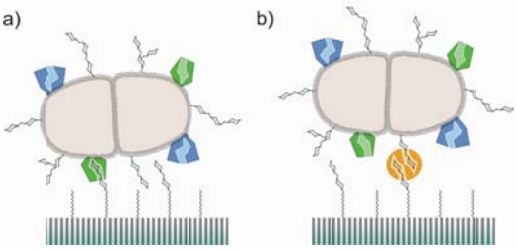

Figure 6.2. Envisioned binding of a *N. gonorrhoeae* diplococcus (displaying several adhesins and carbohydrate epitopes) onto lactosylated PAA, either directly (a) or mediated by peanut agglutinin (b).

This study consists of several parts. First, the functionalization of PAA with lactosyl moieties was studied. To this aim, an alkyne-terminated PAA surface was reacted with 11-azido-undecyl (α- or β-) lactoside. Functionalized surfaces were characterized with infrared (IR) spectroscopy and X-ray photoelectron spectroscopy (XPS). Second, the adsorption of fluorescently labeled PNA onto these surfaces was studied using fluorescence microscopy. Third, the subsequent adsorption of *N. gonorrhoeae* onto these PNA-exposed surfaces was investigated. Gonococcal adsorption directly onto the lactosyl-terminated PAA was also studied. The study concludes with the investigation of the adsorption of *C. albicans* onto lactosyl-terminated PAA.

6.3 Materials and methods

Materials. Glassware used for surface modification was cleaned with organic solvents and etched overnight in basic detergent solution. Before use, it was rinsed with ultrapure water and dried at 120 ºC. Chemicals were obtained from Sigma-Aldrich unless stated otherwise. Porous anodic alumina samples (36 × 8 mm, Anopore™) with an average pore size of 200 nm, were obtained from Whatman Scientific. 1,15-Hexadecadiyne was synthesized from 1,12-dibromododecane and lithium acetylide ethylene diamine complex as described elsewhere,[26] and was purified by recrystallization and vacuum distillation. 11-Azido-1-undecanol was synthesized from 11-bromo-1-undecanol and sodium azide as described elsewhere.[27] Hydrochloric acid (37 %, analytical grade) was obtained from Acros. Solvents used

were either of analytical grade or distilled prior to use. Optical rotation values were measured at 589 nm on a Perkin-Elmer 241 polarimeter. NMR spectra were recorded on a Bruker Avance III 400 spectrometer. HRMS data were collected on an Exactive high resolution MS (Thermo Scientific) equipped with a DART probe.

Synthesis of 2,3,4,6-tetra-O-acetyl-β-D-galactopyranosyl-(1→4)-1-iodo-2,3,6-tri-O-acetyl-D-glucopyranoside (3). Lactose (3.4 g, 10 mmol) was suspended in acetic anhydride (7.8 ml, 82 mmol) and the suspension was stirred under nitrogen. Iodine (50 mg, 0.20 mmol) was added, and the mixture was stirred for 6 h at 35 °C, yielding the octa-O-acetyl-β-lactose (**2**). Dry dichloromethane (10 ml) was added, followed by iodine (2.53 g, 10 mmol) and hexamethyldisilane (2.08 ml, 10 mmol), and the mixture was stirred for 20 h at room temperature. More dichloromethane (20 ml) was added and the mixture was quenched with a 10 % aqueous solution of $Na_2S_2O_3$ (20 ml). The organic layer was further quenched with saturated $NaHCO_3$ solution (3 × 50 ml) and saturated NaCl solution (2 × 50 ml), after which it was dried over Na_2SO_4. After filtration, the organic layer was concentrated under reduced pressure to yield a white solid. This crude product was further purified by column chromatography (eluent: petroleum ether / ethyl acetate 1:1) to give the pure 2,3,4,6-tetra-O-acetyl-β-D-galactopyranosyl-(1→4)-1-iodo-2,3,6-tri-O-acetyl-D-glucopyranoside (**3**) (5.66 g, 7.6 mmol, 76%).

$[\alpha]^{20}_D$ + 136.6° (*c* 1.2, $CHCl_3$), *lit.* $[\alpha]^{23}_D$ + 137.0° (*c* 1.0, $CHCl_3$).[28] ^{1}H NMR (400 MHz, $CDCl_3$): δ 6.91 (1H, d), 5.43 (1H, t), 5.33 (1H, d), 5.09 (1H, dd), 4.93 (1H, dd), 4.50 (1H, d), 4.46 (1H, dd), 4.04 – 4.19 (4H, m), 3.84 – 3.96 (3H, m), 2.13 (3H, s, OAc), 2.10 (3H, s, OAc), 2.06 (3H, s, OAc), 2.04 (3H, s, OAc), 2.03 (6H, s, OAc), 1.94 (3H, s, OAc). ^{13}C NMR (100 MHz, $CDCl_3$): δ 170.2, 170.0, 170.0, 169.9, 169.6, 169.1, 168.9 (7 × C=O), 100.7 (CH), 75.6 (CH), 74.6 (CH), 72.6 (CH), 71.1 (CH), 70.9 (CH), 70.7 (CH), 70.5 (CH), 69.0 (CH), 66.6 (CH), 60.9 (CH_2), 60.8 (CH_2), 20.9, 20.7, 20.7, 20.7, 20.6, 20.5, 20.4 (7 × CH_3-C(O)-, two peaks overlap). HRMS: *m/z* 745.0832, calculated for $C_{26}H_{34}IO_{17}$ ($[M-H]^-$): 745.0835.

Synthesis of β-D-galactopyranosyl-(1→4)-1-(11-azido-undecanyl)-α-D-glucopyranoside (5a). A solution containing **3** (3.00 g, 4.0 mmol), 11-azido-1-undecanol (1.7 g, 8 mmol) and mol sieves (2.0 g, 4 Å) in dry dichloromethane (10 ml) was cooled

to 0 °C under nitrogen atmosphere. Iodine (2.03 g, 8 mmol) was added and the mixture was stirred overnight, in the course of which it was slowly allowed to warm up to room temperature. Ethyl acetate (120 ml) was added, the mol sieves were filtered off and the filtrate was subsequently quenched with 1 M $Na_2S_2O_3$ solution (2 × 75 ml). The top layer (mainly containing ethyl acetate) was further washed with saturated NaCl solution (1 × 75 ml), after which it was dried over Na_2SO_4, filtered and finally concentrated under reduced pressure. The crude product was further purified by column chromatography (eluent: petroleum ether : ethyl acetate 1:1) to yield the 2,3,4,6-tetra-O-acetyl-β-D-galactopyranosyl-(1→4)-1-(11-azido-undecanyl)-3,6-di-O-acetyl-α-D-glucopyranoside (**4a**) as a colorless syrup. This intermediate was dissolved in dry methanol (10 ml) after which a solution of sodium methoxide in methanol (1.0 M, 0.12 ml) was added. The mixture was stirred overnight during which a white suspension formed. Additional methanol (20 ml) was added and the reaction was monitored by TLC (eluens: ethyl acetate). After complete conversion, the mixture was quenched by adding Amberlite 120 H, until the pH was reduced to 7. The mixture was filtered over celite and the filtrate was concentrated under reduced pressure to yield the β-D-galactopyranosyl-(1→4)-1-(11-azido-undecanyl)-α-D-glucopyranoside (**5a**) as a cream-colored solid (1.32 g, 2.5 mmol, 61%).

$[\alpha]^{20}_D$ + 61.6° (*c* 1.1, CH_3OH). ^1H NMR (400 MHz, CD_3OD): δ 4.76 (1H, d, H_{Glc-1}, *J* 4.8 Hz), 4.35 (1H, d, H_{Gal-1}, *J* 7.6 Hz), 3.75 – 3.88 (5H, m), 3.68 – 3.72 (3H, m), 3.53 – 3.60 (3H, m), 3.42 – 3.51 (3H, m), 3.27 (2H, t, *J* 6.9 Hz), 1.55 – 1.65 (4H, m), 1.29 – 1.40 (16H, m, -$(CH_2)_8$-). ^{13}C NMR (100 MHz, CD_3OD): δ 105.1 (CH, C_{Gal-1}), 99.9 (CH, C_{Glc-1}), 81.1 (CH), 77.1 (CH), 76.4 (CH), 74.9 (CH), 73.5 (CH), 73.3 (CH), 72.6 (CH), 70.3 (CH), 69.3 (-CH_2O-), 62.5 (CH_2, C_{Gal-6}), 61.9 (CH_2, C_{Glc-6}), 52.5 (-CH_2-N_3), 30.7, 30.7, 30.6, 30.6, 30.6, 30.3, 29.9, 27.8, 27.3 (9 x CH_2, two peaks overlap). HRMS: *m/z* 536.2811, calculated for $C_{23}H_{43}N_3O_{11}$ ([M-H]$^-$) 536.2814.

Synthesis of β-D-galactopyranosyl-(1→4)-1-(11-azido-undecanyl)-β-D-glucopyranoside (5b). Performing the 11-azido-1-undecanol coupling in acetonitrile instead of dichloromethane changes the stereospecificity, resulting in the formation of 2,3,4,6-tetra-O-acetyl-β-D-galactopyranosyl-(1→4)-1-(11-azido-undecanyl)-2,3,6-tri-O-acetyl-β-D-glucopyranoside (**4b**), which was deprotected in a similar fashion to

obtain the β-D-galactopyranosyl-(1→4)-1-(11-azido-undecanyl)-β-D-glucopyranoside (**5b**) in 37 % yield.

$[\alpha]^{20}_{D}$ – 8.2° (*c* 1.1, CH_3OH), *lit.* $[\alpha]^{23}_{D}$ –7.9° (*c* 1.0, CH_3OH).[29] ^{1}H NMR (400 MHz, CD_3OD): δ 4.27 (1H, d, H_{Gal-1}, *J* 7.5 Hz), 4.18 (1H, d, H_{Glc-1}, *J* 7.8 Hz), 3.75 – 3.82 (2H, m), 3.71 – 3.73 (1H, m), 3.66 – 3.69 (1H, m), 3.58 – 3.62 (1H, m), 3.37 – 3.50 (6H, m), 3.28 – 3.32 (1H, m), 3.12 – 3.19 (2H, m), 1.45 – 1.54 (4H, m), 1.19 – 1.34 (16H, m, -$(CH_2)_8$-). ^{13}C NMR (100 MHz, CD_3OD): δ 105.1 (CH, C_{Gal-1}), 104.2 (CH, C_{Glc-1}), 80.8 (CH), 77.1 (CH), 76.5 (CH), 76.4 (CH), 74.9 (CH), 74.8 (CH), 72.6 (CH), 71.0 (CH), 70.3 (-CH_2O-), 62.5 (CH_2, C_{Gal-6}), 62.0 (CH_2, C_{Glc-6}), 52.5 (-CH_2-N_3), 30.8, 30.7, 30.7, 30.6, 30.6, 30.3, 29.9, 27.8, 27.1 (9 × CH_2, two peaks overlap). HRMS: *m/z* 536.2824, calculated for $C_{23}H_{43}N_3O_{11}$ ([M-H]$^-$): 536.2814.

Preparation of alkyne-terminated surfaces. A PAA substrate was cleaned by sonication in acetone (5 min) and ultrapure water (5 min). The substrate was then immersed for 30 min in a freshly made 1:1 (v:v) mixture of 37% hydrochloric acid and methanol. Afterwards, it was rinsed and sonicated (5 min) with ultrapure water and then with methanol. The cleaned substrate was transferred to a flask containing neat 1,15-hexadecadiyne (~ 1.5 g). In order to dry the sample, the pressure was decreased to ~ 15 mbar. The flask was subsequently immersed in an oil bath of 80 °C. When the 1,15-hexadecadiyne was molten and the substrate was immersed, the flask was filled with argon and kept under a slight overpressure for 16 h at 80 °C. Following the reaction, the substrate was removed from the flask, rinsed copiously with dichloromethane, sonicated in ethanol and dichloromethane (5 min per solvent), and finally dried in air.

Preparation of lactosyl-terminated surfaces. The 1,15-hexadecadiyne-modified substrates were reacted with 11-azido-undecyl-lactoside (either α or β) using the Cu(I)-catalyzed azide-alkyne cycloaddition reaction (CuAAC). Two equivalents of copper sulfate were added to a reaction tube containing a solution of the lactoside in water (1 eq). The tube was also equipped with a stirring bar and a platform. The alkyne-terminated substrate was immersed and placed onto the platform, which protected the fragile PAA from the stirring bar. Adsorbed air bubbles were removed by sonication. To generate Cu(I), two equivalents of sodium ascorbate were added, resulting in a final lactoside concentration of 0.1 mM. The reaction tube was then

placed in a microwave oven (CEM Discover), set to operate at 70 ºC for 30 min under continuous stirring. Following the reaction, the substrate was copiously rinsed with water, then sonicated in water, ethanol and dichloromethane (5 min per solvent), and finally dried in air. Modified samples were cut into four pieces, thereby reducing the sample size to ~ 9 × 8 mm.

Peanut agglutinin adsorption. Samples were incubated in a fresh solution of BSA (0.1 % w/v) in 1 × PBS buffer (900 µl, pH 7.4) for 30 min at 25 °C on a rotating table. A suspension of fluorescein-labeled peanut agglutinin (100 µl, 1 mg/ml) was added, and the samples were incubated for another 2 h. The samples were then washed with BSA-containing PBS buffer (3 × 1 ml, 10 min incubation between each washing step), and directly imaged with fluorescence microscopy. For competition experiments, 20 mM of competing sugar (glucose, lactose) was present during both the adsorption and washing steps. Measurements have been performed in triplicate. Efforts were taken to reduce the light exposure of fluorescein-containing solutions and substrates to a minimum.

***Neisseria gonorrhoeae* adsorption.** Gonococci were obtained as a clinical isolate from Hospital Jeroen Bosch ('s Hertogenbosch, the Netherlands). Lactosyl-terminated PAA surfaces (with or without pre-adsorbed PNA) were placed on a culture plate and washed with phosphate buffered saline (PBS, pH 7.4). An aliquot of a turbid solution, containing ~ 5×10^8 *N. gonorrhoeae* cells/ml in PBS buffer, was added and the surface was incubated on a rotating table at 60 rpm for 2 h at room temperature. Subsequently, the surface was washed with PBS buffer (3 × 1 ml). An aliquot of Syto 9 solution (5 µM in PBS buffer) was added during the last washing step and the PAA surface was incubated on a rotating table for 30 min at room temperature, after which it was imaged by fluorescence microscopy.

***Candida albicans* adsorption.** *C. albicans* was obtained as a clinical isolate from Hospital Jeroen Bosch ('s Hertogenbosch, the Netherlands). Lactosyl-terminated PAA surfaces were placed on a culture plate and washed with phosphate buffered saline (PBS, pH 7.4). An aliquot of a turbid solution, containing ~ 10^8 *C. albicans* cells/ml in PBS buffer, was added and the surface was incubated on a rotating table at 60 rpm for 2 h at room temperature. Subsequently, the surface was washed with PBS buffer (3 × 1 ml). An aliquot of iodonitrotetrazolium chloride solution (INT, 0.02 % (w/v) in PBS

buffer) was added during the last washing step for staining, and the PAA surface was incubated on a rotating table for 30 min at room temperature, after which the PAA was imaged and cell binding was quantified by with transmission light microscopy. Measurements have been performed four times.

Infrared spectroscopy. IR spectra were obtained with a Bruker Tensor 27 FT-IR spectrometer in transmission mode. Spectra were collected using a spectral resolution of 2 cm^{-1} and 256 scans in each measurement. The raw data were divided by the data recorded on a freshly cleaned reference substrate.

X-ray Photoelectron Spectroscopy. XPS analyses were performed using a JPS-9200 photoelectron spectrometer (JEOL). The spectra were obtained under ultrahigh vacuum (UHV) conditions using monochromatic Al Kα X-ray radiation at 12 kV and 25 mA, with an analyzer pass energy of 10 eV for narrow scans and 50 eV for wide area scans. The X-ray incidence angle and the electron acceptance angle were 80º and 10º to the surface normal, respectively. To prevent surface charging during measurements, samples were irradiated with electrons with a kinetic energy of 3.0 eV. Peaks were shifted using the C_{1s} peak at 285.0 eV as a reference. Spectra were corrected using background subtraction (linear or Tougaard) before quantification and any peak deconvolution. Peaks were deconvoluted using GL(30) line shapes (Gaussian/Lorentzian product formulas with 30 % of Lorentzian weight).

Fluorescence microscopy. PAA substrates were imaged directly (without coverslip, immersion oil, or fixative) using an Olympus BX-41 fluorescence microscope. The microscope was equipped with U-MWIBA filters (Olympus Japan, excitation at 460 to 490 nm, dichroic mirror splitting at 505 nm, and emission window of 515 to 550 nm) for fluorescence imaging of substrates stained with Syto 9 or adsorbed with fluorescein-labeled PNA. Images were taken with a × 4 or × 10 dry objective lens using a b/w Kappa DX3 CCD camera. The total magnification was × 40 and × 100, respectively. Images were processed with the Image J program,[30] and normalized to allow comparison.

Transmission light microscopy and yeast cell counting. Substrates stained with INT were imaged using an Olympus BX-41 microscope equipped with a Kappa DX3 CCD camera at a total magnification of × 500. The threshold function of ImageJ was used to convert images of cells and microcolonies to monochrome b/w images. The

objects function was used to determine the amount of cells per field-of-view (FOV). Objects smaller than 1/3 of an average yeast cell were excluded. Objects partially in the FOV were still counted.

6.4 Results and discussion

6.4.1 Preparation of lactosyl-terminated PAA.

The successful demonstration of the CuAAC reaction on alkyne-terminated PAA (Chapter 5) prompted us to prepare lactosyl-terminated surfaces by coupling 11-azidoundecyl lactoside. A similar approach was recently used to create mannose-terminated silicon surfaces, which were demonstrated to selectively bind Concanavalin A and fimbriated *Escherichia coli*.[31]

11-Azido-undecyl-lactoside was prepared according to scheme 1. Lactose was peracetylated (a), followed by selective iodination of the anomeric carbon (b). Substitution of the iodine by 11-azido-undecanol (c) yields the protected product. The choice of solvent in this step determines the preferential formation of either the α or β anomer. Finally, purification and deprotection (d) yields the pure 11-azido-undecyl-(α/β)-lactoside (**5a**/**5b**).

Alkyne-terminated PAA was prepared as reported previously (Chapter 5), and was reacted with the 11-azido-undecyl-lactoside (either pure α or pure β) using the Cu(I)-catalyzed azide-alkyne cycloaddition reaction. The attachment of the hydrophilic carbohydrate moiety to the alkyne-terminated surface changed the surface wetting properties from hydrophobic to hydrophilic.

The resulting lactosyl-terminated surfaces were characterized with IR spectroscopy (Figure 6.3). Surfaces coupled with either epimer gave identical spectra. Comparison with the IR spectrum of the alkyne-terminated surface revealed the (partial) loss of the absorptions at 3320 and 1610 cm^{-1}, confirming that the alkyne group has been consumed in the reaction. Similar to previous results (Chapter 5), the decreased absorption at 1610 cm^{-1} indicates that some alkyne desorption has occurred, presumably due to the reductive coupling conditions. On the other hand, the increased absorption at the frequencies corresponding to the CH_2 bending and stretching modes (at 1460 cm^{-1} and around 2900 cm^{-1}), combined with a strong and broad absorption in

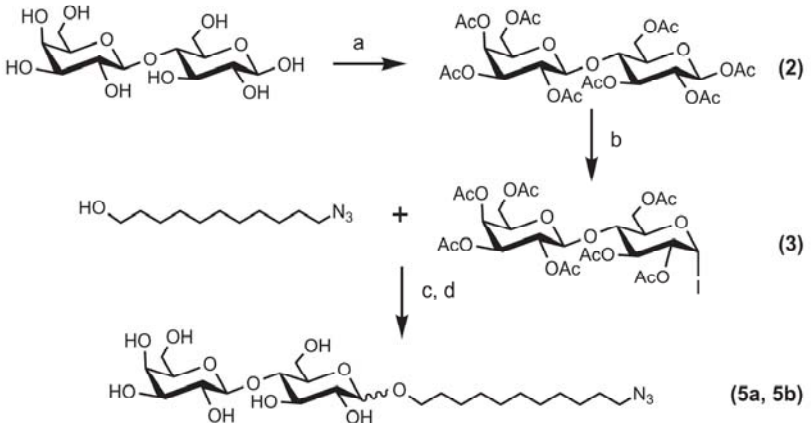

Scheme 6.1. Synthesis of 11-azido-undecyl-lactoside (α or β). (a) Ac_2O, I_2, 35 °C, 6 h; (b) I_2, HMDS in CH_2Cl_2, RT, 16 h; (c) I_2, CH_2Cl_2 (α) or MeCN (β), RT , 0 °C → RT, 16 h; (d) NaOMe in MeOH, RT, 16 h.

the ν_{OH} region (3750 - 3000 cm^{-1}), confirm the coupling of the 11-azido-undecyl-lactoside. Due to the hydrophilic nature of the lactosyl moiety, the latter absorption may be partially caused by adsorbed water, which can also explain the broad adsorption at 1670 cm^{-1}.

Characterization of the reacted surface with XPS revealed the presence of the elements C, O, Al and N, as well as trace amounts of P, I and Cu (Figure 6.4b). Phosphorus is present as a contamination in the PAA, and the P/Al ratio thus did not change notably upon reaction with lactoside. The presence of I likely resulted from a contamination in the lactosyl azide, as its precursor is iodine-containing compound (**3**), and that of Cu is explained by its use as a catalyst in the coupling reaction.

Comparison of the wide-area spectrum with that of alkyne-terminated PAA showed the introduction of nitrogen, as well as an increase in the ratios of C/Al and O/Al Figure 6.4). These changes are in line with the coupling of a carbohydrate to the surface via a triazole linkage. The ratio of N/C (~ 1 : 18) was used to estimate the degree of surface coupling, returning a coupling efficiency of roughly 45%, which is in line with previous results (chapter 5).

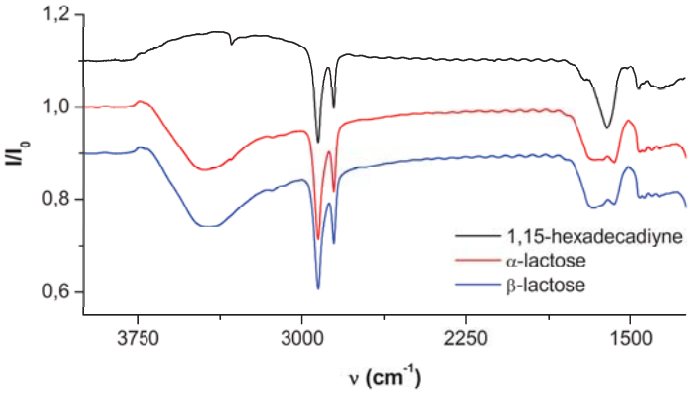

Figure 6.3. Infrared spectra of PAA modified with 1,15-hexadecadiyne prior to (top curve) and after reaction with 11-azido-undecyl-α-lactoside (middle curve) and 11-azido-undecyl-β-lactoside (bottom curve).

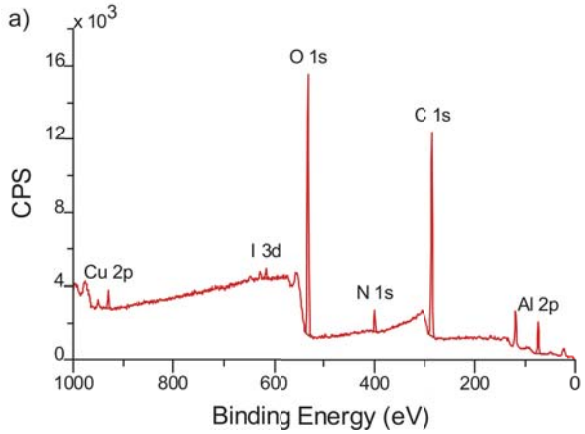

b) Ratio	Alkyne-term.	Lactosyl-term.
C/Al	2.25	3.97
O/Al	1.47	1.84
N/Al	0.00	0.22
P/Al	0.05	0.04
Cu/Al	0.00	0.01
I/Al	0.00	< 0.01

Figure 6.4. XPS wide area spectrum of alkyne-terminated PAA after reaction with 11-azido-undecyl α-lactoside (a), and surface composition prior to and after reaction (b).

6.4.2 Adsorption of peanut agglutinin onto α-lactosyl-terminated PAA

A set of α-lactosyl-terminated PAA samples were exposed to a solution of fluorescently-labeled PNA in BSA-containing PBS buffer, and were subsequently washed with buffer. Immediately afterwards, the degree of PNA adsorption was assessed by measuring the sample fluorescence. To investigate the binding specificity,

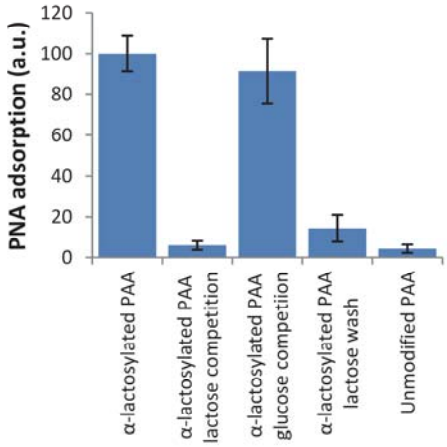

Figure 6.5. Quantification of fluorescently labeled PNA adsorption onto α-lactosyl-terminated PAA by fluorescence microscopy (n = 3).

PNA adsorption was performed in the presence and absence of competing sugars (lactose and glucose) in the solution, whereas binding reversibility was studied by washing with a buffer containing 20 mM lactose. The results are displayed in Figure 6.5.

These results show that PNA adsorbs significantly onto lactosylated PAA, whereas it hardly adsorbs onto unmodified PAA. The adsorption is almost completely inhibited by the presence of 20 mM lactose, but not at all by 20 mM glucose. This shows that PNA adsorbs specifically onto the lactosylated PAA surface, and that there is competition for the PNA binding sites between surface-bound lactose and free lactose in solution. Washing PNA-adsorbed, lactosylated PAA surfaces with lactose solution results in ~ 90 % PNA desorption, revealing that the PNA adsorption is (largely) reversible. This is in line with the reported PNA-lactose binding strength of 1.3×10^3 M^{-1} at 25 °C,[32] which is weak enough to allow receptor desorption by competition, even when divalent binding is considered.

6.4.3 Comparison of PNA adsorption onto α- and β-lactosyl-terminated PAA

Compared to α-lactosylated PAA, the β-lactosylated PAA shows distinctly more PNA adsorption, i.e. about 35 % (Figure 6.6). The adsorption in the presence of free lactose

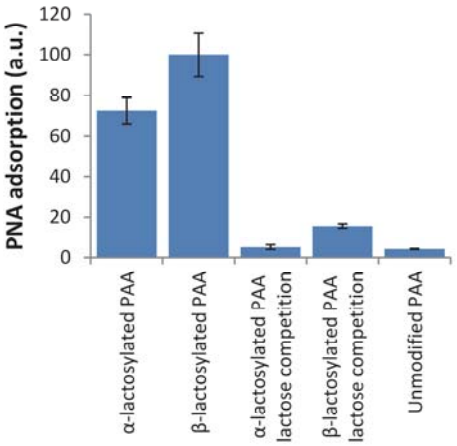

Figure 6.6. Quantification of fluorescently labeled PNA adsorption onto α- and β-lactosyl-terminated PAA by fluorescence microscopy (n = 3).

is somewhat higher as well. This may partially be explained by a different surface coverage, but since the IR spectra of α- and β-lactosylated PAA display nearly identical intensities (Figure 6.3), large variation in surface coverage is unlikely. Instead, the difference in PNA adsorption may originate from the different binding affinity or accessibility of the α- and β-anomer.

Neurohr et al. found that the binding constant of β-methyl lactoside was identical to that of lactose (ratio α/β = 40:60), indicating that the configuration of the anomeric carbon does not affect the binding to PNA.[16] This conclusion was confirmed by the crystal structure of the PNA-lactose complex, which showed that the glucose moiety is exposed at the protein surface, and that this moiety only forms hydrogen bonds with PNA at C_3.[33] Thus, the anomeric carbon is not involved in the complex formation and therefore its configuration is not likely to directly influence the binding affinity. On the other hand, the crystal structure showed that the galactose moiety is heavily involved in the complex formation, with seven hydrogen bonds and additional water bridges.[33] Thus, for the complex to form, the galactose moieties should be accessible. The surface-bound α-lactoside is oriented parallel to the surface (assuming an all-trans

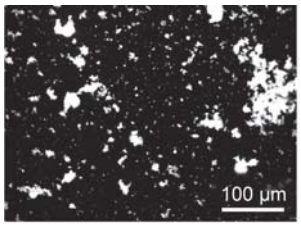

Figure 6.7. Fluorescence image showing agglutination of *N. gonorrhoeae* cells by fluorescein-labeled peanut agglutinin.

alkyl conformation), whereas the β-lactoside has a perpendicular orientation. This implies that the surface-bound β-lactoside is better accessible, which can explain the increased PNA adsorption onto this surface.

6.4.4 Adsorption of N. gonorrhoeae onto PNA-exposing PAA surfaces

Peanut agglutinin (PNA) is a tetravalent lectin, and thus may bind up to four sugar molecules. Because of steric hindrance at the aluminum oxide surface, it is likely that only one or two binding sites participate in surface adsorption, thereby leaving at least two binding pockets available for further interactions, e.g. with molecules or micro-organisms. *N. gonorrhoeae* is known to be agglutinated by peanut agglutinin, as it exposes lipo-oligosaccharides with a Gal-(β1→4)-GlcNAc- terminus. This sequence is known to bind to PNA even slightly stronger than lactose, and is expressed by the majority of gonococcal strains.[34] To validate the expression in the clinical isolate used in this study, fluorescein-labeled PNA was added to a suspension of *N. gonorrhoeae*. The resulting gonococcal agglutination (Figure 6.7) strongly indicated that Gal-(β1→4)-GlcNAc- residues were expressed.

However, determination of gonococcal adsorption onto the PNA-exposing PAA surfaces was complicated by high backgrounds obtained after microbial staining. Several dyes including Syto 9 and iodonitrotetrazolium chloride were tested, but all either suffered from high backgrounds or did not properly stain the organisms. In a previous study, Syto 9 could stain *N. gonorrhoeae* on PAA without complications.[35]

This shows that the high backgrounds observed in the present study are due to interactions of Syto 9 with either the organic adlayer or the adsorbed PNA. As no

suitable staining method was available, it was impossible to draw conclusions on the specificity of N. gonorrhoeae adsorption onto PNA-exposing PAA surfaces. Nonetheless, as the specific adsorption of *N.gonorrhoeae* may have medical significance, further research for suitable staining methods is highly desirable.

6.4.5 Adsorption of N. gonorrhoeae directly onto lactosyl-terminated PAA

It is known that *N. gonorrhoeae* can bind to LacCer.[11] Based on this observation, one might expect direct colonization onto lactosyl-terminated surfaces as well. However, determination of gonococcal adsorption onto these surfaces was again complicated by high backgrounds in the microbial staining. As unmodified PAA is hardly stained, this background staining has to be caused by interactions of the dye with the organic adlayer. Investigation of background staining with various dyes revealed that several fungal dyes were compatible with the lactosyl-modified surfaces. Therefore, we shifted our focus to the adsorption of the pathogenic yeast *C. albicans*.

6.4.6 Interaction of C. albicans with α-lactosyl-terminated PAA

PAA surfaces that were modified with α-lactoside were exposed to a suspension of yeast cells, after which the adsorbed cells were stained with a tetrazolium dye (INT) and subsequently studied with light microscopy. The number of adsorbed cells per field-of-view was counted (Figure 6.8). Lactosyl-modified PAA surfaces showed increased yeast adsorption compared to unmodified PAA, but only to a limited extent. Moreover, competition with free lactose in solution was only found to have effect at very high concentrations (250 mM), whereas competition with glucose did not have any effect.

These results can be explained by selective adsorption of *Candida albicans* onto lactosyl-terminated PAA surfaces. The limited incremental adsorption may be the result of the partial coverage of the cell wall with mannoproteins, which limits the interactions between the β-glucan and the modified PAA surface. Previous studies indeed indicate that the β-glucan is masked in in-vitro experiments,[36] whereas it becomes exposed in growing cultures on (mucosal) surfaces.[37] Moreover, antibody studies indicate a large cell-to-cell variance in β-glucan exposure.[38] Nevertheless,

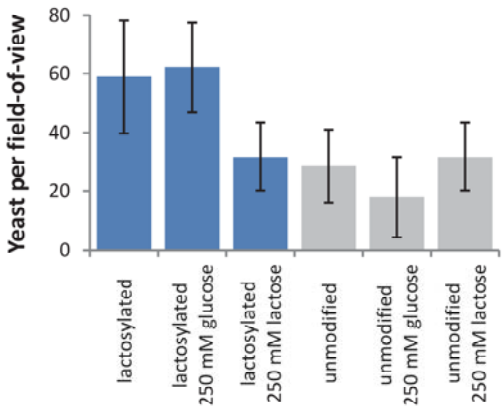

Figure 6.8. Quantification of adsorbed *C. albicans* cells onto lactosyl-terminated and unmodified PAA surfaces, and the effect of competing sugars. Quantification was performed by counting the number of cells per area after staining with INT (n = 4).

partial masking may still allow strong binding to the surface. This was indirectly observed from the high concentrations of lactose necessary in the competition experiment. The need for high concentrations to induce competition points to high binding affinity between cell and surface. This usually results from multivalent binding, which is not unlikely as both the adsorbing yeast and the surface have multiple binding sites.

Adsorption experiments in this study were performed at room temperature. However, the binding of *C. albicans* as well as its β-glucan to LacCer was shown to be enhanced at higher temperatures (37 °C).[10,24] This may relate to improved accessibility of the β-glucan binding sites at higher temperatures. Thus, incubation at higher temperature would likely further increase *C. albicans* adsorption to lactosyl-terminated PAA.

Due to the complexity of the surface of living cells, it cannot be ascertained that the binding to the surface is (solely) due to interactions involving β-glucan. Instead, there may be alternative or additional interactions involved. For example, it is known that *C. albicans* can express a fimbrial protein that binds selectively to glycosphingolipids (such as asialo-GM_1, but not LacCer).[39] Possibly, the cell wall may incorporate adhesins

that are able to bind lactosyl moieties as well. In addition, less specific secondary interactions may also contribute to the binding strength.

The results can be alternatively interpreted when considering that *C. albicans* β-glucan was shown to bind to natural LacCer, but not notably to a synthetic LacCer analog.[10,24] The latter mainly differed from natural LacCer in the saturation of the sphingosine double bond, and thus, these observations indicate that the sphingosine moiety also contributes to *C. albicans* binding. Since the free lactose does not contain this moiety, the high lactose concentration necessary for effective competition would merely reflect the low binding affinity of the yeast with free lactose, instead of indicating the strength of the lactosyl surface-yeast interaction. Moreover, as the surface lactosyl groups are coupled to the PAA via an alkyl chain instead of a sphingosine moiety, strong surface-yeast interactions may not be self-evident. While qualitatively showing the selective adsorption, further research - in which e.g. natural LacCer is used as a competitor - is thus necessary to quantitatively judge the binding affinity of *C. albicans* with lactosylated PAA surfaces. Ideally, these experiments should also use well-characterized fungal species, since species determination of clinical isolates may sometimes be erroneous and different strains of the same species may show large variation in surface characteristics. The current study shows that appropriately modified PAA surfaces would be a highly suitable platform for such studies.

6.5 Conclusions

Lactosyl-terminated PAA surfaces can be prepared by reacting 11-azido-undecyl-lactoside with alkyne-terminated PAA. The resulting surfaces interact specifically and reversibly with peanut agglutinin, as was demonstrated with competition experiments. The lectin adsorption was higher on surfaces that exposed the β-lactoside than on those that displayed the α anomer. As such differences have not been observed in solution, this effect has to relate to the surface confinement of the lactosyl moieties.

Both lactosylated and lectin-exposing surfaces were used for the adsorption of *N. gonorrhoeae*, but attempts for quantification were hampered by high background

staining. *C. albicans*, on the other hand, did show increased colonization onto lactosylated surfaces compared to unmodified surfaces. This effect may originate from interactions involving the cell wall β-glucan, but other interactions may also play a role.

These experiments show that PAA surfaces can be modified to induce specific adsorption of microorganisms. Given the need for rapid detection of microbial infections, further research is highly desirable. This may result in diagnostics that integrate molecular characterization of the cell surface (via specific capture) with subsequent growth. It may also be possible to create carbohydrate arrays that display a library of different molecules and these can thus be used to screen for microorganisms that have a high affinity for specific molecules – possibly isolating microorganisms of industrial importance as well as those with medical significance.

6.6 References

(1) Finlay, B. B.; Cossart, P. *Science* **1997**, *276*, 718-725.

(2) Merz, A. J.; So, M. *Annu. Rev. Cell Dev. Biol.* **2000**, *16*, 423-457.

(3) Karlsson, K. A. *Annu. Rev. Biochem* **1989**, *58*, 309-350.

(4) Wennekes, T.; van den Berg, R.; Boot, R. G.; van der Marel, G. A.; Overkleeft, H. S.; Aerts, J. *Angew. Chem. Int. Edit.* **2009**, *48*, 8848-8869.

(5) Sharon, N. *Trends Biochem. Sci* **1993**, *18*, 221-226.

(6) Ingham, C. J.; Sprenkels, A.; Bomer, J.; Molenaar, D.; van den Berg, A.; Vlieg, J.; de Vos, W. M. *P. Natl. Acad. Sci. USA* **2007**, *104*, 18217-18222.

(7) Finlay, B. B.; Falkow, S. *Microbiol. Mol. Biol. Rev.* **1997**, *61*, 136-169.

(8) Lin, J.; Huang, S. X.; Zhang, Q. J. *Microbes Infect.* **2002**, *4*, 325-331.

(9) Paruchuri, D. K.; Seifert, H. S.; Ajioka, R. S.; Karlsson, K. A.; So, M. *P. Natl. Acad. Sci. USA* **1990**, *87*, 333-337.

(10) Jimenezlucho, V.; Ginsburg, V.; Krivan, H. C. *Infect. Immun.* **1990**, *58*, 2085-2090.

(11) Stromberg, N.; Deal, C.; Nyberg, G.; Normark, S.; So, M.; Karlsson, K. A. *P. Natl. Acad. Sci. USA* **1988**, *85*, 4902-4906.

(12) Deal, C. D.; Krivan, H. C. *J. Biol. Chem.* **1990**, *265*, 12774-12777.

(13) Harvey, H. A.; Swords, W. E.; Apicella, R. A. *J. Autoimmun.* **2001**, *16*, 257-262.

(14) John, C. M.; Griffiss, J. M.; Apicella, M. A.; Mandrell, R. E.; Gibson, B. W. *J. Biol. Chem.* **1991**, *266*, 19303-19311.

(15) Allen, P. Z.; Connelly, M. C.; Apicella, M. A. *Can. J. Microbiol.* **1980**, *26*, 468-474.

(16) Neurohr, K. J.; Bundle, D. R.; Young, N. M.; Mantsch, H. H. *Eur. J. Biochem.* **1982**, *123*, 305-310.

(17) Neurohr, K. J.; Mantsch, H. H.; Young, N. M.; Bundle, D. R. *Biochemistry-US* **1982**, *21*, 498-503.

(18) Pereira, M. E. A.; Kabat, E. A.; Lotan, R.; Sharon, N. *Carbohydr. Res.* **1976**, *51*, 107-118.

(19) Staib, P.; Wirsching, S.; Strauss, A.; Morschhauser, J. *Int. J. Med. Microbiol.* **2001**, *291*, 183-188.

(20) Chaffin, W. L.; Lopez-Ribot, J. L.; Casanova, M.; Gozalbo, D.; Martinez, J. P. *Microbiol. Mol. Biol. Rev.* **1998**, *62*, 130-180.

(21) Ruiz-Herrera, J.; Elorza, M. V.; Valentin, E.; Sentandreu, R. *Fems Yeast Res.* **2006**, *6*, 14-29.

(22) Ohno, N.; Uchiyama, M.; Tsuzuki, A.; Tokunaka, K.; Miura, N. N.; Adachi, Y.; Aizawa, M. W.; Tamura, H.; Tanaka, S.; Yadomae, T. *Carbohydr. Res.* **1999**, *316*, 161-172.

(23) Iorio, E.; Torosantucci, A.; Bromuro, C.; Chiani, P.; Ferretti, A.; Giannini, M.; Cassone, A.; Podo, F. *Carbohydr. Res.* **2008**, *343*, 1050-1061.

(24) Zimmerman, J. W.; Lindermuth, J.; Fish, P. A.; Palace, G. P.; Stevenson, T. T.; DeMong, D. E. *J. Biol. Chem.* **1998**, *273*, 22014-22020.

(25) Sato, T.; Iwabuchi, K.; Nagaoka, I.; Adachi, Y.; Ohno, N.; Tamura, H.; Seyama, K.; Fukuchi, Y.; Nakayama, H.; Yoshizaki, F.; Takamori, K.; Ogawa, H. *J Leukocyte Biol.* **2006**, *80*, 204-211.

(26) Smith, W. N.; Beumel, O. F. *Synthesis-Stuttgart* **1974**, 441-442.

(27) Juan, Y.; Wang, Y. L.; Rassat, A.; Zhang, Y. M.; Sinay, P. *Tetrahedron* **2004**, *60*, 12163-12168.

(28) Mukhopadhyay, B.; Kartha, K. P. R.; Russell, D. A.; Field, R. A. *J. Org. Chem.* **2004**, *69*, 7758-7760.

(29) Andersen, S. M.; Ling, C. C.; Zhang, P.; Townson, K.; Willison, H. J.; Bundle, D. R. *Org. Biomol. Chem.* **2004**, *2*, 1199-1212.

(30) Rasband, W. S. *Image J,* Image J 1.43u, **1997-2010**; U.S. National Institutes of Health: Bethesda, Maryland.

(31) Qin, G. T.; Santos, C.; Zhang, W.; Li, Y.; Kumar, A.; Erasquin, U. J.; Liu, K.; Muradov, P.; Trautner, B. W.; Cai, C. Z. *J. Am. Chem. Soc.* **2010**, *132*, 16432-16441.

(32) Neurohr, K. J.; Young, N. M.; Mantsch, H. H. *J. Biol. Chem.* **1980**, *255*, 9205-9209.

(33) Banerjee, R.; Das, K.; Ravishankar, R.; Suguna, K.; Surolia, A.; Vijayan, M. *J. Mol. Biol.* **1996**, *259*, 281-296.

(34) Mandrell, R. E.; Griffiss, J. M.; Macher, B. A. *J. Exp. Med.* **1988**, *168*, 107-126.

(35) Ingham, C. J.; van den Ende, M.; Pijnenburg, D.; Wever, P. C.; Schneeberger, P. M. *Appl. Environ. Microbiol.* **2005**, *71*, 8978-8981.

(36) Wheeler, R. T.; Fink, G. R. *Plos Pathog.* **2006**, *2*, 328-339.

(37) Dongari-Bagtzoglou, A.; Kashleva, H.; Dwivedi, P.; Diaz, P.; Vasilakos, J. *Plos One* **2009**, *4*, e7967.

(38) Torosantucci, A.; Chiani, P.; Bromuro, C.; De Bernardis, F.; Palma, A. S.; Liu, Y.; Mignogna, G.; Maras, B.; Colone, M.; Stringaro, A.; Zamboni, S.; Feizi, T.; Cassone, A. *Plos One* **2009**, *4*, e5392.

(39) Yu, L.; Lee, K. K.; Sheth, H. B.; Lanebell, P.; Srivastava, G.; Hindsgaul, O.; Paranchych, W.; Hodges, R. S.; Irvin, R. T. *Infect. Immun.* **1994**, *62*, 2843-2848.

Chapter 7

General Discussion

From the previous chapters it follows that 1-alkenes and 1-alkynes are reactive towards various inorganic surfaces. Whereas such reactivity could sometimes be predicted from solution-phase chemistry (e.g. hydrosilylation on silicon), on other surfaces it is quite unexpected (e.g. 1-alkenes on silica). This is especially surprising when one considers that several studies in the past[1,2] have dealt with the reactivity of (terminally) unsaturated hydrocarbons with inorganic surfaces. As these often focused on the catalytic properties of inorganic surfaces, the modification of the surface may have simply been overlooked.

There is no general mechanism for the reaction of terminally unsaturated compounds with inorganic surfaces. Instead, the various proposed mechanisms[3-5] seem to be applicable to specific sets of substrates only. Yet the availability of multiple mechanisms makes it even more likely that the reactivity of 1-alkenes and 1-alkynes is not limited to the reported substrates. Preliminary experiments performed in our laboratory indeed indicated that 1-alkenes are reactive towards indium tin oxide and stainless steel as well, and more inorganic surfaces will undoubtedly be added to the list of reactive substrates in the future.

In contrast to the well-known classes of self-assembled monolayers, 1-alkene/1-alkyne monolayers are often disordered. This reflects the covalent coupling of the molecules to the surface, which does not allow lateral redistribution. Yet disordered monolayers may still have a surface coverage of over 80 % of that of well-ordered monolayers, as is known from experiments with alkylcarboxylates on alumina.[6] Moreover, studies on 1-alkyne monolayers on silicon have shown that covalent coupling does not necessarily preclude formation of well-packed monolayers: it may just require careful tuning of the coupling conditions.[7] With increasing knowledge of the modification mechanisms, it is likely that in the future 1-alkene/1-alkyne monolayers with an improved surface coverage and possibly even molecular order will be obtained on other substrates as well.

From our efforts to obtain functionalized monolayers on alumina, it follows that several functional groups are reactive towards the surface. For example, the adsorption of 1-dodecanal seemed to result in monolayer formation. Presumably, this reactivity is not limited to alumina, but can be extended to other oxide surface as well.

This clearly shows that there is much to be explored in the surface modification of inorganic surfaces.

In addition to these general points, more specific comments and recommendations can be linked to the individual chapters. **Chapter 2** introduces light-enhanced microcontact printing, a technique that can be used for the local modification of H-Si. Such a technique could be useful for electrochemical sensing applications, as it can introduce chemical heterogeneity within limited distance from the semiconductor interface. However, electrochemical detection requires almost defect-free monolayers, which have not been obtained with LE-μCP so far. Backside inking, as reported by Balmer et al,[8] may improve the surface coverage as it omits solvents from the process, and maintains a high concentration of ink at the stamp-substrate interface. Further improvement of the surface coverage may be realized by using stamp materials that are less prone to contaminate the surface. Finally, one could also increase the reactivity of the adsorbent, e.g. by using enyne compounds as an ink.[9] Even so, it may be that the required high surface coverages cannot be obtained. In this case, modification of the H-Si surface with propenyl magnesium bromide could be an interesting alternative, as this gives a high surface coverage and protection against oxidation, whereas the surface can be further functionalized and the distance to the silicon interface is minimal.[10]

Microcontact printing may also be used to locally oxidize the silicon surface. When printing experiments were performed under ambient conditions, the stamp pattern was negatively transferred to the surface. Presumably, illumination enhances oxide formation on the non-contacted areas, whereas the contacted areas are protected against oxidation by the stamp.[11] When the stamp is inked, an organic monolayer may grow simultaneously on the contacted areas, although this does not seem to be required for patterning. Alternatively, the non-oxidized areas can be functionalized afterwards in solution, which can yield high-density monolayers. Therefore, inkless microcontact printing may provide an alternative and simple means to pattern the silicon surface.

Chapter 3 deals with the modification of silica surfaces with 1-alkenes. It shows that the modification reaction is a photochemical process, and indicates that the adsorbate binds to the surface in Markovnikov fashion, which is characteristic of an ionic reaction. Further research on the detailed mechanism is required, specifically given the unclear role of the polymerization that seems to follow the initial monolayer formation. This could involve verification of the adsorbate structure with ultraviolet photoelectron spectroscopy (UPS), which can give the energy levels of the valence electrons involved in surface binding, and in-situ IR spectroscopy on well-defined Si surfaces that are partially covered with –OH moieties.[12] In addition, surface modification can be performed in the presence of a radical scavenger, which will suppress any occurring radical reactions.

One interesting phenomenon that was encountered in the IR spectra of the modified samples is the substrate band. The intensity of this band correlates nicely with that of the methylene vibrations. However, as the band is purely caused by an optical effect, it can be used to determine the adsorbed layer thickness. This would be beneficial since, unlike XPS-based estimations, such thickness determination is almost independent of the composition of the adsorbed film.[13] Initial calculations using an optical model[14,15] were promising, but yielded negative absorption. Performing these quantitative IR measurements would put additional requirements to the experiment, such as such as a stable IR source intensity and a reliable detector signal. Moreover, as the substrate band results from the substrates' specific optical properties, thickness determination is only feasible for a specific set of substrates.

The applicability of the developed modification method mainly depends on the stability of the adsorbed layer. The initial stability experiments with TG-MS and atomic layer deposition have been performed on a multilayer-covered substrate, and therefore may not be representative for the monolayer-covered substrates. Therefore, the stability of these monolayers should be tested in biologically relevant media with future applications in mind.

The developed surface modification method is especially useful for modification of enclosed surfaces. In **Chapter 4**, this method was therefore used to locally couple strands of DNA to the inner surface of a capillary, starting from modification with

2,2,2-trifluoroethyl undec-10-enoate (TFEE). Interestingly, the coverage obtained by grafting this molecule to the surface is lower than that obtained by grafting 1-hexadecene, even though the functional group stays intact. Such differences may be used to derive information on the mechanism, analogously to studies on diamond.[4] Therefore, comparison of the coupling efficiency of several functional components, including trifluoroacetic acid-protected 10-aminodec-1-ene (TFAAD), may be worthwhile as well. Knowledge on the mechanism is useful for further application, since it allows the selection and fine-tuning of functional groups and coupling conditions.

The surface concentration of DNA is dependent on both the TFEE grafting density and the DNA coupling efficiency. Since the publication of Chapter 4, the latter could be improved by performing the reaction at higher amine concentrations, i.e. at 50 instead of 5 μM.[16]

It follows from the hybridization and dehybridization experiments that hybridization may be thwarted by non-specific interactions of the ssDNA with the surface. Such non-specific adsorption may be tested by performing a control experiment in which fluorescently-labeled ssDNA is adsorbed onto a surface that is modified with ethyl undec-10-enoate. This surface closely resembles the TFEE-modified surface, but does not show reactivity towards amines, which implies that all possible adsorption is due to non-covalent interactions. If it follows that non-specific adsorption is significant, further tuning of the organic monolayer is necessary, e.g. by incorporating oligoethylene glycol moieties or zwitterionic polymer linkers that are known to reduce non-specific interactions with biomolecules.[17-19]

The method reported in Chapter 4 has recently been used to immobilize enzymes to the wall of the capillary.[16] In addition, it has allowed the construction of a three-step enzymatic cascade process, in which each step takes place in a discrete zone of the modified capillary. This is particularly useful to reduce enzymatic inhibition by intermediate products, or to force selectivity wherever multiple enzymes can convert the same substrate.

Facile exchange of inactivated surface-bound enzymes is enabled by the reversibility of the DNA conjugation. This reversibility may also be exploited in other applications, such as the preconcentration and separation of DNA-labeled analytes. As

this can be performed directly within a microchannel, these processing steps can be easily integrated in microfluidic devices.

In **Chapter 5** it is shown that adsorption of 1-alkynes onto alumina yields a surface-bound 2-hydroxy carboxylate. Whereas 1-alkynes are known to oxidize into several species, the formation of 2-hydroxy-carboxylates has not been reported before. Therefore, the major issue that still needs to be addressed is the mechanism of adsorbate formation. Mechanistic information may be available in literature on surface catalysis, or may be obtained by adsorbing structurally related compounds, such as 1-alkenes or 3-substituted 1-alkynes. Testing for reactivity differences on various types of (pretreated) alumina may further contribute to mechanistic understanding. Finally, these experimental observations may be supported by quantum chemical calculations on models of the alumina surface.

In addition to elucidating the adsorption mechanism, it would be interesting to further explore direct monolayer formation of 2-hydroxy carboxylic acids. Since these are chiral compounds, adsorption of the individual enantiomers can show the influence of chirality on monolayer formation. Unfortunately, as the commercial availability of 2-hydroxy carboxylic acids is limited, synthetic methods need to be developed to introduce this moiety into other functionalized compounds. On the other hand, the oxidative adsorption of 1-alkynes onto alumina may itself be a means to obtain 2-hydroxy carboxylic acids, especially when the chemisorption would turn out to be reversible under certain conditions.

This last argument also stresses the importance of further stability studies. The stability studies performed in chapter 5 are limited, and the observed hydrolytic stability may be dependent on pH. This is also indicated by the limited stability of the 2-hydroxy carboxylate-aluminium complex in acidic solutions.[20] For further biochemical applications, the hydrolytic stability of the modified surfaces should be tested at a wide pH range in several different buffers.

In our stability experiments, we have compared the stability of PAA that was modified with 1-hexadecene and with 1-hexadecyne. Adsorption of the 1-alkene also resulted in monolayer formation, but this was not further explored because the 1-alkyne-modified surfaces showed superior stability. Nevertheless, it is interesting to

study the structure of 1-alkene-derived monolayer, both from a fundamental point of view and because it can further elucidate the oxidation mechanism of unsaturated compounds on alumina.

Finally, since we have introduced an additional surface chemistry to modify alumina, there is a need to compare the different known modification methods on relevant parameters. These could include e.g. thermal and hydrolytic stability, packing density and ease of functionalization. Such a study would be beneficial from the perspective of further application.

The choices for the adsorptive species in **Chapter 6** have partially been driven by pragmatism. Therefore, the studied carbohydrate-adhesin systems may not have been optimal in all cases. This can explain why peanut agglutinin does and *N. gonorrhoeae* does not show selective adsorption onto lactose-terminated PAA surfaces: Whereas the former is selective for D-galactose residues (i.e. the terminus of the lactosyl moiety), the latter shows higher affinity for carbohydrate sequences that are more complex than lactose, such as asialo-GM_2 (GalNac(β1-4)Gal(β1-4)Glc(β1-1)Cer). Future studies on selective microbial adsorption should therefore start from a careful design of the target carbohydrate. Ideally, this design should also take into account the effect of the ceramide, even though incorporation of this moiety may further complicate carbohydrate synthesis.

An interesting phenomenon that was observed is the adsorption difference of PNA between α- and β-lactosylated surfaces. We have suggested that this is due to increased steric hindrance at the α-lactosylated surface. However, this suggestion was done based on the limited experimental evidence that adsorption of each epimer yields equal surface coverage, which should be further validated by XPS analysis. If these experiments support a steric effect, it would also be interesting to further study the effect of lactosyl surface concentration on lectin adsorption, e.g. by performing the azide-alkyne cycloaddition with a mixture of a lactosylated and a non-functional azide.

Since lectins have multiple binding pockets, lectin-modified surfaces can be used to further adsorb antigen-expressing molecules, nanoparticles, proteins and even cells. This was attempted in Chapter 6 by adsorbing *N. gonorrhoeae*. Since PNA gave rise to gonnococcal agglutination in solution, selective adsorption to the surface was also

expected. However, this selectivity could not be observed by traditional staining methods due to a high background intensity. Other methods for staining or fluorescent labeling should therefore be investigated. This could include a sandwich assay in which fluorescently labeled PNA is adsorbed subsequently to *N. gonorrhoeae*. Alternatively, label-free methods such as Raman spectroscopy could be used to (qualitatively) determine the presence of *N. gonorrhoeae* on the PAO surface. Finally, the monolayer constituents could be tuned to prevent non-specific dye adsorption, e.g. by the incorporating of oligoethyleneglycol moieties or poly-zwitterionic linkers.

Direct adsorption of microorganisms onto lactosylated PAO surfaces was difficult to observe, which in the case of *N. gonorrhoeae* was primarily due to staining problems. But even so, the gonococcal affinity for lactosyl moieties may have been limiting. Since *N. gonorrhoeae* binds more avidly to asialo-GM_1 and asialo-GM_2 than to lactose,[21] and the adhesin involved in this interaction has been identified,[22] surface functionalization with these more complex carbohydrates would be an interesting subject for future studies. These studies could be further extended by adsorbing other pathogens such as *Neisseria meningitidis* and *Moraxella catarrhalis*, which are also known to selectively bind to asialo-GM_1 and asialo-GM_2.[23,24]

The interaction of *Candida albicans* with lactosyl ceramide is rather unusual. Whereas selective binding usually involves a carbohydrate and a protein, this interaction is carbohydrate-based only.[25] As it involves β-glucan, a structural cell wall component, it seems that this interaction is coincidental, and thus is unlikely to be exploited in the colonization of human tissue. On the contrary, there is even limited evidence that this interaction is exploited by the human immune system to counter colonization![25,26] For the selective adsorption of *C. albicans* onto PAO surfaces, other interactions may therefore prove to be more effective. Examples include the fimbrial adhesion of *C. albicans* to asialo-GM_1 and asialo-GM_2,[27] and the fucose-specific binding of candidal germ tubes.[28] Interestingly, such interactions may also be exploited for phenotypic selection, as the adhesins involved are only expressed in certain fungal forms.

In conclusion, the selective adsorption of microorganisms onto surfaces is a very interesting field that is still largely unexplored. Selective adsorption can be achieved by functionalizing the surface with carbohydrates (mimicking the binding between a

glycosphingolipid and an adhesin), or with adhesins that target bacterial carbohydrate sequences (analogously to lectin-LPS binding). Alternatively, the surface may be equipped with antibodies that target bacterial antigens. Whatever approach is selected, the selective adsorption of microorganisms has great potential in the fields of medical diagnostics and microbial screening, and may eventually be applied in a range of products, including a rapid test for sexually transmitted diseases.[29]

References

(1) Trombetta, M.; Busca, G.; Rossini, S.; Piccoli, V.; Cornaro, U.; Guercio, A.; Catani, R.; Willey, R. J. *J. Catal.* **1998**, *179*, 581-596.

(2) Corma, A. *Chem. Rev.* **1995**, *95*, 559-614.

(3) Cicero, R. L.; Chidsey, C. E. D.; Lopinski, G. P.; Wayner, D. D. M.; Wolkow, R. A. *Langmuir* **2002**, *18*, 305-307.

(4) Nichols, B. M.; Butler, J. E.; Russell, J. N.; Hamers, R. J. *J. Phys. Chem. B* **2005**, *109*, 20938-20947.

(5) Sun, Q. Y.; de Smet, L. C. P. M.; van Lagen, B.; Giesbers, M.; Thune, P. C.; van Engelenburg, J.; de Wolf, F. A.; Zuilhof, H.; Sudholter, E. J. R. *J. Am. Chem. Soc.* **2005**, *127*, 2514-2523.

(6) Sondag, A. H. M.; Raas, M. C. *J. Chem. Phys.* **1989**, *91*, 4926-4931.

(7) Scheres, L.; Arafat, A.; Zuilhof, H. *Langmuir* **2007**, *23*, 8343-8346.

(8) Balmer, T. E.; Schmid, H.; Stutz, R.; Delamarche, E.; Michel, B.; Spencer, N. D.; Wolf, H. *Langmuir* **2005**, *21*, 622-632.

(9) Rijksen, B.; Scheres, L.; Zuilhof, H. *manuscript in preparation*.

(10) Puniredd, S. R.; Assad, O.; Haick, H. *J. Am. Chem. Soc.* **2008**, *130*, 13727-13734.

(11) Rosso, M.; Giesbers, M.; Schroen, K.; Zuilhof, H. *Langmuir* **2010**, *26*, 866-872.

(12) Michalak, D. J.; Amy, S. R.; Aureau, D.; Dai, M.; Esteve, A.; Chabal, Y. J. *Nat. Mater.* **2010**, *9*, 266-271.

(13) Thickness determination using the substrate band would be dependent on the refractive index of the adsorbed layer.

(14) Dijt, J. C.; Stuart, M. A. C.; Fleer, G. J. *Adv. Colloid Interfac.* **1994**, *50*, 79-101.

(15) These calculations were performed by Remco Fokkink (Laboratory of Physical Chemistry and Colloid Science).

(16) Vong, T.; Schoffelen, S.; van Dongen, S. F. M.; van Beek, T. A.; Zuilhof, H.; van Hest, J. C. M. *Chem. Sci.* **2011**, *2*, 1278-1285.

(17) Holmlin, R. E.; Chen, X. X.; Chapman, R. G.; Takayama, S.; Whitesides, G. M. *Langmuir* **2001**, *17*, 2841-2850.

(18) Jiang, S. Y.; Cao, Z. Q. *Adv. Mater.* **2010**, *22*, 920-932.

(19) Prime, K. L.; Whitesides, G. M. *J. Am. Chem. Soc.* **1993**, *115*, 10714-10721.

(20) Corain, B.; Longato, B.; Sheikhosman, A. A.; Bombi, G. G.; Macca, C. *J. Chem. Soc.-Dalton Trans.* **1992**, 169-172.

(21) Stromberg, N.; Deal, C.; Nyberg, G.; Normark, S.; So, M.; Karlsson, K. A. *P. Natl. Acad. Sci. USA* **1988**, *85*, 4902-4906.

(22) Paruchuri, D. K.; Seifert, H. S.; Ajioka, R. S.; Karlsson, K. A.; So, M. *P. Natl. Acad. Sci. USA* **1990**, *87*, 333-337.

(23) Ahmed, K.; Suzuki, Y.; Miyamoto, D.; Nagatake, T. *Med. Microbiol. Immun.* **2002**, *191*, 5-10.

(24) Hugosson, S.; Angstrom, J.; Olsson, B. M.; Bergstrom, J.; Fredlund, H.; Olcen, P.; Teneberg, S. *J. Biochem.* **1998**, *124*, 1138-1152.

(25) Zimmerman, J. W.; Lindermuth, J.; Fish, P. A.; Palace, G. P.; Stevenson, T. T.; DeMong, D. E. *J. Biol. Chem.* **1998**, *273*, 22014-22020.

(26) Sato, T.; Iwabuchi, K.; Nagaoka, I.; Adachi, Y.; Ohno, N.; Tamura, H.; Seyama, K.; Fukuchi, Y.; Nakayama, H.; Yoshizaki, F.; Takamori, K.; Ogawa, H. *J Leukocyte Biol.* **2006**, *80*, 204-211.

(27) Yu, L.; Lee, K. K.; Sheth, H. B.; Lanebell, P.; Srivastava, G.; Hindsgaul, O.; Paranchych, W.; Hodges, R. S.; Irvin, R. T. *Infect. Immun.* **1994**, *62*, 2843-2848.

(28) Vardar-Unlu, G.; McSharry, C.; Douglas, L. J. *FEMS Immunol. Med. Mic.* **1998**, *20*, 55-67.

(29) Bijlsma, E. Snelle soatest in ontwikkeling. *Sp!ts*, Sept 11, 2009, p 1.

Appendix A

Supplementary information to Chapter 4

A.1 Electronic core level calculations

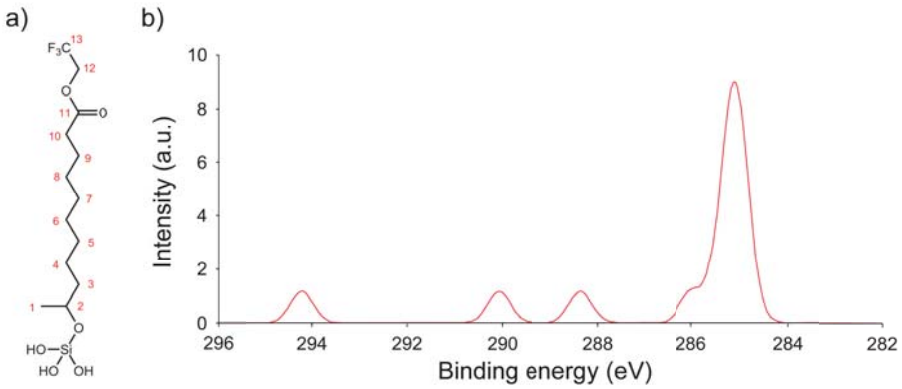

Figure A-1. a) Simplified model of the surface-bound TFEE molecule, and b) the simulated C_{1s} electron energies that was obtained by calculating the corresponding C_{1s} electron energies with Gaussian03 (B3LYP/6-311G(d,p) level of theory with natural bond orbital analysis).

Table A-1. Calculated C_{1s} electron energies for the model depicted in Figure A-1a.

Atom	eV	Atom	eV	Atom	eV
C_1	285.4	C_6	285.1	C_{10}	286.0
C_2	285.0	C_7	285.1	C_{11}	290.1
C_3	285.1	C_8	285.1	C_{12}	288.3
C_4	284.8	C_9	285.3	C_{13}	294.2
C_5	285.0				

A.2 XPS C_{1s} spectra of a TFEE monolayer on borosilicate

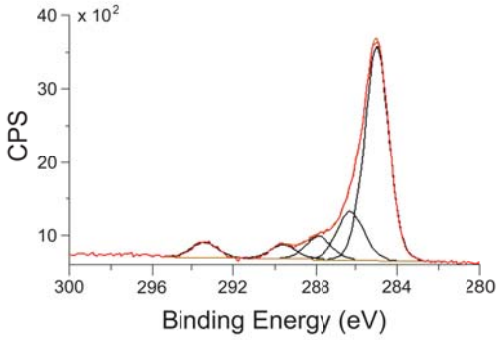

Figure A-2. C_{1s} narrow scan of TFEE-modified borosilicate surface after 4 hours of modification.

A.3 Determination of DNA hybridization coverage

To determine the amount of dehybridized DNA, a calibration curve was made by spiking known amounts of the complementary, fluorescently-labeled strand (AC-Cy5) into an unmodified microchannel under constant buffer flow. The areas of the resulting peaks in the graph of the fluorescence spectrometer were then plotted against the amount of injected AC-Cy5, from which a linear relation could be established (Figure A-3). This calibration graph was used to determine the amount of dehybridized DNA from the signal of the fluorescence spectrometer in the dehybridization experiments. These numbers were then converted to molecules per cm^2 using Avogadro's number and the area of the modified surface (0.188 cm^2).

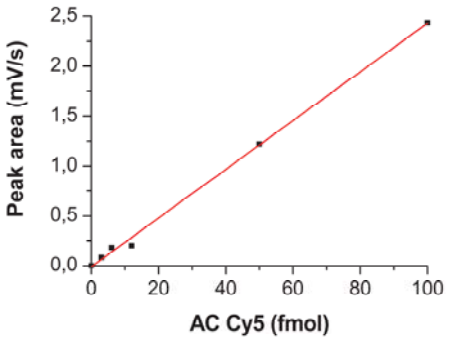

Figure A-3. Calibration of the fluorescence spectrometer response on the spiking of different amounts of fluorescently labeled, complementary DNA.

Appendix B

Supplementary information to Chapter 5

B.1 Surface sensitivity of XPS on porous anodic alumina

In our experimental setup, the angle between the X-ray beam and the surface normal is 80°, while the angle between the detector and the surface normal is 10°. While only a fraction of the X-rays is absorbed by the alumina, we assume that the X-ray intensity in the sample is uniform. Absorption of X-rays results in the emission of electrons in all directions. However, due to attenuation, only the electrons originating from the first 10 nm of the surface are able to escape the surface. Of these electrons, only those will be detected that are emitted at the same angle as the detector. For flat samples, the depth of analysis (the surface sensitivity), is dependent on the angle between the sample and the detector. Assuming that the depth of analysis for a sample normal to the detector is 10 nm, tilting it by 10° will reduce this depth by a factor equal to the cosine of this angle, i.e. to 9.8 nm.

Porous alumina, however, contains pores that run perpendicularly to the surface. Due to the sample tilt, electrons originating from the inner surface of the pore will be able to reach the detector. Since the angle between the inner surface and the detector is not 10 but 80°, the depth of analysis of the inner surface is only 1.7 nm, i.e. the signal obtained from the inner surface is very sensitive to adsorbed species (Figure B-1).

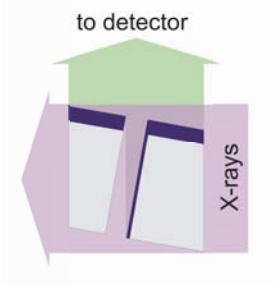

Figure B-1. Schematic cross section of a fragment of the PAA surface during XPS acquisition. The depth of analysis is highlighted by the dark areas.

The total signal of a PAA surface during acquisition consists of contributions arising from both the internal and the external surface, whereas that of a flat, non-porous surface only consists of external surface contributions. Correspondingly, measurements on PAA surfaces will show increased surface sensitivity compared to flat surfaces. As simple attenuation calculations do not take into account porosity effects, the resulting adsorbed layer thickness will therefore be overestimated.

B.2 Electronic core level calculations

To confirm whether the proposed binding model fits with the obtained XPS data, the energies of the core electrons were calculated using the Gaussian09 program.[1] Since the detailed surface structure of the amorphous PAA is unknown, an (over)simplified structure was used to model the surface sites. The final model is depicted in Figure B-2. The system geometry was optimized at the B3LYP/6-311G(d,p) level of theory, and natural bond orbital analysis[2] was employed to obtain the core orbital energies. The energy of C_5 was set to 285 eV by multiplying the calculated value of 277.6 eV with a scaling factor; this scaling factor was then applied to the other carbon atoms as well.

Figure B-2. Simplified model used for the theoretical calculations of XPS data.

B.3 Monolayers of 2-hydroxy-hexadecanoic acid onto PAA

The XPS spectra of PAA surface modified with 1-hexadecyne and with 2-hydroxy-hexadecanoic acid have been obtained, and are reported below. The strong analogy clearly points to the presence of the same surface-bound species.

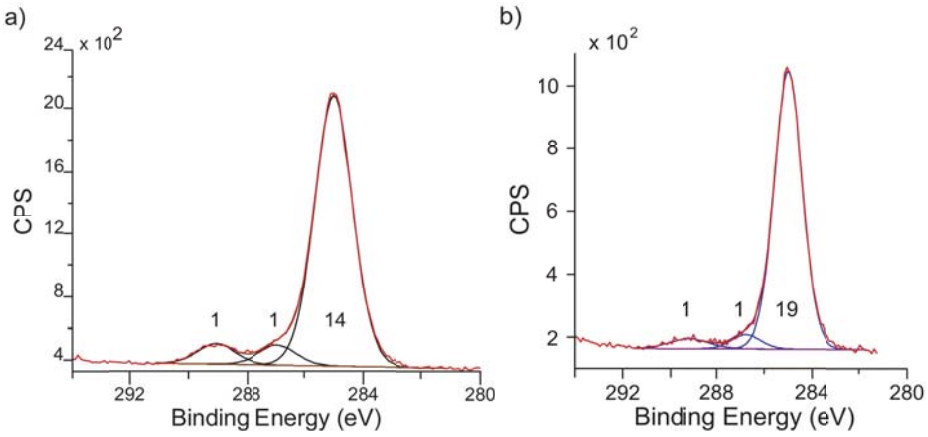

Figure B-3. X-ray photoelectron spectrum of the C_{1s} region of 1-hexadecyne-modified PAA (left), 2-hydroxy hexadecanoic acid-modified PAA (right) and their deconvolutions.

B.4 XPS wide area spectra of functionalized surfaces.

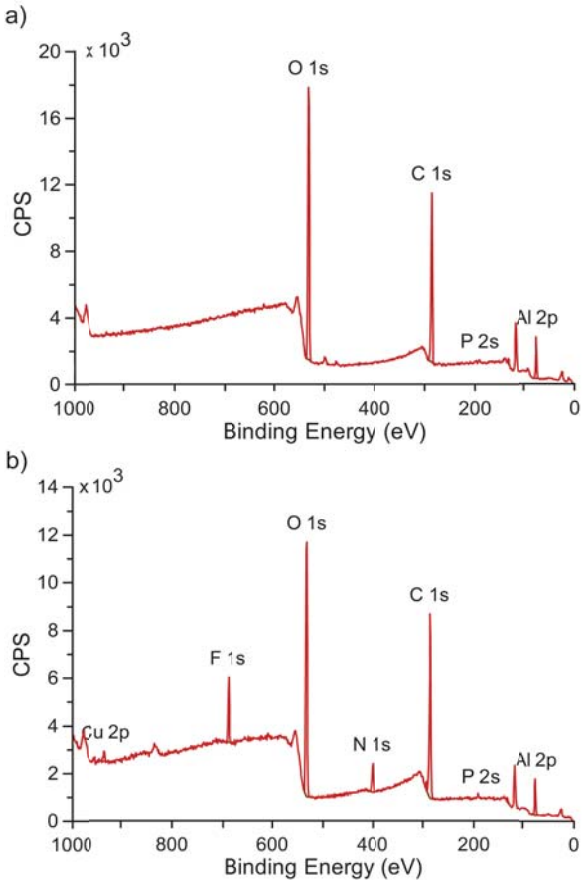

Figure B-4. XPS wide area spectra of alkyne-terminated PAA before (a), and after reaction with 11-azido-3,6,9-trioxaundecyl-trifluoro-acetamide (b).

B.5 References

(1) Frisch, M. J.et al. *Gaussian 09, Revision A.1,* **2009**; Gaussian, Inc.: Wallingford CT.

(2) Glendening, E. D.; Reed, A. E.; Carpenter, J. E.; Weinhold, F. *NBO, Version 3.1,*

Summary

Surface modification is important because it allows the tuning of surface properties, thereby enabling new applications of a material. It can change physical properties such as wettability and friction, but can also introduce chemical functionalities and binding specificity. Several techniques are available to modify the surface, such as Langmuir-Blodgett adsorption, protein adsorption or monolayer formation. Of these, organic monolayers have the advantages that they are easily tunable, fairly stable, and do not change the structural properties of the surface.

Most studies on monolayer formation deal with self-assembled monolayers (SAMs), which form spontaneously under ambient conditions. However, in the last two decades studies on the coupling of unsaturated hydrocarbons to the surface have also emerged. The formation of such monolayers requires activation, e.g. by heating or illumination. Nevertheless, these monolayers are of particular interest because of their high stability, resulting from the covalent coupling and the weakly polarized surface bond.

From the overview given in **Chapter 1**, it follows that terminally unsaturated hydrocarbons (1-alkenes and 1-alkynes) form covalently coupled monolayers on a variety of substrates, such as silicon-based materials and diamond. The mechanism by which this takes place is dependent on the substrate material and reaction conditions. The reactions on silicon and diamond are well-understood, and studies can now focus on applications. Conversely, the understanding of the UV-mediated reactions on silicon nitride and silicon carbide is limited, and these reactions thus require further fundamental investigation. In addition, terminally unsaturated hydrocarbons may modify other inorganic materials as well. This is the subject of this thesis.

Chapter 2 deals with the well-known modification of silicon surfaces. In this chapter, a method for the direct patterning of 1-alkynes onto hydrogen-terminated silicon is presented. The method combines microcontact printing with illumination by visible light through the stamp, and results in the local formation of an alkenyl monolayer. The method was named light-enhanced microcontact printing (LE-μCP), since monolayer formation was clearly enhanced by visible light illumination. Extended contact times (~3 h) and high ink concentrations (100 mM) are required for optimal results. This yields monolayers with a moderate surface coverage, which is comparable to other μCP-based methods on silicon. The features of the stamp are well-transferred to the surface, and pattern broadening remains limited in spite of the prolonged reaction times. Chemically heterogeneous surfaces can be prepared by backfilling the uncontacted areas with a functional second ink. Interchanging the inks results in contrast inversion, showing that LE-μCP is also compatible with functional inks.

In **Chapter 3** the modification of fused silica substrates with 1-alkenes was investigated. Functionalization of these transparent substrates is of major importance in the field of sensing and diagnostics. Currently, the surface modification of these materials is based on organosilane chemistry, but this has several disadvantages. Therefore, a new modification method was developed, which is based on a photochemical reaction of terminal alkenes with the surface. This yielded highly hydrophobic surfaces with high thermal stability. The adsorbed layer prevents atomic layer deposition of platinum, and thus provides proper chemical passivation of the underlying surface. The alkenes initially bind to the surface hydroxyl groups in Markovnikov fashion, but at prolonged reaction oligomerization takes place, resulting in an increased layer thickness. The reaction is photochemically initiated, requiring light with a wavelength below 275 nm, which enables the use of photolithography to constructively pattern the silica surfaces. As this was previously impossible, the newly developed method therefore forms a valuable addition to the existing modification methods.

The method developed in Chapter 3 was applied in **Chapter 4** to locally furnish silica surfaces with a functional linker. This allowed the selective attachment of single-stranded DNA onto the modified areas. Such selective modification can be performed onto plain surfaces, but also onto curved, enclosed surfaces, as was demonstrated by the functionalization of the inner surface of a microchannel. By using fluorescently labeled DNA, sharp pattern boundaries could be visualized. The surface-bound DNA can be selectively and reversibly hybridized with a strand of complementary DNA. From the hybridization cycles, it follows that $\sim 7 \times 10^{11}$ fluorescently labeled DNA molecules are hybridized per cm^2. By furnishing target compounds with the complementary DNA strand, this hybridization approach may be applied for the selective, localized binding of proteins, antibodies and other biomolecules to the surface.

In Chapters 5 and 6 the material of interest is porous anodic alumina (PAA). In **Chapter 5**, a new method for the organic modification of PAA is presented, which is based on the reaction of terminal alkynes with the alumina surface. The reaction results in the formation of a monolayer within several hours at 80 °C and is dependent on both oxygen and light. These monolayers are well-defined and consist of an oxidation product of the 1-alkyne, namely its α-hydroxy carboxylate. The obtained monolayers are fairly stable in water and at elevated temperatures. Modification with 1,15-hexadecadiyne results in a surface with available alkyne endgroups. These can be used for further surface chemistry, such as the alkyne-azide coupling reaction.

In **Chapter 6**, the biofunctionalization of PAO is explored by coupling 11-azido-undecyl-lactoside to the alkyne-terminated surface and studying the subsequent adsorption of lectin peanut agglutinin (PNA). The PNA binds selectively and reversibly to the lactosylated surfaces. Moreover, PNA adsorption is higher on surfaces that expose the β-lactoside than on those that display the α-anomer. This effect can be attributed to surface-associated steric hindrance.

Selective adsorption of pathogenic micro-organisms to functionalized surfaces is potentially interesting for medical diagnostics, as it can reduce the time to diagnosis. Therefore, the adsorption of *Neisseria gonorrhoeae* and *Candida albicans* onto

lactosylated porous anodic alumina (PAA) surfaces was also investigated. *N. gonorrhoeae* was adsorbed either directly onto the lactosylated surface or subsequently to PNA adsorption. Yet in both cases, quantification of the adsorbed *N. gonorrhoeae* was hampered by high background staining. *C. albicans*, on the other hand, did show increased colonization onto lactosylated surfaces compared to unmodified surfaces, presumably due to interactions involving the cell wall β-glucan. Thus, Chapter 6 shows that aluminum oxide surfaces can be modified to induce selective adsorption of proteins and micro-organisms.

This thesis includes several studies on the surface modification of silicon, silicon oxide and aluminum oxide with 1-alkenes and 1-alkynes. **Chapter 7** contains recommendations for further research on the modification of these materials. It is highly likely that terminally unsaturated hydrocarbons show reactivity towards other relevant inorganic surfaces as well, which can be worthwhile investigating. Moreover, in the course of this study, it was found that other functionalities are also able to modify oxidic surfaces. This clearly shows that there is much to be explored in the surface modification of inorganic surfaces!

The modified surfaces have been used for the selective binding of DNA, proteins and micro-organisms. These will likely develop a rapidly growing importance in a wide range of devices. Especially the selective adsorption of microorganisms onto surfaces is a very interesting field, as it still largely unexplored with respect to both fundamental and more applicable aspects. Following up on the coupling of organic and (bio)functional compounds, surface modification with living cells and biofilms will therefore be a research topic of prime interest for the coming years!

Samenvatting

Het modificeren van oppervlakken is belangrijk omdat het ons in staat stelt de eigenschappen van het oppervlak aan te passen. Zo kunnen fysische eigenschappen als bevochtiging en frictie worden aangepast, maar ook kunnen functionele chemische groepen worden geïntroduceerd. Dit laatste geeft ons de mogelijkheid om verdere chemie aan het oppervlak te bedrijven, bijvoorbeeld voor het maken van moleculaire apparaten of voor het selectief binden van van bepaalde stoffen. Er zijn verschillende technieken om een oppervlak te modificeren, zoals de adsorptie van polymeren, eiwitten of Langmuir-Blodgett lagen, maar ook de vorming van organische monolagen. Juist deze laatste zijn interessant omdat deze de structurele eigenschappen van het oppervlak niet veranderen, gemakkelijk te variëren en betrekkelijk stabiel zijn.

Veel studies op het gebied van monolaagvorming zijn gericht op zelfvormende monolagen, welke al bij kamertemperatuur spontaan aan het oppervlak binden. Daarnaast zijn er monolagen die activeringsenergie vereisen om te worden gevormd, bijvoorbeeld in de vorm van belichting of verwarming. Een belangrijke klasse van verbindingen die zulke monolagen vormt, zijn de eindstandig onverzadigde koolwaterstoffen (EOKs). Monolagen van deze verbindingen staan in de belangstelling vanwege hun hoge stabiliteit, wat het resultaat is van een covalente, zwak gepolariseerde binding met het oppervlak.

Uit het overzicht in **hoofdstuk 1** volgt dat EOKs (ofwel 1-alkenen en 1-alkynen) covalent gebonden monolagen vormen op verscheidene substraten, zoals silicium-houdende materialen en diamant. Het mechanisme waarmee deze koppeling plaatsvindt, is afhankelijk van het materiaal en de reactiecondities. Er is al veel bekend over de koppelingsreactie op silicium en diamant, maar de monolaagvorming op

andere siliciumhoudende materialen behoeft nog verder onderzoek. Daarnaast is het waarschijnlijk dat EOKs ook op andere anorganische materialen monolagen kunnen vormen. Dit is het onderwerp van dit proefschrift.

In **hoofstuk 2** wordt een toepassing van de organische modificatie van silicium oppervlakken behandeld. Er wordt een methode gepresenteerd om monolagen van 1-alkynen patroonsgewijs op waterstof-getermineerde oppervlakken te vormen. Deze methode combineert microcontact printen (μCP, een stempeltechniek) met belichting door de stempel heen. Daar waar de stempel in contact met het oppervlak is, wordt een alkenyl monolaag gevormd, terwijl de belichting het proces bevordert. Om optimale resultaten te verkrijgen is een lange contacttijd (> 3 u) en een hoge inktconcentratie (100 mM) nodig. De resulterende monolagen hebben een aanzienlijke dichtheid, vergelijkbaar met monolagen die via andere μCP-methoden zijn gevormd. De patronen van de stempel worden goed overgebracht naar het oppervlak en ondanks de lange contacttijd blijft de patroonverbreding beperkt. Chemisch heterogene oppervlakken kunnen worden bereid door na de stempelstap de nog ongereageerde gebieden te laten reageren met een functionele tweede inkt. Tenslotte is de ontwikkelde methode ook goed toepasbaar met functionele inkt.

In **hoofdstuk 3** wordt de modificatie van fused silica substraten met 1-alkenen onderzocht. Functionalizering van deze transparante substraten is van groot belang voor toepassingen op het gebied van biochemische detectie en diagnostiek. De huidige modificatiemethoden zijn gebaseerd op organosilaanchemie en hebben een aantal beperkingen. Daarom is een nieuwe methode ontwikkeld, gebaseerd op een fotochemische reactie van eindstandige alkenen met het oppervlak. De reactie wordt geïnitieerd door licht met een golflengte < 275 nm en resulteert in hydrofobe oppervlakken met een hoge thermische stabiliteit. De gevormde laag verhindert atomaire laagdepositie van platina en biedt dus een goede passivering van het oppervlak. De alkenen binden in eerste instantie aan het oppervlak via Markovnikov additie, maar bij langere reactietijden groeit de laag dikker door oligomerizatie. Bijzonder aan deze reactie is de mogelijkheid om het oppervlak lokaal te modificeren

middels fotolithografie. De nieuw ontwikkelde modificatiemethode vormt daarom een belangrijke aanvulling op de bestaande methoden.

De methode uit hoofdstuk 3 wordt in **hoofdstuk 4** gebruikt om silica oppervlakken lokaal te voorzien van een functionele groep. Dit maakt het mogelijk om specifiek op deze plaatsen enkelstrengs DNA te binden. Dit kan zowel op vlakke als op gekromde, omsloten oppervlakken, zoals is gedemonstreerd door de binnenkant van een silica microkanaal te functionalizeren. Door het DNA van een fluorescent label te voorzien, kan zichtbaar worden gemaakt dat de patronen scherp begrenst zijn. Het gebonden DNA kan selectief en reversibel gehybridizeerd worden met een streng van de complementaire sequentie. Uit de hybridizatiecycli volgt dat er $\sim 7 \times 10^{11}$ fluorescent gelabelde DNA moleculen per cm^2 kunnen hybridizeren. Door eiwitten, antilichamen en andere biomoleculen te voorzien van een complementaire DNA streng, wordt het mogelijk om deze verbindingen selectief aan het oppervlak te binden.

In hoofdstukken 5 en 6 wordt de oppervlaktemodificatie van poreus anodisch alumina (PAA) behandeld. In **hoofdstuk 5** wordt hiervoor een nieuwe methode gepresenteerd, die is gebaseerd op een reactie van eindstandige alkynen met het oppervlak. De reactie leidt bij 80 °C binnen enkele uren tot de vorming van een monolaag en is afhankelijk van zowel zuurstof als licht. Deze monolaag is goed gedefinieerd en bestaat uit een oxidatieproduct van het 1-alkyn, namelijk zijn α-hydroxy carboxylaat. De verkregen monolagen zijn redelijk stabiel in water en bij hogere temperaturen. Modificatie met 1,15-hexadecadiyn geeft een oppervlak dat nog vrije alkyngroepen beschikbaar heeft voor verdere oppervlaktereacties. Dit is gedemonstreerd door hier vervolgens een azideverbinding aan te koppelen.

In **hoofdstuk 6** wordt de biofunctionalizering van PAA verkend door een lactoside aan het alkyn-getermineerde oppervlak te koppelen en hier vervolgens het lectine pinda agglutinine (PNA) aan te adsorberen. Het PNA bindt selectief en reversibel aan de gemodificeerde oppervlakken, maar wel meer aan die waarop het β-lactoside gekoppeld is dan aan die met het α-anomeer. Dit effect kan worden verklaard door oppervlakte-gerelateerde sterische hinder.

Daarnaast is de adsorptie van de pathogenen *Neisseria gonorrhoeae* en *Candida albicans* aan het lactose-getermineerde PAA onderzocht. Selectieve adsorptie van zulke pathogenen is van mogelijk belang voor de medische diagnostiek, omdat het de diagnosetijd potentieel kan verkorten. *N. gonorrhoeae* is zowel direct op het gefunctionaliseerde PAA oppervlak geadsorbeerd, alsook na adsorptie van PNA. Het was echter niet mogelijk om het aantal geadsorbeerde bacteriën te bepalen door problemen met het aankleuren van de microorganismen. Experimenten met *C. albicans* lieten daarentegen meer kolonizatie zien op lactosyl-getermineerd PAA dan op ongemodificeerde oppervlakken. Dit is vermoedelijk te wijten aan interacties van het lactose met het β-glucan van de celwand. Hoofdstuk 6 laat daarom zien dat aluminium oxide oppervlakken zo gemodificeerd kunnen worden dat eiwitten en micro-organismen hier selectief op adsorberen.

Dit proefschrift omvat verschillende studies waarin een aantal materialen gemodificeerd wordt met 1-alkenen en 1-alkynen. **Hoofdstuk 7** bevat aanbevelingen voor verder onderzoek aan de modificatie van deze materialen. Daarnaast is het goed denkbaar dat EOKs ook reageren met andere relevante anorganische oppervlakken. Ook is tijdens dit onderzoek gebleken dat andere functionele groepen eveneens in staat zijn om met oxidische oppervlakken te reageren. Dit laat duidelijk zien dat er nog veel te ontdekken valt op het gebied van oppervlaktemodificatie van anorganische oppervlakken!

De gemodificeerde oppervlakken zijn gebruikt om er DNA, eiwitten en micro-organismen selectief aan te laten binden. Zulke biofunctionele oppervlakken zullen steeds belangrijker worden in een scala aan toepassingen. Vooral de selectieve adsorptie van micro-organismen aan oppervlakken is bijzonder interessant, omdat hier nog weinig onderzoek aan is gedaan. In navolging van oppervlaktemodificatie met organische en biochemische verbindingen, zal oppervlaktemodificatie met levende cellen en biofilms ongetwijfeld een belangrijk onderzoeksonderwerp worden in de komende jaren!

Dankwoord

Tijdens mijn promotie-onderzoek heb ik met veel mensen samengewerkt. In deze sectie wil ik hen graag bedanken.

Veel dank ben ik verschuldigd aan mijn promotor Han Zuilhof. Han, ik heb veel bewondering voor je enorme ambitie. Bedankt voor de vrijheid die je me hebt gegeven in mijn onderzoek en je aansporingen om toch vooral het werk aan die glasmodificatie voort te zetten. Ook dank ik je voor je geduld tijdens de periode dat mijn promotiewerk op een wat lager pitje stond.

Ernst Sudhölter wil ik bedanken voor zijn begeleiding aan het begin van het project. Ernst, je verwondering werkt motiverend!

In the first year of my PhD, I had the opportunity to visit the group of Matt Linford at the Brigham Young University. It was very inspiring to experience the result-oriented, teamwork-driven approach of this group. In particular, I would like to thank Michael Lee for teaming up with me in that period. Thank you, Matt and Michael, for you warm hospitality.

I would also like to thank Stacey Bent and Marja Mullings from Stanford University. Your work on atomic layer deposition has been a great addition to Chapter 3.

Ik heb het genoegen gehad om vier jaar lang een kamer te delen met Luc Scheres. Ook al zaten we soms allebei in onze eigen wereld, in die vier jaar is hier toch een goede vriendschap uit voortgekomen. Luc, ik wil je hartelijk bedanken voor alle kopjes koffie, tafelvoetbalwedstrijden, rondjes om de golfbaan, barbeques op de boerderij, brainstormsessies, en wat al niet meer. Ik koester onze vriendschap en wens je bijzonder veel succes in de toekomst .

Eind 2008 kreeg ik de mogelijkheid om een student te begeleiden in zijn eindopdracht. Dit bleek Remco Regeling: 'hardcore to the bone' inclusief kaalgeschoren hoofd en Feyenoord-bomberjack, maar ook leergierig en voorzien van een enorme werklust. We vormden een goed team samen, ook later toen je als technicus werd aangesteld. Remco, dank je voor al je energie en zeker ook voor de vrijdagse vis! Te gek dat je net als Luc mijn paranimf wilt zijn!

TuHa Vong wil ik bedanken voor de samenwerking die uiteindelijk tot hoofdstuk 4 heeft geleid. Maar ook bedankt ook voor je gezelligheid tijdens de studiereis in Zweden en je pogingen het spel Munchkin uit te leggen.

With Menglong Yang around, there is always a laugh. But there are also wise lessons and reflections. There are many moments I cherish: the Chinese parties at my place, the making of the movie, and of course the fantastic holiday you organized for us in China. I'm glad I could have my first scientific baby with you! Thank you for everything and hopefully we meet again soon!

At the end of my stay in Wageningen, I had the honor of working together with two experienced researchers, Carel Weijers and Colin Ingham. It was very inspiring to work in such a multidisciplinary team, which produced so many ideas, that it was often difficult to stay on the same track. It made science great fun, thank you for that! I am also grateful to Willem de Vos for his initiative to set up this collaboration and for his contribution to this work.

I want to thank Michel and Milena for their friendship. It was a lot of fun to share a lab with you, but also outside the lab during cheese fondue parties, Bassie & Adriaan karaoke and bunny hunting we had good times. No wonder that Anouk and I followed you to Leiden to become your neighbors!

Ook Tijs Lammens wil ik bedanken voor zijn vriendschap. Het was fijn om een vriend in de buurt te hebben waarmee ik ook mijn labervaringen kon delen. Zeker als het iemand is die zo relaxed in het leven staat als jij!

Bart Rijksen, ik ben jou toch vooral dankbaar voor het introduceren van SpongeBob in mijn leven! Maar ook bedankt voor je deelname aan Team Diacetylene (een echte kwallenclub!) en je fantastische rol in het kikkeravontuur in China!

In de vier jaar dat Luc en ik een kamer deelden in de kelder, hebben we toch twee voetbaltafels weten te verslijten. Veel plezier heb ik hieraan beleefd met Luc, Michel,

Remco en Bart, maar ook met onze buurmannen Ruud Cuijpers en Murali Sukumaran. Ruud, aan jouw enthousiasme kan iedereen een voorbeeld nemen, bedankt hiervoor! Murali, it was a pleasure having you around, good luck in India!

Thanks to Louis de Smet and Ahmed Arafat for teaching me the art of silicon surface modification. Ahmed, thanks for introducing me to the upgraded Bizza Bollos at Sfinx and the after-dinner coffees at Albert Heijn as well!

Dan wil ik ook graag Rosalie Teeuwen bedanken: met jou als kamergenoot is er altijd leven in de brouwerij! En huisbaas Gregor Pilzak, bedankt voor je raad op het gebied van organische chemie!

Met Erik Faber vormde ik een team tijdens alle NanoNed activiteiten. Erik, bedankt voor de prettige samenwerking! En over NanoNed gesproken: Marjan Fretz, hartelijk dank voor je belangstelling en het faciliteren van mijn onderzoeksproject.

Marcel Giesbers en Barend van Lagen, bedankt voor jullie ondersteuning en wijze raad op het gebied van spectroscopie. Maar ik ben jullie minstens zo dankbaar voor de plezierige werksfeer! En Marcel, wil je Monique namens mij bedanken voor het bemannen van de XPS hotline?

Maarten Posthumus wil ik bedanken voor de exacte massabepalingen en zijn markante aanwezigheid bij Organische Chemie. Frank en Elbert ben ik dankbaar voor hun ondersteuning bij de gaschromatografie en voor de toevoer van al die argoncilinders. Ronald de Bruin wil ik bedanken voor het afhandelen van alle bestellingen, maar ook voor het bijzondere kaartje uit Wit-Rusland.

Met veel plezier heb ik deelgenomen aan allerlei sociale activiteiten bij Organische Chemie, variërend van borrels en spelavonden tot sportdagen en studiereizen. Met name Kim de Lange en Teris van Beek ben ik dankbaar voor hun inzet om deze activiteiten van de grond te krijgen. Maar ook Alexandre, Anke, Jos, Mabel, Loes, Wouter, Rokus, Jacob, Ed, Evan, Niels, Jaime, Nishant, Nagesh, Ai, Willem, Jerome, Tin, Jacinthe, Aliaksei, Suzanne, Marloes, Feng, Annemarie, Ioan, Kishore, Melle, Cindy, Remko, Ganesan, Elly, Aleida, Maurice, Michel, Ton, Erik, Frans, Anne-Marie, Cees en alle andere collega's wil ik bedanken voor alle gezelligheid!

In de afgelopen twee jaar was ik nog af en toe bij Organische Chemie te vinden. In deze tijd zijn er veel nieuwe projecten opgestart gestart. Vooral Tom Wennekes en Aline Debrassi wil ik veel succes wensen met de voortzetting van het werk op poreus

anodisch alumina! And to Siddhu, Yan, Radostina, Florine and Umesh: good luck to you as well!

Martin Hessing en Colin Ingham, ik wil jullie bedanken voor de mogelijkheid die jullie me boden om bij MicroDish aan de modificatie van poreus anodisch alumina te blijven werken. Dit heeft zeker bijgedragen aan het totstandkomen van dit proefschrift. Martin en Colin, ik wens jullie veel succes op jullie hengelexpeditie en mochten jullie niets vangen, dan staat mijn nagelstudio klaar voor gebruik!

Na het dagelijkse werk in het laboratorium was ik 's avonds vaak te vinden bij Budo Academy Physical in Ede. Het beoefenen van Yoseikan ju-jutsu en aikido is tijdens mijn promotieperiode een belangrijke uitlaatklep voor me geweest. Daarom wil ik iedereen bedanken bij en met wie ik daar de afgelopen jaren heb getraind, en met name Edgar, Matthieu, Erwin, Minh, Bart-Jan, Sam en Esther.

Mijn familie en vrienden heb ik geprobeerd niet te veel lastig te vallen met al mijn werkzaamheden. Maar gelukkig had ik naast mijn promotieproject in 2009 nog een ander groot project om over te praten: Ik wil iedereen bedanken die met Anouk en mij van onze bruiloft in de berghut een fantastisch feest heeft gemaakt!

Mijn ouders Gerard en Dinie en schoonouders André en Maria wil ik bedanken voor hun interesse, steun en vertrouwen. In dat kader dank ik ook generaal IJlemans voor zijn niet-aflatende woordenbrij.

Maar aan Anouk ben ik nog wel de meeste dank verschuldigd. Anouk, dank je wel voor je onvoorwaardelijke steun. En ook al komt het citaat van Dr. Paul Armstrong je misschien wel heel bekend voor, je wist me toch telkens weer te verrassen en zo uit de dagelijkse sleur te trekken. Ik hoop nog lang met jou van het leven te genieten!

On the author

Jurjen ter Maat (1980) was born and raised in Warnsveld, the Netherlands. In 1998 he started a study in Chemical Engineering at Twente University. After an internship at BASF in Ludwigshafen, his interest in surface chemistry was raised within the group of Supramolecular Chemistry and Technology, where he performed his graduation project under the supervision of Jurriaan Huskens. He obtained his MSc degree *cum laude* and for his final thesis, he was awarded the Unilever Research prize.

In 2005, Jurjen cut off his hair and started a PhD project. He resumed working on surface chemistry in the group of Organic Chemistry at Wageningen University, under the supervision of Han Zuilhof. The main results of his work are described in this thesis. Because of his experience with porous anodic alumina, he was employed as a researcher at MicroDish BV in 2009. There, he further developed his skills in surface modification and microfabrication. As of March 2012, Jurjen is working as a research technologist at AkzoNobel Industrial Chemicals in Deventer.

Aside from his professional education, Jurjen is enrolled at Budo Academy Physical, where he practices Yoseikan Ju-Jutsu and Aikido. He also enjoys mountaineering and playing tennis with or against his lovely wife Anouk.

List of Publications

Photochemical covalent attachment of alkene-derived monolayers onto hydroxyl-terminated silica, ter Maat, J.; Regeling, R.; Yang, M.; Mullings, M. N.; Bent, S. F.; Zuilhof, H. *Langmuir* **2009**, *25*, 11592.

Light-enhanced microcontact printing of 1-alkynes onto hydrogen-terminated silicon, ter Maat, J.; Yang, M. L.; Scheres, L.; Kuypers, S.; Zuilhof, H. *Chem. Commun*. **2010**, *46*, 8005.

Organic modification and subsequent biofunctionalization of porous anodic alumina using terminal alkynes, ter Maat, J.; Regeling, R.; Ingham, C. J.; Weijers, C.; Giesbers, M.; de Vos, W. M.; Zuilhof, H. *Langmuir* **2011**, *27*, 13606.

Site-specific immobilization of DNA in fused silica microchannels via photolithography, Vong, T. H.; ter Maat, J.; van Beek, T. A.; van Lagen, B.; Giesbers, M.; van Hest, J. C. M.; Zuilhof, H. *Langmuir* **2009**, *25*, 13952.

Microcontact printing onto oxide-free silicon via highly reactive acid fluoride-functionalized monolayers, Scheres, L.; ter Maat, J.; Giesbers, M.; Zuilhof, H. *Small* **2010**, *6*, 642.

Where bio meets nano: The many uses for nanoporous aluminum oxide in biotechnology, Ingham, C. J.; ter Maat, J.; de Vos, W. M. *Biotechnol. Adv.* **2012**, doi:10.1016/j.biotechadv.2011.08.005.

Micro- and nanopatterning of functional organic monolayers on oxide-free silicon by laser-induced photothermal desorption, Scheres, L.; Klingebiel, B.; ter Maat, J.; Giesbers, M.; de Jong, H.; Hartmann, N.; Zuilhof, H. *Small* **2010**, *6*, 1918.

Preparation of metal-SAM-dendrimer-SAM-metal junctions by supramolecular metal transfer printing, Nijhuis, C. A.; ter Maat, J.; Bisri, S. Z.; Weusthof, M. H. H.; Salm, C.; Schmitz, J.; Ravoo, B. J.; Huskensa, J.; Reinhoudt, D. N. *New J. Chem.* **2008**, *32*, 652.

Molecular printboards on silicon oxide: Lithographic patterning of cyclodextrin monolayers with multivalent, fluorescent guest molecules, Mulder, A.; Onclin, S.; Peter, M.; Hoogenboom, J. P.; Beijleveld, H.; ter Maat, J.; Garcia-Parajo, M. F.; Ravoo, B. J.; Huskens, J.; van Hulst, N. F.; Reinhoudt, D. N. *Small* **2005**, *1*, 242.

Photochemical modification of solid materials, Zuilhof, J. T.; ter Maat, J. European Patent EP2356082, October 17, 2008.

Overview of completed training activities

Discipline-specific courses	**Organized by**	**Year**
From membrane transport to neurosciences	Portuguese Society of Biophysics	2005
Chemical surface analysis of materials	EPFL Lausanne	2006
Fundamentals of nanotechnology	Twente University	2006
General courses		
VLAG PhD week	VLAG	2007
Personal efficacy	Meijer & Meijaard	2008
PhD scientific writing	Language Services	2009
Career perspectives	Meijer & Meijaard	2009
Intellectual property	NanoNed	2009
Meetings		
European atomic force microscopy forum	University of Münster	2007
Advanced macromolecular systems	Twente University	2007
European materials research symposium	EMRS Strassbourg	2009
Annual structure and reactivity meetings	NWO Lunteren	2005-2009
Annual MicroNano conference	NanoNed	2005-2010
Optionals		
Preparation PhD research proposal		2005
Exchange project with Linford group, Brigham Young University, Provo (USA)		2006
Organic chemistry study tour to Sweden		2007
Organic chemistry study tour to China		2009
Organic chemistry group meetings		2005-2009
Organic chemistry colloquia		2005-2009
Total ECTS credits		**44.9**

The research described in this thesis was financially supported by NanoNed, funded by the Dutch Ministry of Economic Affairs (project WMM.6975).